University of Alberta

Stabilization of oil sands tailings using vacuum consolidation

by

Ehsan Abazari Torghabeh

A thesis submitted to the Faculty of Graduate Studies and Research
in partial fulfillment of the requirements for the degree of

Doctor of Philosophy
in
Geotechnical Engineering

Civil and Environmental Engineering

Fall 2013
Edmonton, Alberta

ABSTRACT

This research is an experimental design and numerical analysis of a novel technique of the vacuum consolidation of Mature Fine Tailings (MFT). A meso-scale test was conducted to examine the feasibility of the MFT dewatering process. Vacuum consolidation involves applying a negative water pressure to the coke layer overlain by a saturated sand layer and underlain by MFT. Numerical modeling was conducted using the finite element program SoilVision to model the meso-scale experiment. Unsaturated behavior of Suncor coke, Suncor sand and MFT was investigated using Tempe pressure cell and capillary rise in an open tube prior to commencement of tests. Results indicate that a flux of water flows from the MFT layer into the coke layer which is indicative of the MFT dewatering. The modeling analysis indicates that suction has little effect on the settlement while the overburden has the significant effect on consolidation. This thesis also illustrates the importance of recalibrating TDR probes for different materials. The three layered system testing of MFT, Suncor coke and Suncor sand indicates that applying suction causing MFT to dewater, can set the stage for a four layered system in which another layer of MFT is placed on top of the sand layer. The suction applied to the coke layer causes the double-drained MFT to dewater faster.

Table of Contents

List of Figures

List of Tables

Chapter 1 Introduction

1.1 Statement of problem

Oil sands tailings is comprised of water, sand, clay, silt and residual bitumen at a pH typically between 8 to 9. The traditional method of disposing oil sands tailings involves discharging the fine tailings into a settling pond. The discharge flow segregates, with the coarser fraction of the tailings slurry settling out rapidly to form long sand beaches (Kwak et al., 2005). The solids contained in the fresh slurry arriving at the pond settle relatively fast creating a "clean" water cap containing some solids. As hindered sedimentation continues, further de-watering and consolidation of the tailings within the pond occurs very slowly (Yunxin and Sego, 2001).

Over time, three zones form in the tailings ponds. The uppermost 3 m layer is composed of clear to semi-clear water which is recycled continuously through an extraction process. There is a transition zone underneath the clear water which is composed of a mixture of clay, fine sand, bitumen and water with gradually increasing density. This mixture is referred to as Mature Fine Tailings (MFT). MFT at Syncrude, for instance, consists of 85% water, 13% fines and 2% bitumen by volume (Jakubick et al., 2003). The distinction between the different zones in the tailings pond is based on the shear strength and geotechnical parameters such as the grain size distribution, solids content and Atterberg limits (Fine Tailings Fundamentals Consortium 1995).

The main focus of this research program is to study the feasibility of stabilizing MFT by creating a surface capable of supporting light traffic, which is essential for the reclamation process. Capping techniques for soft tailings were first applied to reclaim

phosphatic clay waste ponds where various types of sand caps were placed on the fine tailings. The success of capping techniques depends on the initial solids content of the underlying tailings. The bearing capacity failure of the sand cap occurs if the solids content is less than a critical limit (Bromwell et al., 1977).

The proposed capping technique for oil sands tailings involves placing a layer of coke on top of the tailings surface overlain by a thicker layer of sand. Applying a vacuum to the coke layer with time develops sufficient shear strength and will eventually dewater and consolidate the tailings. Further dewatering and consolidation of the tailings using vertical drains techniques might be implemented afterwards.

1.2 Objective and scope of the thesis

The objective of this research was to examine the feasibility of vacuum consolidation to improve the consolidation behavior of the MFT in a meso-scale column test. In order to achieve this objective, the research was divided into four studies, including laboratory characterization of the materials, instrumentation, meso-scale experiment and the numerical modeling. These studies were combined together to develop the overall understanding of the vacuum consolidation process. The objectives of each component of this research can be listed as followings.

- To determine the unsaturated parameters of Suncor sand, Suncor coke and MFT, including the wetting and drying Soil-Water Characteristics Curves and their permeability functions.

- To design, calibrate and install the instruments required to measure the desired parameters in the meso-scale study.
- To conduct the meso-scale column test on vacuum consolidation of the MFT.
- To numerically model the meso-scale column test using a finite element program.

This study utilized Suncor tailings produced from a tailings extraction plant to create the layered system of Suncor coke and Suncor sand. This research program is limited to Suncor MFT.

1.3 Organization of the thesis

This thesis is organized into 6 chapters. A brief introduction to each chapter follows below.

Chapter 2 includes a brief review of the characterization of Suncor sand, Suncor coke and MFT, and the determination of unsaturated parameters. The theoretical aspect of the Soil-Water Characteristic Curves are discussed and reviewed. Factors affecting the unsaturated behavior of the MFT are discussed and presented. The measured SWCCs are compared with two SWCC models. The measured SWCCs are also compared with the estimated SWCCs obtained using particle size distribution curves. The unsaturated permeability functions of Suncor coke and Suncor sand were determined based on the measured SWCCs. The chapter concludes with the determination of unsaturated permeability function of the MFT based on the large strain consolidation data and its drying SWCC.

Chapter 3 begins with a brief overview of the instrumentation of the large scale column test. The focus of this chapter is the calibration of Time Domain Reflectometry (TDR) devices to measure the water content of the soil at various elevations in the column. The universal formulation, Topp equation (1980), used to correlate the dielectric properties of materials to water contents, is applied to Suncor sand, Suncor coke and MFT. The results indicate that Topp equation (1980) for water content measurement leads to significantly different results in MFT, Suncor sand and Suncor coke which necessitates the need for developing new calibration equations for each material.

Chapter 4, meso-scale experiment is the core of the thesis. This chapter presents a validation of the hypothesis and experimentally simulated tailings pond condition. The experimental performance of vacuum consolidation on dewatering and reclaiming tailings was investigated in the designed PVC column. Interface settlement, pore-water pressure response, suction in the media and water content in each level were monitored and used for the validation purposes.

Chapter 5 describes the numerical modeling of the meso-scale experiment using the finite element code, SoilVision. Various parameters including the settlement, pore pressure dissipation, effective stress, saturation and permeability functions of the materials during the experiment are investigated in this chapter.

Chapter 6 presents a summary of the observations, conclusions and future work.

1.4 REFERENCES

Bromwell, L. G., and Oxford, T. P. (1977). "Waste Clay Dewatering and Disposal." Geotechnical Practice for Disposal of Solid Waste Materials; pp. 541-558.

Fine Tailings Fundamentals Consortium. (1995). Advances in oil sands tailings research. Alberta Dept. of Energy, Edmonton, Alta.

Jakubick, A. T., McKenna, G., and Robertson, A. M. (2003). "Stabilisation of Tailings Deposits: International Experience." Nternational Experience. Mining and the Environment III, Sudbury, Ontario, Canada, 25-28 May pp. 1-9.

Kwak, M., James, D. F., and Klein, K. A. (2005). "Flow behaviour of tailings paste for surface disposal." Int.J.Miner.Process., 77(3), 139-153.

Yunxin, Q., and Sego, D. C. (2001). "Laboratory properties of mine tailings." Canadian Geotechnical Journal, 38(1), 183-190.

Chapter 2 Unsaturated behavior of Coke, Sand and Suncor Mature Fine Tailings

2.1 Introduction

A technique was developed as part of a research initiative to investigate the potential for using vacuum consolidation to strengthen soft oil sands fine tailings. As part of the vacuum technique, Mature Fine Tailings (MFT) was overlain with a layer of saturated coke followed by another layer of uniformly distributed sand. Negative water pressure was then applied to the coke layer, which desaturated the coke and the sand layer. An upward flow of pore-water from the MFT into the coke layer was monitored and provided verification of the consolidation of the underlying tailings. An understanding of the unsaturated material characteristics was necessary to assist with performing a numerical analysis of a large scale simulation of the dewatering process. This paper describes the unsaturated material behavior of Suncor sand, Suncor coke and MFT. These properties form the basis for numerical and experimental modeling of the vacuum consolidation process (Fredlund and Rahardjo, 1993).

Research studies have demonstrated that the unsaturated behavior of soil is related to its Soil-Water Characteristics Curve, (SWCC) (Fredlund and Rahardjo, 1993). The SWCC shows the relationship between the amount of water in a soil and various applied soil suctions (Fredlund et al. 2011) and can be plotted as volumetric water content θ_w versus soil suction. The SWCC can be used to describe the unsaturated soil strength (Vanapalli et al., 1996) and unsaturated permeability properties (Fredlund

and Xing, 1994). The shape of the SWCC varies significantly depending on soil gradation and soil type. An idealized SWCC graph is shown in Figure 2.1.

Research studies have shown that the volumetric water content of soil is not a single unique curve. It has been found that the drying volumetric water content lies above the wetting curve. Consequently there are two different bounding curves. One curve determines the behavior of soil as it is wet, and is referred to as the wetting soil-water characteristic curve (or absorption curve). The other curve is referred to as the drying soil-water characteristic curve (or desorption curve). The difference between the two is known as the hysteresis and is illustrated in Figure 2.1.

Assuming that the soil structure of a sand or coarse-grained soil undergoes negligible volume change, the water content remains fairly constant up to the air-entry value as suction in the soil increases. The matric suction at which the water content starts to decrease is designated as the air-entry value (or ψ_{aev}). The water content decreases in a linear manner (on a semi-log plot) until the residual water content of the soil, θ_r is reached. The residual water content is the lowest water content in which the water phase in the soil remains continuous (Fredlund and Xing, 1993). The soil suction corresponding to the residual water content is known as the residual soil suction. Let us suppose that the soil is dried to a low water content and then re-wetted. The matric suction on the wetting curve at which the water starts to enter the soil matrix is known as the water-entry value, $\psi_{wev.}$ The water-entry value is defined as the soil suction at which the water content starts to increase considerably during the wetting process.

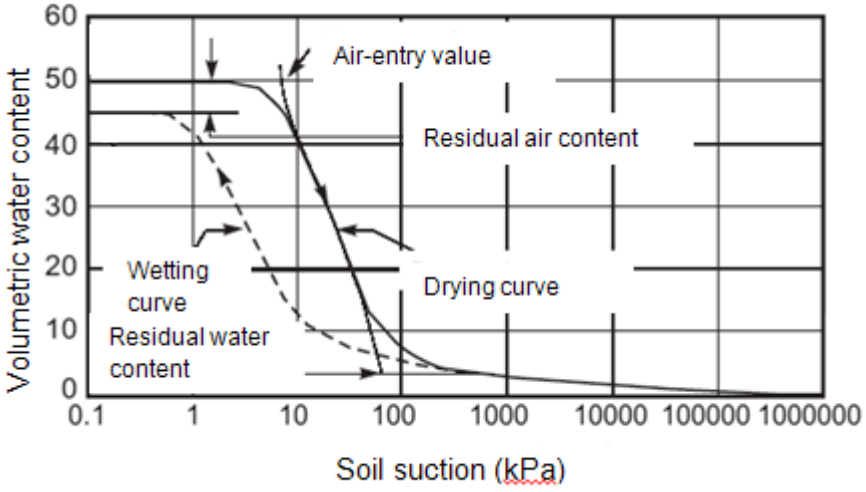

Figure 2.1: Typical SWCC graph (after Fredlund and Rahardjo, 1993)

Numerous studies have been carried out on modeling the SWCC of various soil types (Fredlund and Xing, 1994; Leong and Rahardjo, 1997; Mualem, 1977; Rossi and Nimmo, 1994; Aubertin et al., 1998). The Fredlund and Xing (1994) equation and van Genuchten equation (1980) yield the best-fit for a variety of soil types. The fit between the proposed SWCC equations and data is generally based on a least-square algorithm. Both equations can be best-fit using the SoilVision program (SoilVision Systems Ltd., 1999).

The Fredlund and Xing (1994) equation is expressed as follows:

$$\theta_w = \theta_s \left[1 - \frac{\ln(1+\psi/\psi_r)}{\ln(1+10^6/\psi_r)} \right] \left[\frac{1}{\left\{ \ln\left[e + (\psi/a_f)^{n_f} \right] \right\}^{m_f}} \right] \qquad [2.1]$$

where θ_w is the volumetric water content; θ_s is the saturated water content; a_f is a soil parameter that is related to the suction at the inflection point; n_f is a soil parameter related to the inflection point on the SWCC; m_f is a soil parameter related to the residual water content; ψ is soil suction (kPa); ψ_r is the residual suction (kPa). These parameters define the shape of the SWCC for both wetting and drying situations.

The van Genuchten (1980) equation can be expressed as follows:

$$\theta_w = \theta_r + (\theta_s - \theta_r)\left[1 + (\psi / a_v)^{n_v}\right]^{-m_v} \qquad [2.2]$$

where a_v is a soil parameter related to the inflection point and is somewhat greater than the AEV; n_v is a soil parameter related to the rate of water extraction from the soil and m_v is a soil parameter related to θ_r. These fitting parameters determine the shape of the SWCC.

Several research studies have been performed in an attempt to relate the SWCC of the soil to the particle size distribution (Fredlund et al., 2002).

In this paper, the SWCC's for Suncor coke, Suncor sand and MFT were measured and best-fitted using Fredlund-Xing (1994) and van Genuchten (1980) equations. The fitting parameters were discussed and correlated against the grain-size distributions of the materials. The drying SWCC for the MFT sample was corrected for volume change by using the shrinkage curve to relate soil suction to the gravimetric water content. The SWCC of the soils and the saturated hydraulic conductivities were then used to compute the unsaturated hydraulic conductivity of these materials. The unsaturated soil property functions were used later during the vacuum consolidation analysis.

2.2 Material description

Suncor coke, Suncor sand and MFT were used in this study. All materials are by-products of the oil sand extraction process in Northern Alberta. The materials were shipped to the University of Alberta in Edmonton in barrels from Suncor operation sites in Fort McMurray, Alberta. Black coke particles cover a wide range of particle sizes while the light brown Suncor sand collected from the tailings pond beaches have a fairly uniform distribution. Basic geotechnical properties for these materials were determined without bitumen removal and are tabulated in Table 2.1. Dry sieve analysis was conducted using ASTM D422-63 (ASTM 1997*a*). Specific gravity was measured using ASTM D854-92 (ASTM 1997*b*). A non-dispersed hydrometer test was conducted on MFT based on ASTM D1140-92 (ASTM 1997*c*). Atterberg limits on the MFT sample was conducted according to ASTM D4318-95 (ASTM 1997*f*). The soils were classified according to ASTM D2487-93 (ASTM 1997*e*). The grain-size distribution is given in Figure 2.2. The shrinkage curve of MFT has been determined based on ASTM D427-98 (ASTM 1998) and is shown in Figure 2.3.

Table 2.1. Geotechnical properties of the soils

	Suncor Coke	Suncor sand	MFT
Unified Soil Classification System	GW	SP	ML
Specific Gravity, G_s	1.37	2.65	2.49
Coefficient of uniformity, C_u	10.03	2.12	---
Coefficient of curvature, C_c	2.88	0.83	---
Dry density of soil, γ_d (kN/m^3)	6.79	14.36	4.29
Void ratio, e	0.94	0.77	4.63
Porosity, n (%)	0.48	0.43	0.82
Liquid limit (%)			48
Plastic limit (%)			22

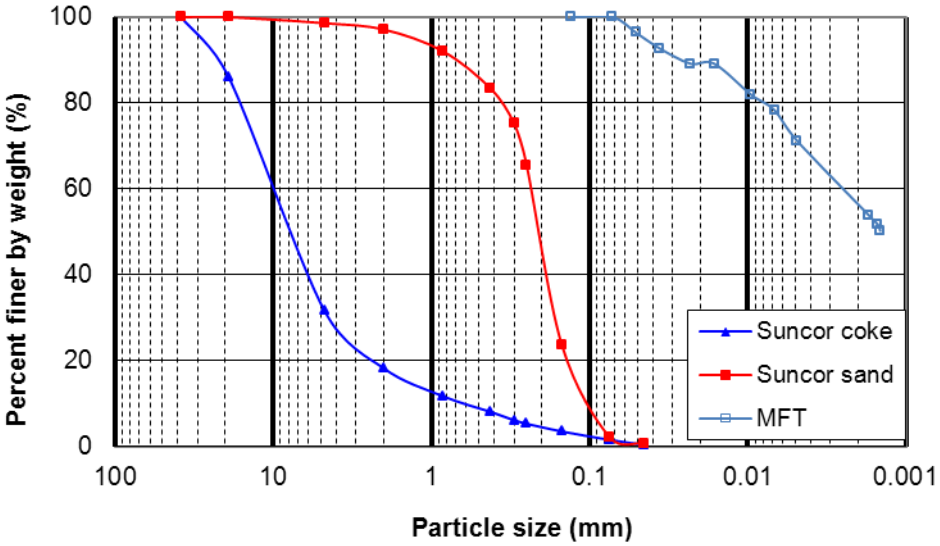

Figure 2.2: Particle size distribution of Suncor coke, Suncor sand and MFT

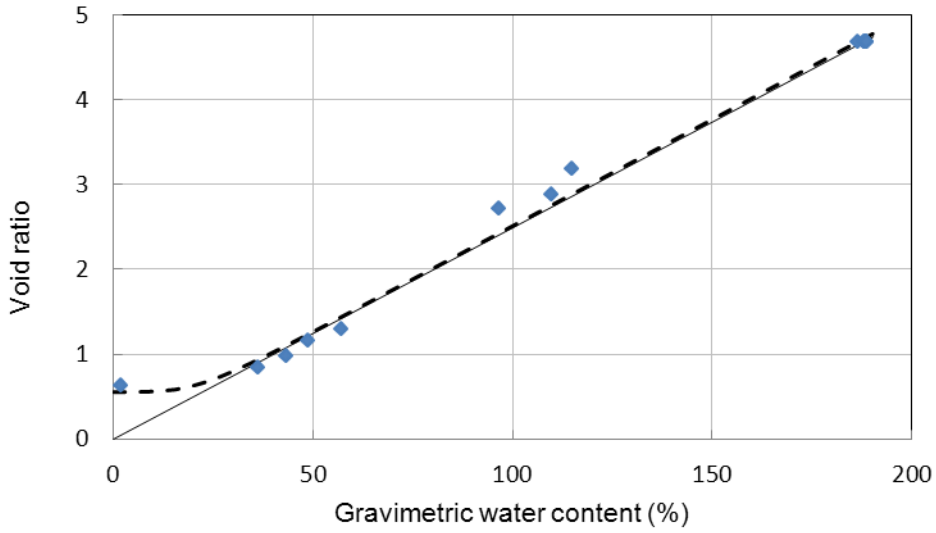

Figure 2.3: Shrinkage curve for MFT

2.3 Tempe pressure cell

The drying SWCC for all of the materials was obtained using a Tempe cell manufactured by the Soilmoisture Corporation (1999). The test procedure when using a Tempe cell is similar to that used for the conventional pressure plate apparatus detailed in D2325-68 (ASTM 1997*d*). The components of a Tempe cell are illustrated in Figure 2.4.

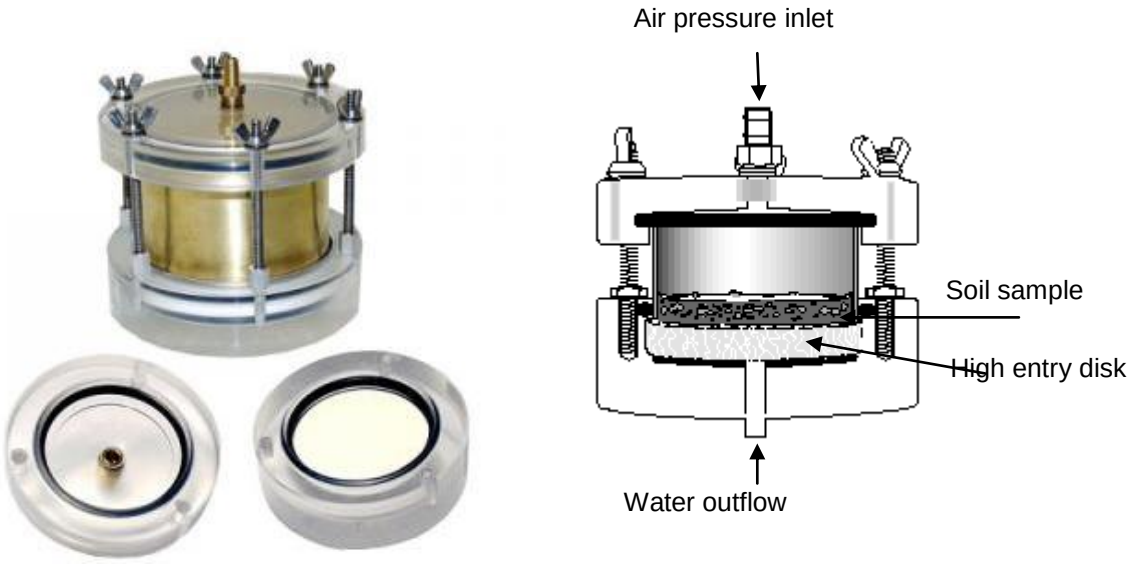

Figure 2.4: Compartments of a Tempe pressure plate

The test procedure associated with the Tempe cell involves placing a known amount of saturated soil in the cell. The size of the Tempe cell was selected at least four times larger than the largest size of the materials tested. The sample can be saturated by submerging the entire cell in water for a few days. The cell allows the water to drain but prevents air from entering the high air-entry ceramic disk once the disk is saturated. The water in the soil specimen can drain through an outlet provided at the bottom of the cell. Hence the water pressure at the bottom of the specimen is maintained at atmospheric (0 kPa gauge) throughout the test. The air pressure is applied to the cell through an inlet tube on the top cap. The O-rings covering the cell keep the cell airtight during the experiment. Excess water will be

drained from the bottom ceramic disk once the air pressure is set to the desired value. The change in water content is measured frequently by measuring the weight of the Tempe cell. To ensure that equilibrium has been attained, the Tempe cell is weighed until no significant change in weight is evident, which is indicative of the sample's stress state equilibrium. Once the highest air pressure is applied to the sample, the sample's final water content is measured. The water contents during previous stages of the experiment are evaluated using back analysis. The equilibrium time in each stage depends on type of the material and generally varies from a few hours to a few days. ASTM D2325-68 recommends using an equilibrium time of 18 to 48h.

As the air-entry value of coarse materials is fairly low, it is desirable to start the experiment with as low a matric suction value as possible (i.e., in the order of 0.1 kPa). Since the air pressure regulator is only accurate to about 10 kPa, in our study an accurate pressure transducer was attached to the Tempe cell to provide accurate pressure application in the low suction range.

The matric suction applied to the cell is the average value of the matric suction between the top and bottom of the soil specimen. As air pressure, u_a (kPa) is applied to the sample, the average matric suction will be equal to the mean value of $u_a + 0.5\rho_w gH$ where ρ_w is the density of water and H is the height of the soil specimen. These calculations are illustrated in Figure 2.5.

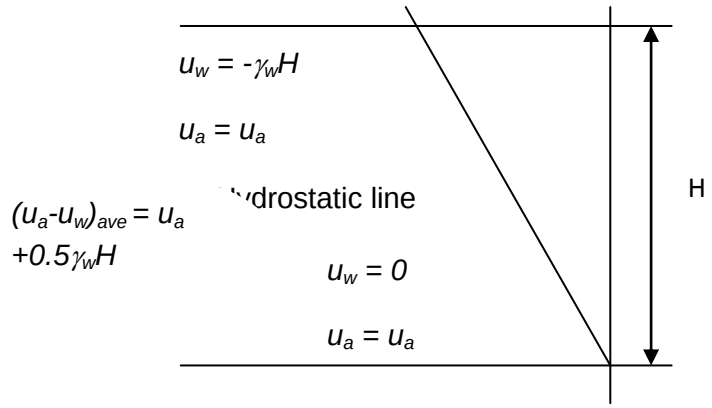

Figure 2.5: Calculation of the average matric suction in the soil specimen

Figure 2.5 shows that in order to get the average matric suction, $0.5\rho_w gH$ must be added to the air pressure. For a soil specimen of 20 mm in height, the adjustment value is 0.1 kPa, indicating that even before applying the air pressure to the sample, the average matric suction is 0.1 kPa.

The volumetric water content is the volume of water divided by the entire volume of the soil and is calculated from gravimetric water content using the following equation:

$$\theta_w = (\rho_d / \rho_w) w \qquad [2.3]$$

where w is the gravitational water content; ρ_d is the dry density of the soil specimen and ρ_w is the density of water.

The soil specimen is initially saturated prior to Tempe cell experiments. Therefore the test results yield a drying SWCC. Measuring the SWCC of a soil is time consuming. The time required for the experiment depends on the soil type, specimen size, applied air pressure and type of ceramic disk. The ceramic disk used for tests on Suncor coke and Suncor sand had an air-entry value of 100 kPa. The ceramic disk for the test on the MFT sample had an AEV of 500 kPa.

2.4 Capillary rise open tubes

The wetting SWCC of Suncor coke and Suncor sand was obtained using open tubes. Capillary rise open tubes can be filled with dry material and compacted to the desired density. The open end of the tube is placed in a tray with water maintained at a

particular level. The water table is maintained at the same level for the entire test. The top of the tube is covered with aluminum foil to prevent evaporation. Due to the capillary phenomenon, water will start to rise in the tube and eventually reach equilibrium after some elapsed time. The matric suction in the soil is equal to the negative water pressure since the air pressure in the tube is atmospheric, ($u_a = 0$).

The height of the sample above the water level is assumed to be equal to the capillary head. Once equilibrium is reached, soil samples are taken at various elevations in the tube to determine the gravimetric water content. The water content can then be calculated using equation [2.3] and plotted as volumetric water content versus soil suction. The tubes utilized in this series of experiments were 0.1 m in diameter and 0.5 m in length. The samples were allowed to wet for 60 days. Figure 2.6 shows the configuration of the open tube arrangement.

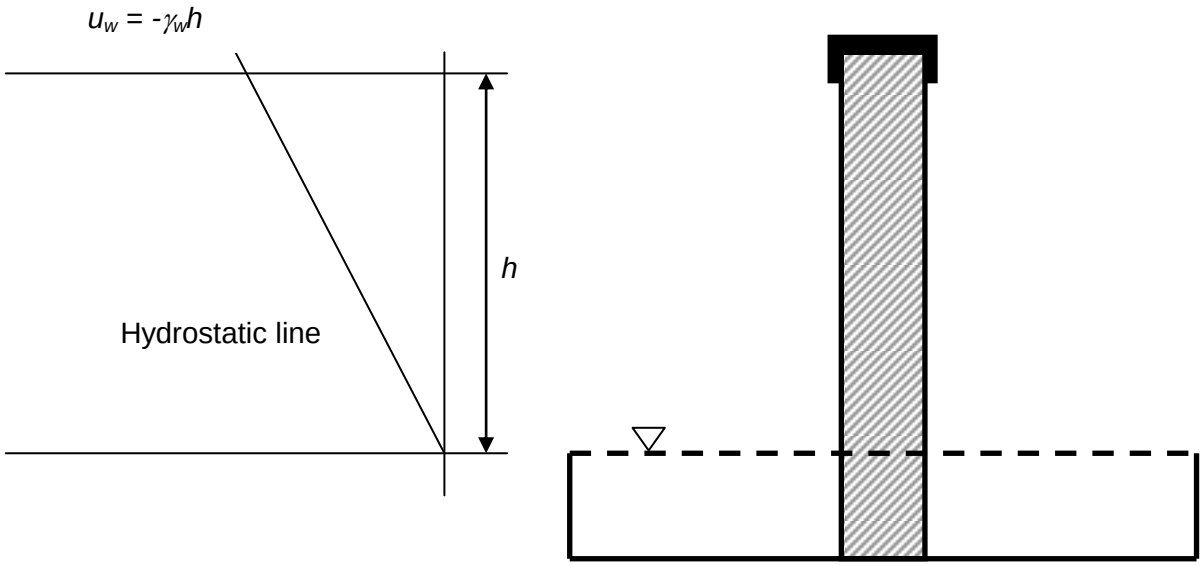

Figure 2.6: Schematic diagram of a capillary rise in the open tube

2.5 Results and discussions

The drying and wetting SWCC of Suncor sand and Suncor coke were determined using Tempe pressure cells and open capillary rise tubes, respectively. Only the drying curve for the MFT was determined and corrected for volume change. The results were best-fit using Fredlund-Xing (1994) and van Genuchten (1980) models. The air-entry value, residual matric suction and fitting parameters of the SWCC were determined using SoilVision database systems (SVD v.4.0 1999) and listed in Table 2.2. Figures 2.7 To 2.9 show the test data as well as the best-fit results. FX denotes the Fredlund-Xing (1994) model and VG denotes the van Genuchten (1980) model. WC stands for wetting curve and DC stands for drying curve.

Table 2.2: Fitting parameters for the Fredlund-Xing (1994) and the van Genuchten (1980) models

Description	Symbol	Suncor coke	Suncor sand	MFT
Unified Soil Classification System		GW	SP	ML
Drying curve				
Saturated volumetric water content	θ_s	0.47	0.42	0.88
Air-entry value (kPa)	ψ_a	0.01	1.07	5.09
Residual matric suction (kPa)	ψ_r	2.06	6.69	27.35
Residual volumetric water content	θ_r	0.049	0.019	0.055
Fredlund and Xing parameters	a_f	0.032	2.11	9.02
	n_f	1.061	2.58	2.96
	m_f	1.218	1.47	1.21
van Genuchten parameters	a_v	0.0806	0.092	0.024
	n_v	0.451	1.69	2.066
	m_v	7.99	8	8
Wetting curve				
Fredlund and Xing parameters	a_f	0.0219	4.48	
	n_f	1.295	1.059	
	m_f	2.59	12.31	
van Genuchten parameters	a_v	80.94	0.23	
	n_v	0.414	1.31	
	m_v	7.08	8	

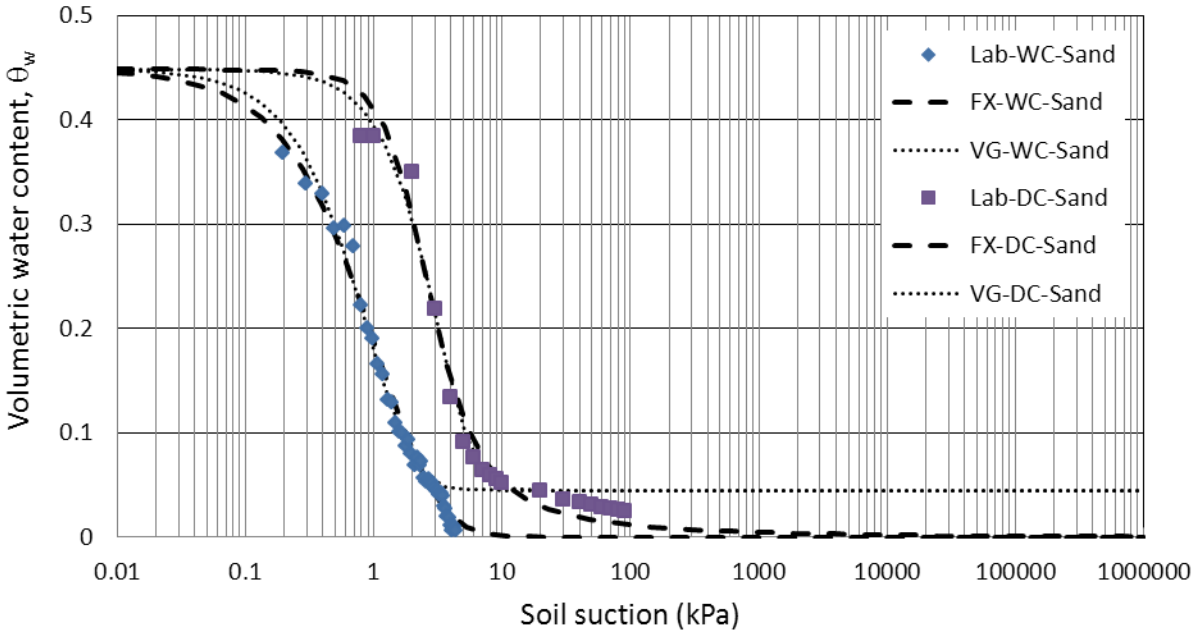

Figure 2.7: Drying and wetting curves for Suncor sand

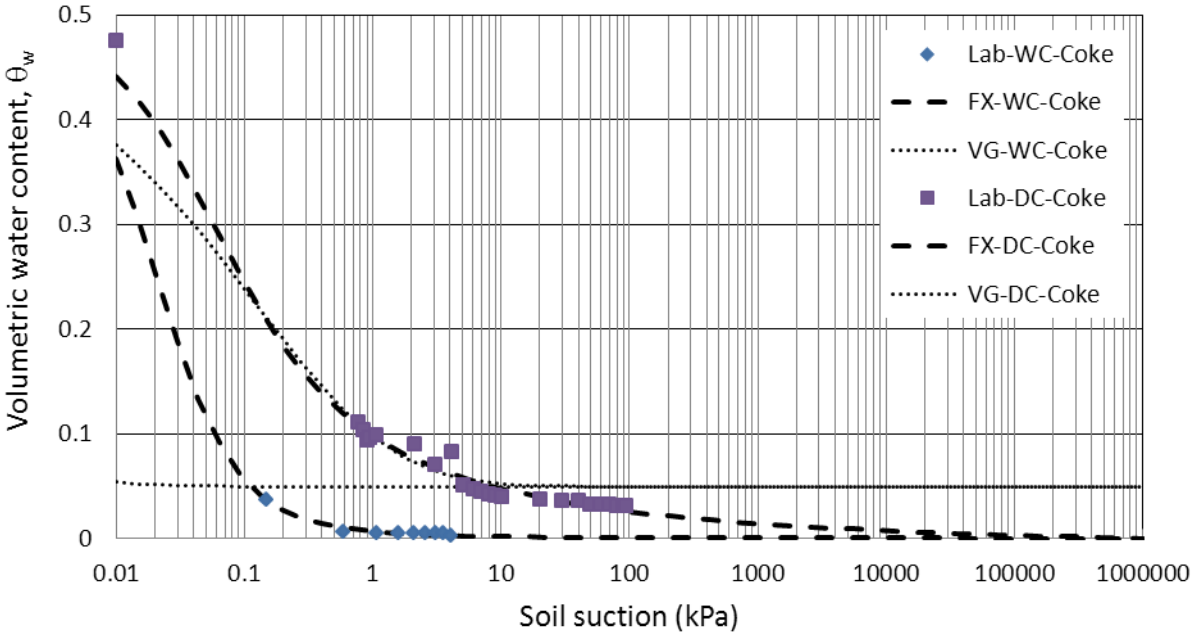

Figure 2.8: Drying and wetting curves for Suncor coke

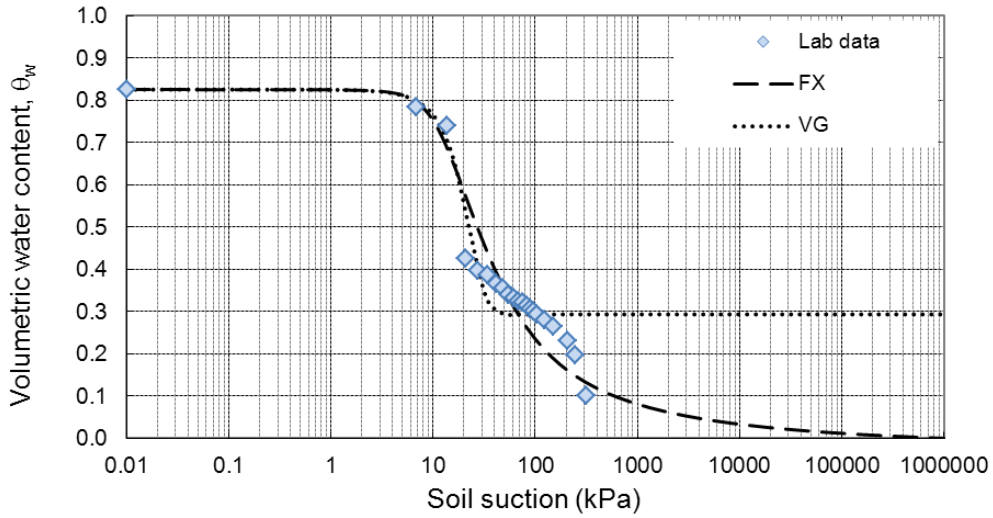

Figure 2.9: Drying curve for MFT

2.5.1 Fitting parameters

The SWCC characteristics can be correlated with the model fitting parameters. For example, the air-entry value of the soil, ψ_a, is related to the soil parameter a_f. This relationship is shown in Figure 2.10. Yang et al. (2004) observed a linear relationship between these two parameters. The values obtained for the a_f parameter fit well with the linear relationship proposed by Yang et al. (2004). A larger air-entry value yields a larger a_f parameter.

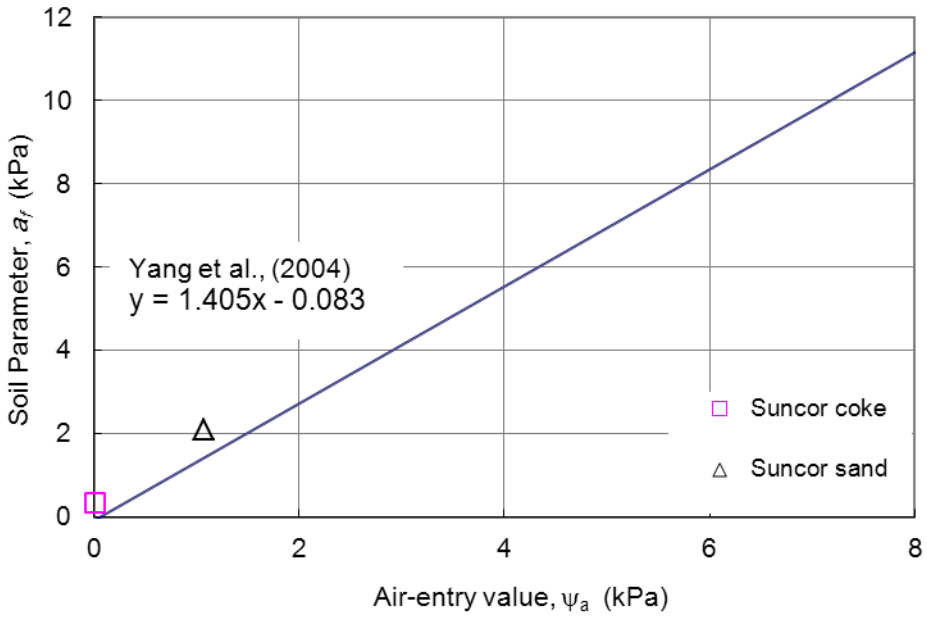

Figure 2.10: Soil parameter a_f in Fredlund-Xing (1994) versus air-entry value for the drying curves

In a similar manner, the soil parameter, m_f, in Fredlund-Xing model (1994) can be related to residual suction ψ_r. As shown in Figure 2.11 there is a direct relationship between the soil suction and the soil parameter m_f. For comparison reasons, the data are compared with the data presented by Yang et al., (2004) where a linear but inverse relationship was shown between soil parameter m_f and residual suction. The results do not agree with the data points obtained from Yang's experiments (Yang et al., 2004). The reason of disagreement may be due to the errors associated with the measurement of water content in the Tempe Cell experiment. More data points are needed to further investigate the trend of the soil parameter m_f, with the residual suction.

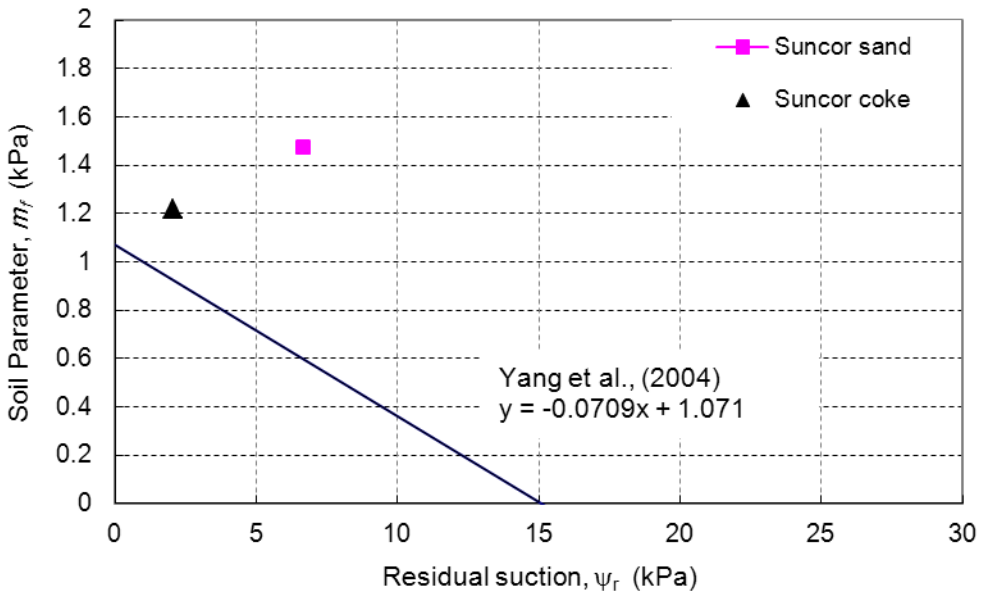

Figure 2.11: Soil parameter m_f in Fredlund-Xing (1994) versus residual suction value for the drying curves

The parameter *n* has been correlated with the slope of SWCC, which is determined by $(\theta_s - \theta_r)/(log\ \psi_r - log\ \psi_a)$. According to Yang et al. (2004), there is a linear relationship between the slope of the SWCC and the soil parameter n_f. Figure 2.12 shows a similar linear equation but with a different slope. The trend of the results shows an increasing effect with the SWCC slope, consistent with the results obtained by Yang (Yang et al., 2004). However, due to the limited number of materials tested, it would not be feasible to draw a general conclusion about the discrepancy.

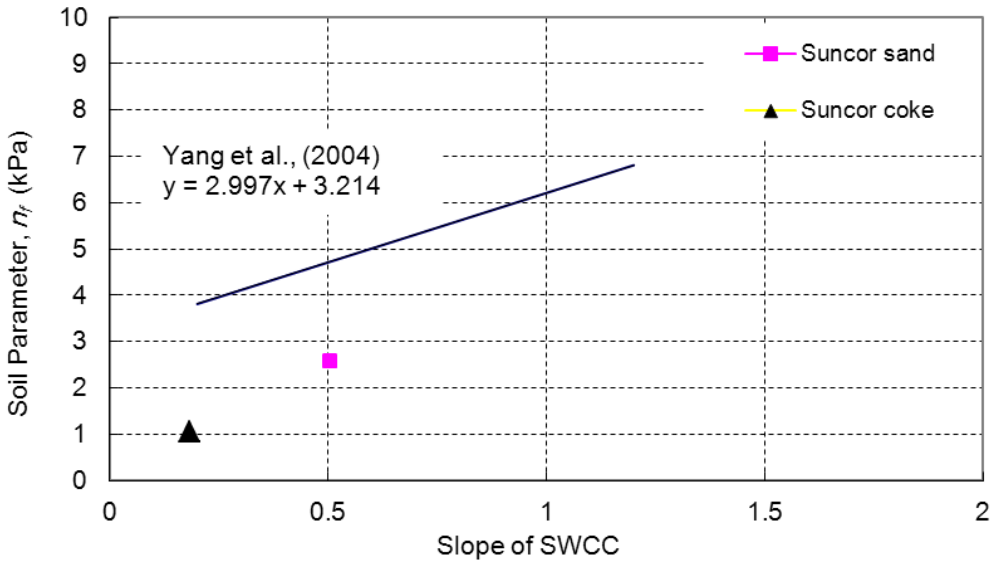

Figure 2.12: Soil parameter n_f in Fredlund-Xing (1994) versus the slope of the SWCC

2.5.2 Relationship between the SWCC and the particle size distribution

It is common to relate the SWCC to the grain-size distribution curve of a specific soil type. Data presented by Yang et al. (2004) show a direct relationship between the air-entry value and the residual suction with D_{10} (i.e., the diameter at 10% passing on the grain-size curve). Figure 2.13 shows the relationship between AEV and residual suction ψ_r with D_{10} along with the trend lines presented by Yang et al. (2004). As illustrated in the Figure 2.13, the data follows the trend lines closely, indicating that a finer soil has a higher air-entry value and a higher residual suction, ψ_r. The increase in the pore size of the soil leads to a decrease in the air-entry value and residual suction. The difference between soil suction and the air-entry value also decreases to zero as the D_{10} increases.

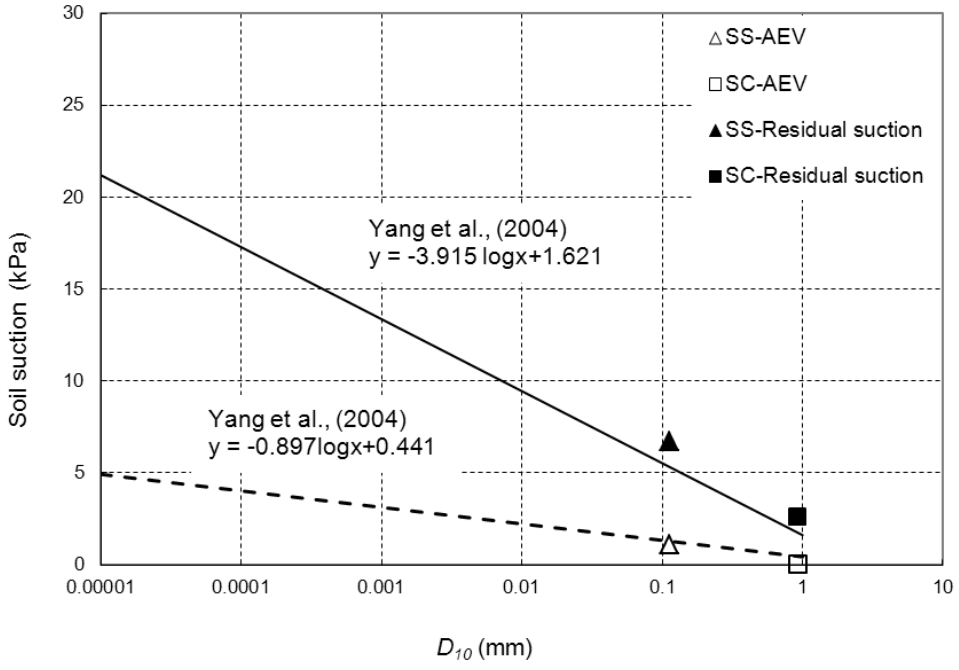

Figure 2.13: Soil suction versus D_{10} of Suncor sand and Suncor coke

(SS denotes Suncor sand; SC denotes Suncor coke)

The slope of the SWCC is comparable with the slope of soil particle distribution. A flatter slope leads to a flatter SWCC (Figure 2.14). For comparison reasons, the data points are plotted with the linear equation presented by Yang et al., (2004). The plot is consistent with the results shown by Yang et al. (2004), in which a linear relationship was shown between the SWCC and the particle size distribution curve.

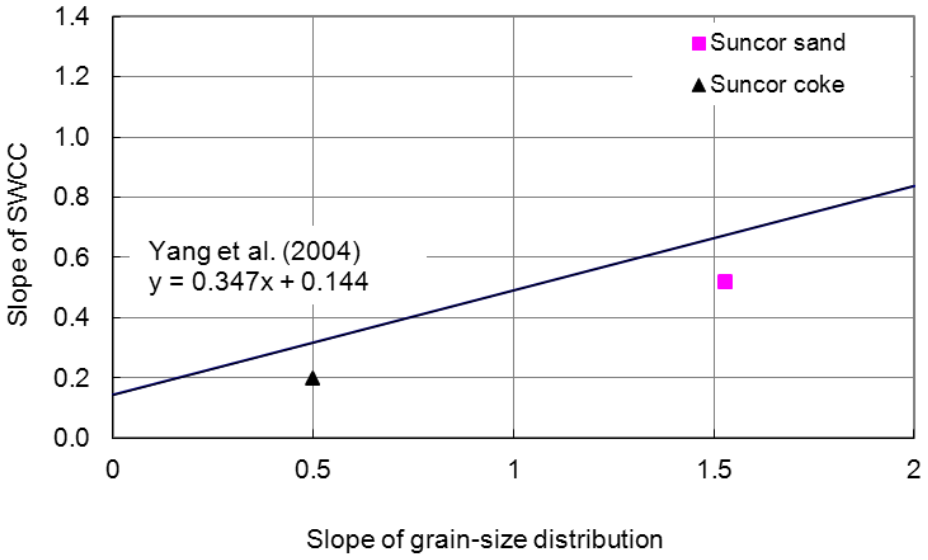

Figure 2.14: Slope of the SWCC versus the slope of the grain-size distribution curve

2.5.3 Estimations of the SWCC from the particle size distribution

Several models have been developed for the purpose of estimating the drying SWCC from the soil particle size distribution (Arya and Paris, 1981; Aubertin et al., 2003; Aubertin et al., 1998; Barbour, 1998; Pham et al., 2003; Gupta and Larson, 1979; Haverkamp and Parlange, 1986; Johari et al., 2006; Mualem, 1984). Various Pedo-transfer Functions (PTF) have been proposed and developed. The success of each PTF depends on the correlation coefficient R^2, air-entry value and a maximum slope. Figures 2.15 to 2.17 compare the estimated SWCC from various researchers with the lab data presented in this thesis. The figures indicate a good relationship between the Fredlund-Wilson (2002) PTF and the lab data for coke and sand. All the estimations differ considerably from the MFT lab data. This might be due to the fine-grained nature of the MFT and extreme volume change in MFT which creates a significant distinction between the MFT and granular materials such as coke and sand. It appears that the models do not work properly for materials with water contents higher than their liquid limit.

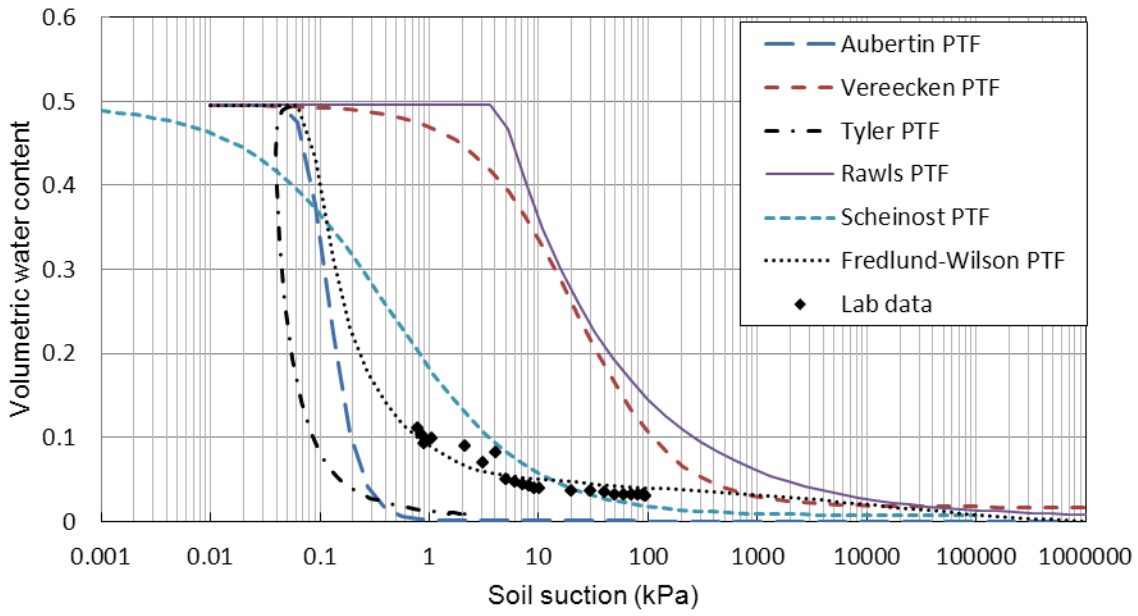

Figure 2.15: Various estimations of the SWCC for Suncor coke based on the particle size distribution

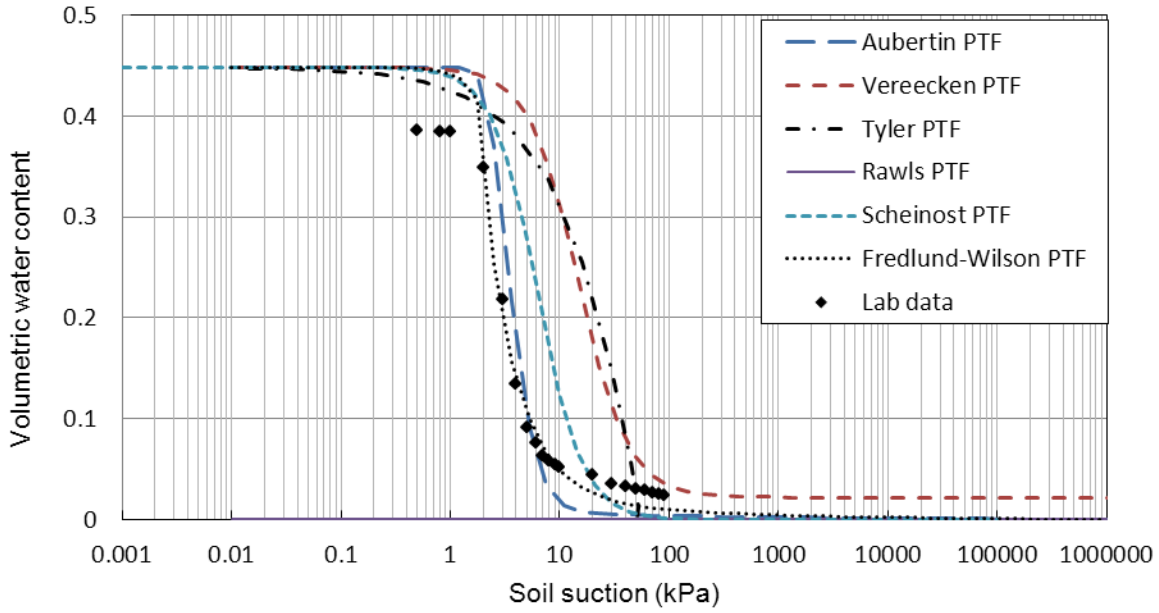

Figure 2.16: Various estimations of the SWCC for Suncor sand based on the particle size distribution

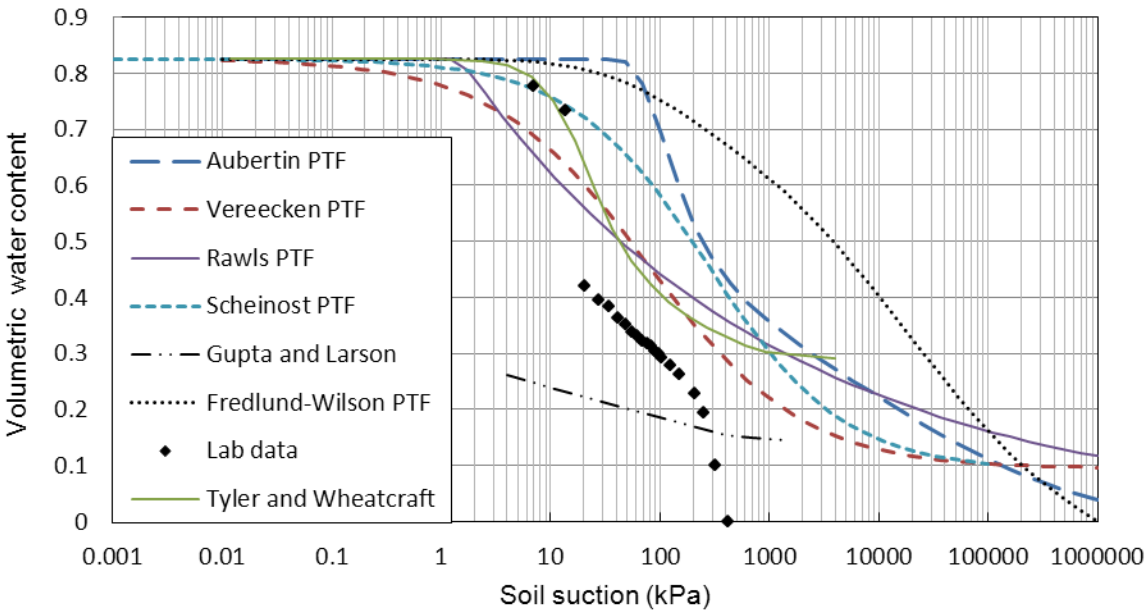

Figure 2.17: Various estimations of the SWCC for MFT based on the particle size distribution

2.5.4 Analysis of the wetting SWCC

The wetting SWCCs for Suncor coke and Suncor sand vary considerably. The major distinction is related to the significant difference in particle size distribution as shown in Figure 2.2. The fitting parameters for the wetting SWCC shown in Table 2.2 control the shape of the curve. The water-entry value is higher for a finer soil since the small pores are filled with water first. As a result, there is a close relationship between the soil particle distribution indicated by D_{10} and the water-entry value of the soil.

2.5.5 Hysteresis effect

The hysteresis in the wetting and drying curves implies different water content at a specific suction. The plots of drying and wetting SWCCs for both soils indicate a considerable hysteresis for each soil type. Few studies have been carried out to quantify hysteresis in soils; however it is evident that there is a relationship between

the hysteresis and D_{10}, suggesting a lower hysteresis for a small D_{10}. This relationship can be easily observed by comparing the D_{10} of Suncor coke and Suncor sand, which implies a higher hysteresis for the Suncor coke. There is a smaller hysteresis loop for uniform soil (Pham et al., 2003; Hogarth et al., 1988; Jaynes, 1984; Nimmo, 1992; Parlange, 1976).

2.5.6 Unsaturated permeability

Various researchers have tried to relate the SWCC of soil to the unsaturated coefficient of permeability. An indirect statistical method for determining unsaturated hydraulic conductivity, k of the materials was performed using the SoilVision Database System (SoilVision Systems Ltd., 1999). The SWCC and saturated permeability were incorporated into the model to derive the permeability functions of the soils. The equation is similar to the Fredlund and Xing (1994) and the fitting parameters are determined from the SWCC equation. Details of the procedures to obtain a relationship between the permeability function using the SWCC properties and saturated coefficient of permeability are described in Fredlund and Rahardjo (1993).

The statistical model has been found to yield a reasonable permeability function. The unsaturated hydraulic conductivities of Suncor coke and Suncor sand have been determined based on Fredlund-Xing (1994) and van Genuchten-Mualem (1980) equations and can be seen in Figures 2.18 and 2.19 (Fredlund et al., 1994; Laliberte et al., 1968; van Genuchten, 1980).

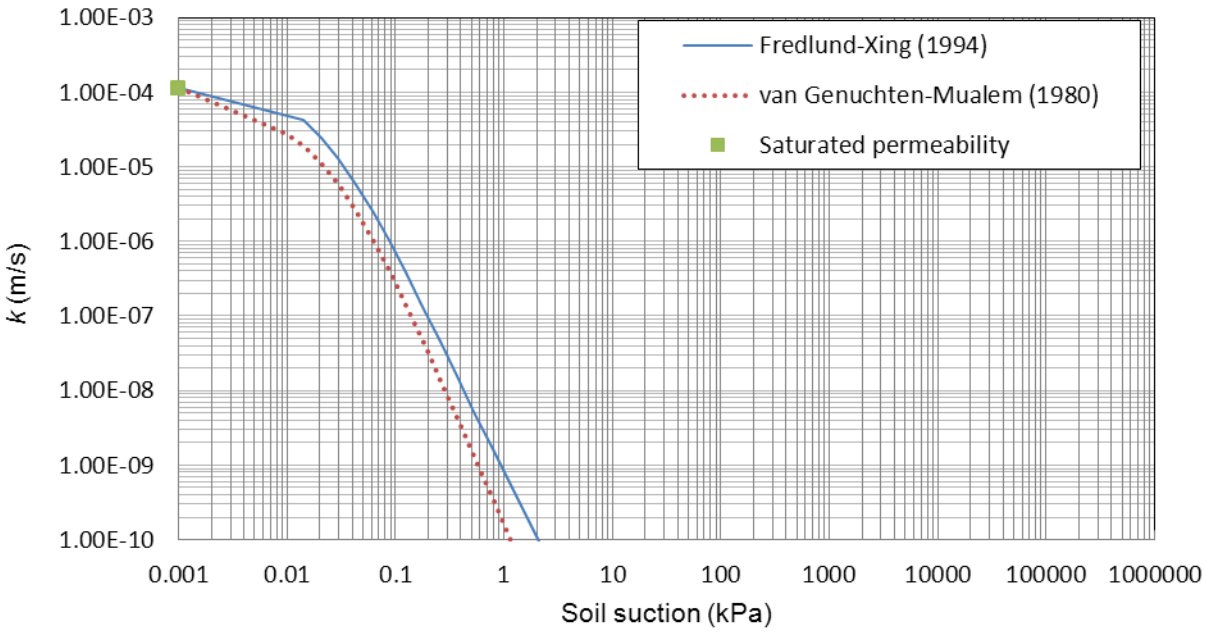

Figure 2.18: Unsaturated permeability function for Suncor coke

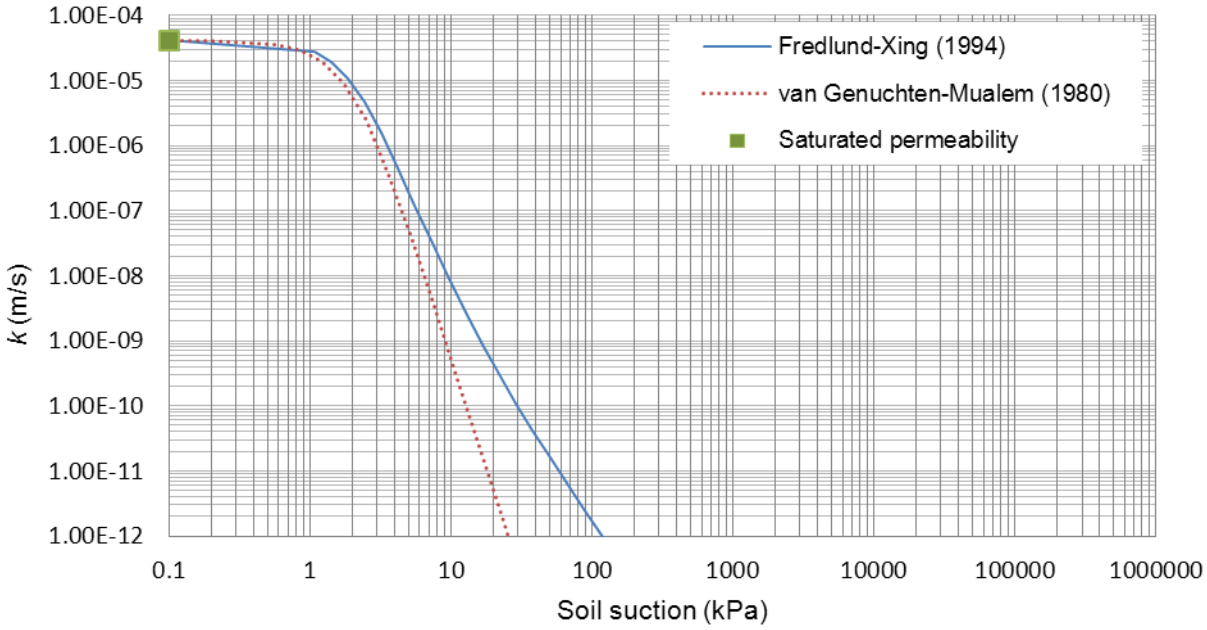

Figure 2.19: Unsaturated permeability function for Suncor sand

To determine the permeability function of MFT, the degree of saturation for the SWCC is calculated and plotted in Figure 2.20. It is observed in the graph that the actual air-entry value of MFT is approximately 2000 kPa, indicating that unlike the volumetric SWCC (Figure 2.9), the MFT will not desaturate until the soil suction exceeds 2000 kPa.

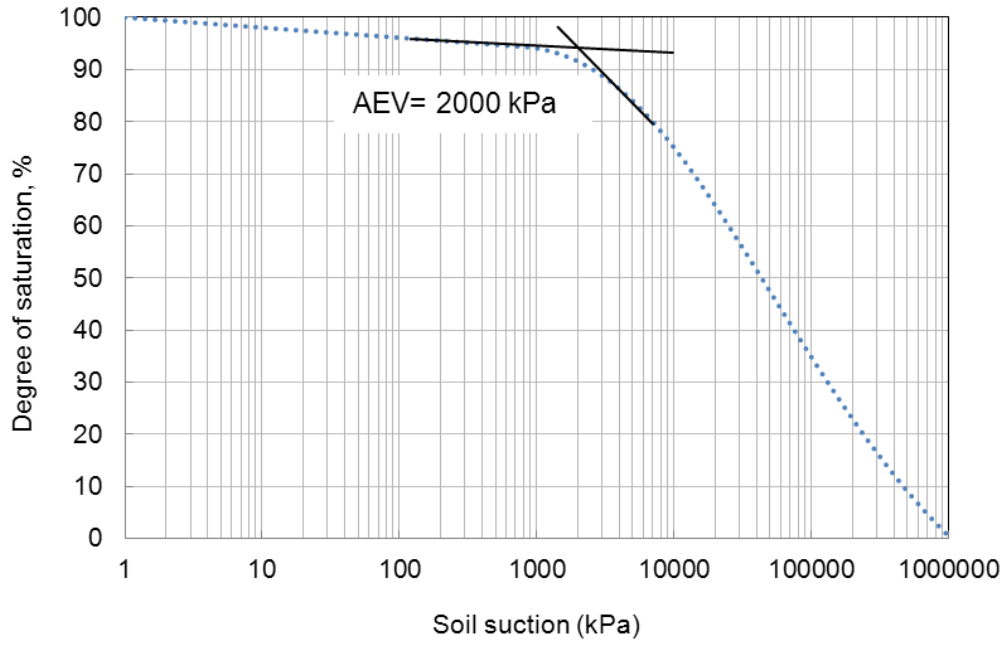

Figure 2.20: Degree of saturation of the SWCC for MFT

The results of a large-strain consolidation test were used to determine the saturated permeability function before the air-entry value of the MFT (Miller et al., 2010). The result of permeability versus effective stress is plotted in Figure 2.21. It should be noted that based on the principle of axis-translation, the effective stress and the soil suction can be used interchangeably, since the material remains saturated. The permeability function also agrees with the Kozeny-Carman relationship in which the saturated permeability is proportional to equation [2.4]:

$$k \propto \frac{e^3}{e+1} \qquad [2.4]$$

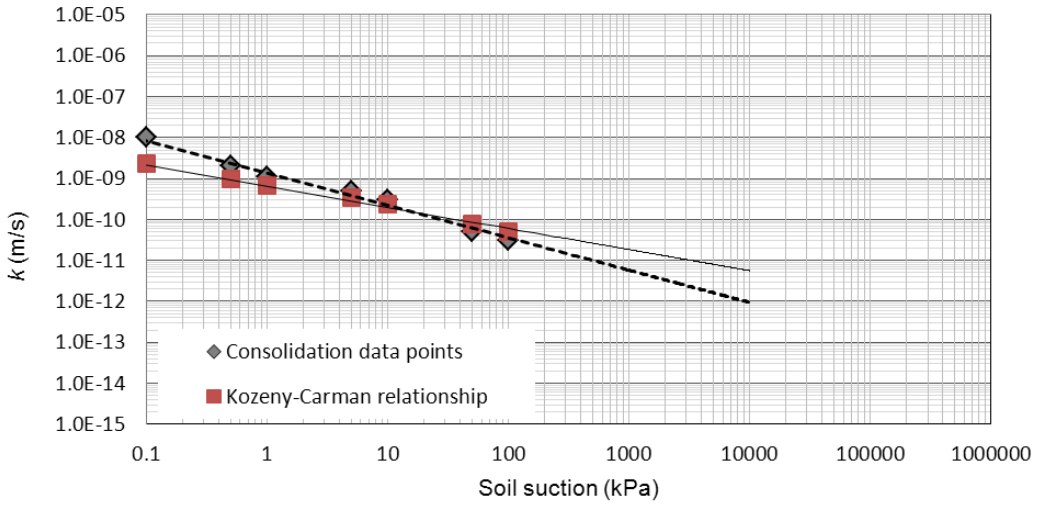

Figure 2.21: Saturated permeability function for the MFT based on a large-strain consolidation test (Miller et al., 2010)

The unsaturated permeability function for MFT is determined using the degree of saturation of the SWCC as input in the SoilVision Database System (SoilVision Systems Ltd., 1999), based on the same algorithm applied to Suncor coke and Suncor sand (Figure 2.22).

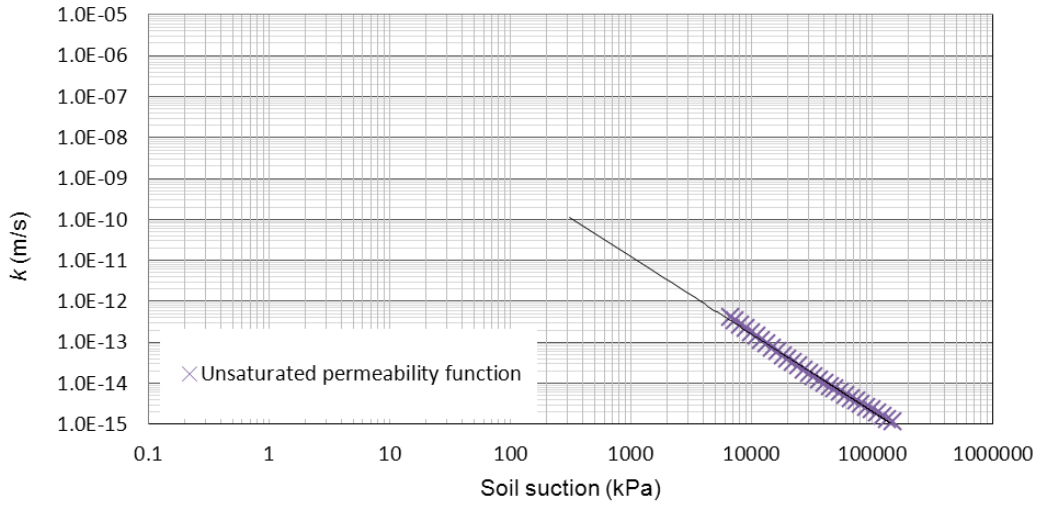

Figure 2.22: Unsaturated permeability function for MFT

The two figures combine to form the complete permeability function is shown in Figure 2.23, which demonstrates a bilinear relationship. The first part incorporates the saturated part where the volume of MFT decreases dramatically and the latter part provides the unsaturated permeability function of MFT as the soil suction exceeds the air-entry value.

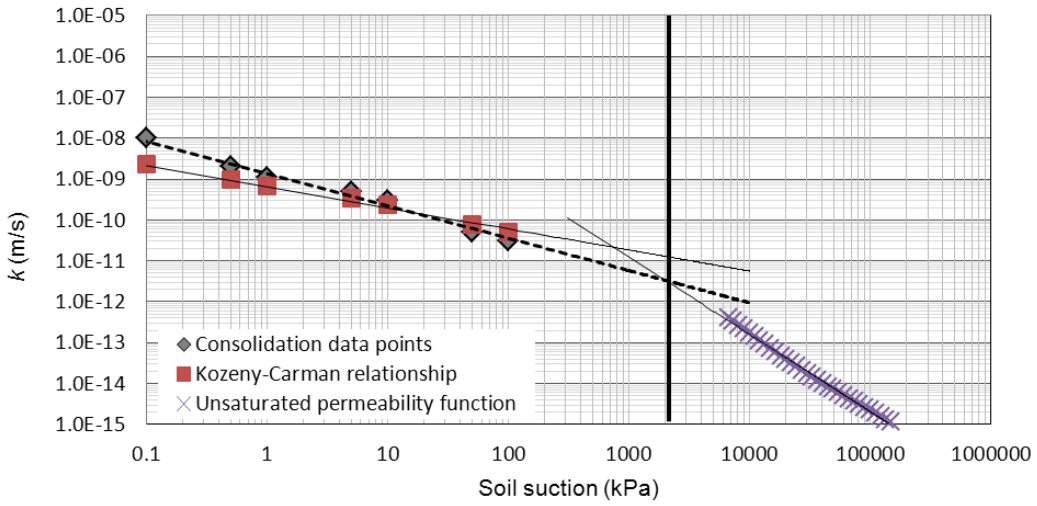

Figure 2,23: Bilinear permeability function of MFT

2.6 Summary and conclusion

The drying and wetting curves for Suncor sand and Suncor coke were experimentally measured. The results of soil-water characteristic curves (SWCC) were then best-fit with the Fredlund-Xing (1994) and van Genuchten (1980) models. The fitting parameters were correlated to the grain-size parameters. There is reasonable agreement between the fitting parameters and particle size distribution of soils. The results also show that coarser materials have a lower air-entry value, a lower residual suction and a lower water-entry value than fine-grained soil. The estimations are also consistent with the laboratory data, except for the MFT, which does not follow the data trend for coarse-grained materials. The unsaturated permeability functions were also estimated based on their SWCCs and the saturated permeabilities.

2.7 REFERENCES

Arya, L. M., and Paris, J. F. (1981). "Physicoempirical model to predict the soil moisture characteristic from particle-size distribution and bulk density data. *Soil Sci.Soc.Am.J.*, 45(6), 1023-1030.

ASTM. 1997*a*. Standard test method for particle size analysis of soils (D422-63). *In* 1997 Annual Book of ASTM Standards, Vol. 04.08. American Society for Testing and Materials (ASTM), Philadelphia, PA. pp. 10-16

ASTM. 1997*b*. Standard test method for specific gravity of soils (D854-92). *In* 1997 Annual Book of ASTM Standards, Vol. 04.08. American Society for Testing and Materials (ASTM), Philadelphia, PA. pp. 88-91.

ASTM. 1997*c*. Standard test method for amount of material in soils finer than the No. 200 (75 μm) sieve (D1140-92). *In* 1997 Annual Book of ASTM Standards, Vol. 04.08. American Society for Testing and Materials (ASTM), Philadelphia, PA. pp. 92-94.

ASTM. 1997*d*. Standard test method for capillary moisture relationships for coarse and medium textured soils by porous plate apparatus (D2325-68). *In* 1997 Annual Book of ASTM Standards, Vol. 04.08. American Society for Testing and Materials (ASTM), Philadelphia, PA. pp. 195-201.

ASTM. 1997*e*. Standard classification of soils for engineering purposes (unified soil classification system) (D2487-93). *In* 1997 Annual Book of ASTM Standards, Vol. 04.08. American Society for Testing and Materials (ASTM), Philadelphia, PA. pp. 217-227.

ASTM. 1997*f*. Standard test method for liquid limit, plastic limit, and plasticity index of soils (D4318-95). *In* 1997 Annual Book of ASTM Standards, Vol. 04.08. American Society for Testing and Materials (ASTM), Philadelphia, PA. pp. 522-532.

ASTM. 1998. Standard test method for shrinkage factors of soil by the mercury method (D 427-98). *In* 1998 Annual Book of ASTM Standards, Vol. 04.08 American Society for Testing and Materials (ASTM), West Conshohocken, PA (2003), pp. 22–25.

Aubertin, M., Mbonimpa, M., Bussiere, B., and Chapuis, R. P. (2003). "A model to predict the water retention curve from basic geotechnical properties." *Canadian Geotechnical Journal*, 40(6), 1104-1122.

Aubertin, M., Ricard, J. -., and Chapuis, R. P. (1998). "A predictive model for the water retention curve: application to tailings from hard-rock mines." *Canadian Geotechnical Journal*, 35(1), 55-69.

Barbour, S. L. (1998). "Nineteenth Canadian geotechnical colloquium: The soil-water characteristic curve: A historical perspective." *Canadian Geotechnical Journal,* 35(5), 873-894.

Fredlund, D.G., and Rahardjo, H. 1993a. Soil mechanics for unsaturated soils. John Wiley & Sons Inc., New York.

Fredlund, D. G., and Xing, A. (1994). "Equations for the soil-water characteristic curve." *Canadian Geotechnical Journal,* 31(4), 521-532.

Fredlund, D. G., Xing, A., and Huang, S. (1994). "Predicting the permeability function for unsaturated soils using the soil-water characteristic curve." *Canadian Geotechnical Journal,* 31(4), 533-546.

Fredlund, M. D., Wilson, G. W., and Fredlund, D. G. (2002). "Use of the grain-size distribution for estimation of the soil-water characteristic curve." *Canadian Geotechnical Journal,* 39(5), 1103-1117.

Gupta, S. C., and Larson, W. E. (1979). "Estimating soil water retention characteristics from particle size distribution, organic matter percent, and bulk density." *Water Resour.Res.,* 15(6), 1633-1635.

Haverkamp, R., and Parlange, J. -. (1986). "Predicting the water-retention curve from particle-size distribution: 1. Sandy soils without organic matter." *Soil Sci.,* 142(6), 325-345.

Hogarth, W. L., Hopmans, J., Parlange, J. -., and Haverkamp, R. (1988). "Application of a simple soil-water hysteresis model." *Journal of Hydrology,* 98(1-2), 21-29.

Jaynes, D. B. (1984). "Comparison of soil-water hysteresis models." *Journal of Hydrology,* 75(1-4), 287-299.

Johari, A., Habibagahi, G., and Ghahramani, A. (2006). "Prediction of soil-water characteristic curve using genetic programming." *J.Geotech.Geoenviron.Eng.,* 132(5), 661-665.

Leong, E. C., and Rahardjo, H. (1997). "Review of soil-water characteristic curve equations." *J.Geotech.Geoenviron.Eng.,* 123(12), 1106-1117.

Miller, W. G., Scott, J. D., and Sego, D. C. (2010c). "Effect of extraction water chemistry on the consolidation of oil sands fine tailings." CIM Journal, 1(2), 113-129.

Mualem, Y. (1984). "Prediction of the Soil Boundary Wetting Curve." *Soil Sci.,* 137(6),.

Mualem, Y. (1977). "Extension of the similarity hypothesis used for modeling the soil water characteristics." *Water Resour.Res.,* 13(4), 773-780.

Nimmo, J.R. (1992): "Semiempirical model of soil water hysteresis." Soil Sci. Soc. Am. J. 56, 1723-1730.

Pham, H. Q., Fredlund, D. G., and Barbour, S. L. (2003). "A practical hysteresis model for the soil-water characteristic curve for soils with negligible volume change." *Geotechnique*, 53(2), 293-298.

Rossi, C., and Nimmo, J. R. (1994). "Modeling of soil water retention from saturation to oven dryness." *Water Resour.Res.,* 30(3), 701-708.

SoilVision Systems Ltd. 1999. SoilVision: a knowledge-based database system for unsaturated–saturated soil properties (computer program), version 2.0. SoilVision Systems Ltd., Saskatoon, Sask.

van Genuchten, M. T. (1980). "Closed-form equation for predicting the hydraulic conductivity of unsaturated soils." *Soil Sci.Soc.Am.J.*, 44(5), 892-898.

Vanapalli, S. K., Fredlund, D. G., Pufahl, D. E., and Clifton, A. W. (1996). "Model for the prediction of shear strength with respect to soil suction." *Canadian Geotechnical Journal,* 33(3), 379-392.

Yang, H., Rahardjo, H., Leong, E., and Fredlund, D. G. (2004). "Factors affecting drying and wetting soil-water characteristic curves of sandy soils." *Canadian Geotechnical Journal,* 41(5), 908-920.

Chapter 3 Time Domain Reflectometry measurement of soil water content and electrical conductivity of MFT, Suncor sand and Suncor coke

3.1 Introduction

A new consolidation technique is proposed to investigate stabilization of the oil sands fine tailings. This technique involves placing a layer of saturated coke on top of the Mature Fine Tailings (MFT) layer followed by another layer of uniformly distributed sand. Applying suction to the coke layer desaturates the coke layer. Monitoring upward flow of pore-water from the MFT layer into the coke layer indicates the start of consolidation of the tailings. This technique is experimentally tested in a large scale column test. As the column is loaded with test materials, instruments measure and monitor the consolidation behavior. Preliminary evaluation tests were conducted to identify the five parameters to be measured in the instrumented column container Instrumentation was selected based on the ability of the gauges to measure the required soil parameters, both in terms of magnitude and frequency. Matric suction and settlement are measured by the jetfill tensiometers and settlement plates mounted in different elevations of the column, respectively. Pore pressure dissipation is measured using the strain gauge piezometers. TDR moisture probes are used to simultaneously measure the water content and electrical conductivity of the MFT, Suncor coke and Suncor sand as the consolidation proceeds.

Time Domain Reflectometry, TDR, is a nondestructive method that has the potential to provide the required soil parameter measurements. The TDR technology can be fully automated for taking readings both for field and laboratory scale research with minimal disturbance of the soil (Drungil et al., 1989). The system has a high portability and safety.

Differences in the amount of water in soil materials make the dielectric constant dependent on its water content (Siddiqui et al., 2000). Fellner-Feldegg (1970) used the TDR method to measure the electrical properties of materials. About ten years later, Topp (1980) extended this method to measure the volumetric water content in coaxial sample holders (Topp et al., 1980). With the aid of appropriate calibrations, the dielectric conductivity can be related to the volumetric water content and the bulk soil electrical conductivity can be related to the electrical conductivity of the pore-water solution (Nichol et al., 2003). The apparent dielectric permittivity is the real component of the complex valued dielectric permittivity which is frequency dependent (Nichol et al., 2003).

The objective of this paper is to describe the steps followed to relate TDR measurements and dielectric properties of MFT, Suncor coke and Suncor sand to the volumetric water content and electrical conductivity. The water content of the materials varied from saturation (33% solids content) to completely dry conditions.

3.2 Theory

A TDR instrument is an electronic device that propagates a short rise time electromagnetic pulse through a coaxial cable to a probe. The probe is a wave guide extension on the end of coaxial cable. TDR probes are inserted or buried in the medium to measure the dielectric constant that allows the water content and electrical conductivity to be determined. If the conductor has no impedance, the entire transmitted pulse will be absorbed and no signal is reflected back towards the TDR. The reflection from the waveguide takes place where impedance changes causing some of the incident signal to reflect to the source. The impedance is related to the geometrical configuration of the probe and is inversely related to the dielectric constant of the surrounding material in the medium. Figure 3.1 illustrates the components of a TDR system. The application of TDR in measuring soil water content and permittivity is based on the velocity of the pulse which travels along a transmission line buried in the material being measured. Change in volumetric water content can readily change the dielectric properties. Change in properties are realized as a change in probe impedance which affects the shape of the reflection and leads to an evaluation of the water content and soil electrical conductivity (Siddiqui et al., 2000). A representative waveform is illustrated in Figure 3.2.

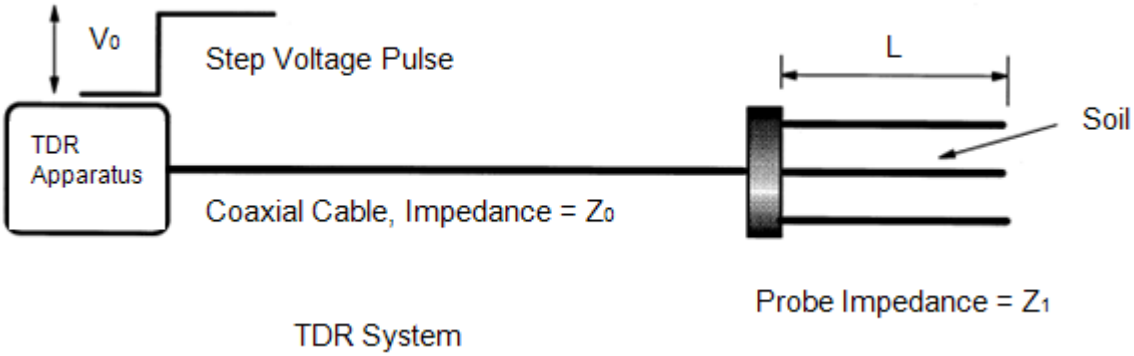

Figure 3.1. A TDR system is composed of a pulse generator, a sampler, an oscilloscope, a coaxial cable, a shielded two wire transmission cable and three parallel metal rods which are inserted in the material (after Pettinelli et al., 2002).

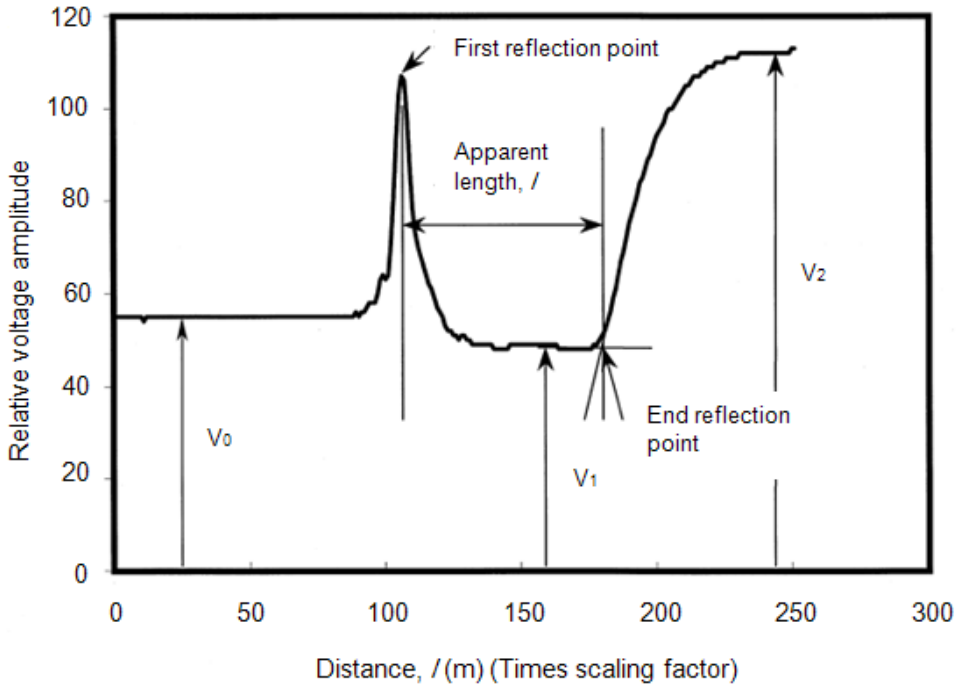

Figure 3.2. A typical TDR waveform (after Siddiqui et al., 2000).

Two well-known techniques are used to determine the dielectric constant of the medium from the waveform. The dual tangent method determines the time that the waveform is deflected by the arrival of energy from the probe head and probe end reflections. The first tangent is the predeflection waveform while the second one is the falling limb of the waveform deflection. The time at the intercept of the predeflection and postelection lines are referred to as the arrival time of the reflected pulse energy (Topp et al., 1980). The waveform can be strongly influenced by the probe dimensions and size of the sample.

If the ion concentration of the medium surrounding the probe is higher than a certain value, tangent lines cannot be accurately fitted to the waveform (Nichol et al., 2003). To improve the waveform interpretation a new technique was devised by Hook (1992) using remotely shorted diodes that provide improved estimates of pulse travel time and eventually more precise determination of moisture content (Hook et al., 1992). The travel waves when using this technique are selectively diverted from the conductor to the ground conductors by positive intrinsic negative diodes. Travel times to the probe head and end are estimated from the arrival of the diverted signal by tangent line analysis of the difference waveform (Hook et al., 1992). In this technique, soil electrical conductivity is obtained from the reflected waveforms by analyzing the change in the voltage signal with travel time.

3.2.1 Determination of soil moisture content

Topp et al., (1980) reported a strong relationship between the dielectric constant of the soil and the volumetric water content for a wide range of soils (Equation 3.1). Other studies also confirmed Topp equation (Dalton and van Genuchten 1986; Zegelin et al., 1989; Heimovaara et al., 1996; Or and Wraith, 1999). The TDR method was also used for measuring the volumetric water content of unsaturated soils. A wide range of soils were tested and the results showed a strong relationship between volumetric water content and dielectric constant.

$$\theta_v = -0.053 + 0.029K_a - (5.5\times10^{-4})K_a^{\,2} + (4.3\times10^{-6})K_a^{\,3} \qquad [3.1]$$

where θ_v is the volumetric water content and K_a is the apparent dielectric constant of the soil.

Topp equation (Topp et al., 1980) has been shown to not provide accurate results for highly plastic clays, organic soils and soils with high or low densities (Siddiqui et al., 2000). Alternative equations to incorporate low bulk density, large porosity and specific surface have also been developed (Noborio, 2001).

Hook et al., (1992) found that there is a linear relationship between the volumetric water content and T/T_{air} ratio:

$$\theta_v = (T/T_{air} - T_s/T_{air})(\varepsilon_w^{\,0.5} - 1) \qquad [3.2]$$

where T, T_{air} and T_s are the travel time of the pulse in soil, oven dried soil and in air respectively and ε_w is equal to 80.362 at 20^0C.

Alharthi et al., (1987) showed that a linear relation exists between $K^{0.5}$ and volumetric water content.

Malicki et al., (1996) proposed a new equation incorporating the bulk density of the soil ρ_b:

$$\theta_v = \frac{K_a{}^{0.5} - 0.819 - 0.168\rho_b - 0.159\rho_b}{7.17 + 1.18\rho_b} \quad [3.3]$$

Hu et al., (2010) established a quadratic equation between $\sqrt{K_a}$ and θ_w for expansive soils:

$$\sqrt{K_a} = a_2 + b_2\theta_w + c_2\theta_w{}^2 \quad [3.4]$$

where a_2, b_2 and c_2 are constants determined through a fitting procedure.

3.2.2 Electrical conductivity measurement

Soil electrical conductivity can be obtained from TDR waveforms by analyzing the change in voltage signal from the probe reflections with respect to travel time (Noborio, 2001). The attenuation of the voltage is due to the concentration of the ions which is used to determine soil electrical conductivity. The electrical conductivity of the soil depends upon a constant to account for the probe geometry, often referred to as K_p.

The most commonly used equation to calculate the electrical conductivity of materials is the Giese-Tiemann method presented by Topp et al., (1988).

$$EC_{G-T} = \left(\frac{K_p}{Z_u}\right)\left(\frac{1-\rho_\infty}{1+\rho_\infty}\right) \quad [3.5]$$

where K_p is the geometric constant of the probe, Z_u is the characteristic impedance of the cable and ρ_∞ is the reflection coefficient at a distant point.

3.3 Testing materials and facilities

3.3.1 Mature Fine Tailings, Suncor coke and Suncor sand

Approximately 400 liters of Suncor mature fine tailings (MFT), Suncor coke and Suncor sand were shipped from the site in Fort McMurray, Alberta to the University of Alberta Geotechnical Laboratory, Edmonton. The basic geotechnical parameters of the materials are summarized in Table 2.1. ASTM D854-92 (ASTM 1997*b*); ASTM D422-63 (ASTM 1997*a*); ASTM D1140-92 (ASTM 1997*c*); ASTM D4318-95 (ASTM 1997*f*); ASTM D2487-93 (ASTM 1997*e*). Grain size distribution for Suncor sand, Suncor coke and MFT are shown in Figure 2.3.

3.3.2 TDR instrument and probes

Twelve three-rod TDR moisture probes referred to as CS640 manufactured by Campbell Scientific Canada Corporation were used in this study. Figure 3.3 shows a CS640 TDR probe. Table 3.2 presents the specifications of the TDR probe used in the experiments.

Table 3.2. Specifications of the TDR probe.

CS640	
Rod exposed length (mm)	75
Cable Length (m)	9.14
Probe constant, *Kp*	6.4
Rod spacing, (mm)	3.0
Probe offset	0.035

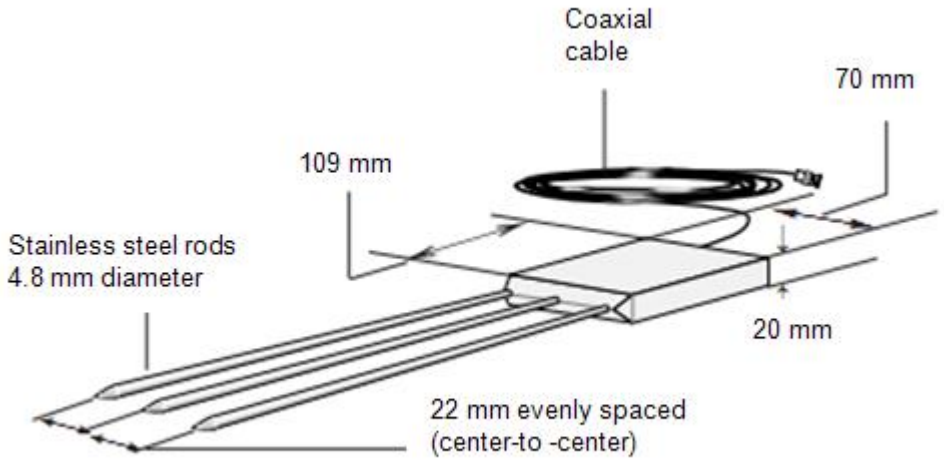

Figure 3.3. Illustration of components of a TDR probe (after Campbell Scientific Canada Corporation).

3.3.3 Data acquisition system

The experimental data of TDR probes were logged on a personal computer running the PCTDR software using a data acquisition board (CR1000) to which all TDR's were connected. Hardware used for data collection includes: (a) TDR100, (b) Two 8 Channel Multiplexers, (c) a power supply, (d) a data logger CR1000 used for data collection, (e) PVC casings and (f) a frame to hold the flexible cables in a consistent shape. Figure 3.4 illustrates the various electronic pieces used as the data acquisition system. The data logger was connected to the computer through an RS232 port to log the data.

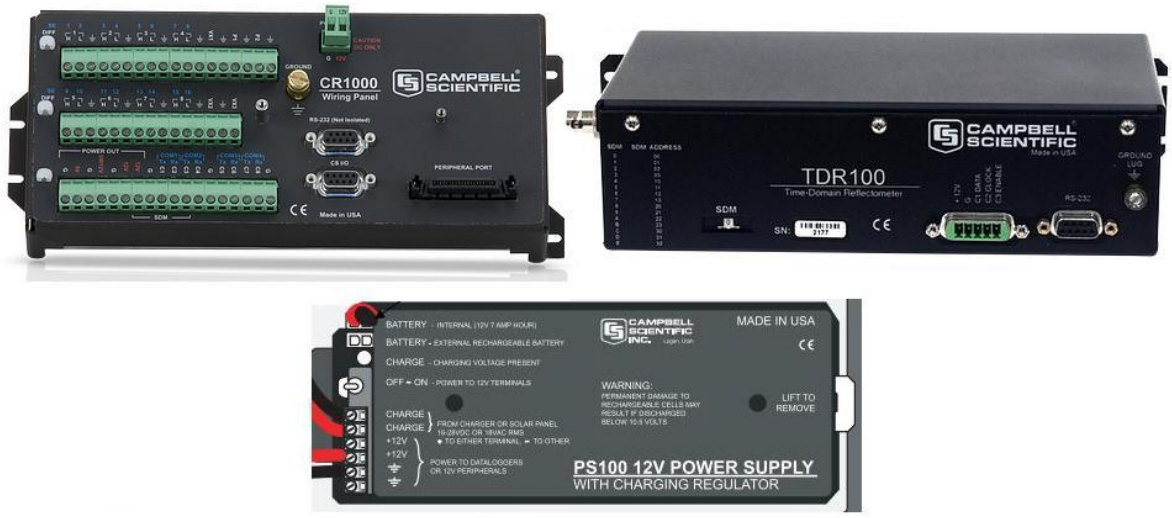

Figure 3.4. Illustration of the data logger CR1000 (top left), TDR100 (top right) and the power supply (bottom).

3.4 Experimental calibration and validation approach

TDR waveforms were collected using the probes with three rod. The raw scan TDR waveforms with 2001 points in time were collected manually using the PCTDR program for detailed waveform analysis. For the remainder of the test, automated readings were taken using a CR1000 data logger connected to a PC running the PC400 program using the dual tangent method. Laboratory calibration work was conducted using 10 m coaxial cables to connect the probe to the TDR100. The exposed metal rods of each TDR probe were immersed in the material to be tested. A probe offset was used to correct for part of the probe which was surrounded by the probe head material. The probes were immersed in both conductive and nonconductive media.

Suncor sand and Suncor coke were placed loosely in PVC containers and saturated with tap water prior to calibration. The container had a cross-section of 350 by 200 mm, which was sufficient to contain the majority of the wave energy of the pulse. The soil surrounding the rods was not compacted since any compaction might leave air voids in the area adjacent to the rods which can produce errors in the readings. TDR measurements were taken from twelve probes at the depths of 100 mm which completely covered the probes. Thirty different measurements were taken using each probe as the material dried. The measured water content was defined as the average of the water content over the length of the probe rods. If any part of the probe was exposed to air the probe would not be able to transform the waveform correctly and the accuracy of the measurements would have been diminished.

After each reading, one sample was taken for oven-dry measurement of water content and the material was allowed to dry for a few hours through evaporation. Before each measurement the soil was mixed thoroughly to homogenize the water content in the soil. This procedure was repeated to the end of the experiment where the soil was almost completely dry. To ensure that no significant temperature variation took place to alter the soil dielectric properties all the measurements were taken at the room temperature (15 ^{0}C to 25 ^{0}C). Figure 3.5 presents the set-up of the calibration of TDR measurements in MFT.

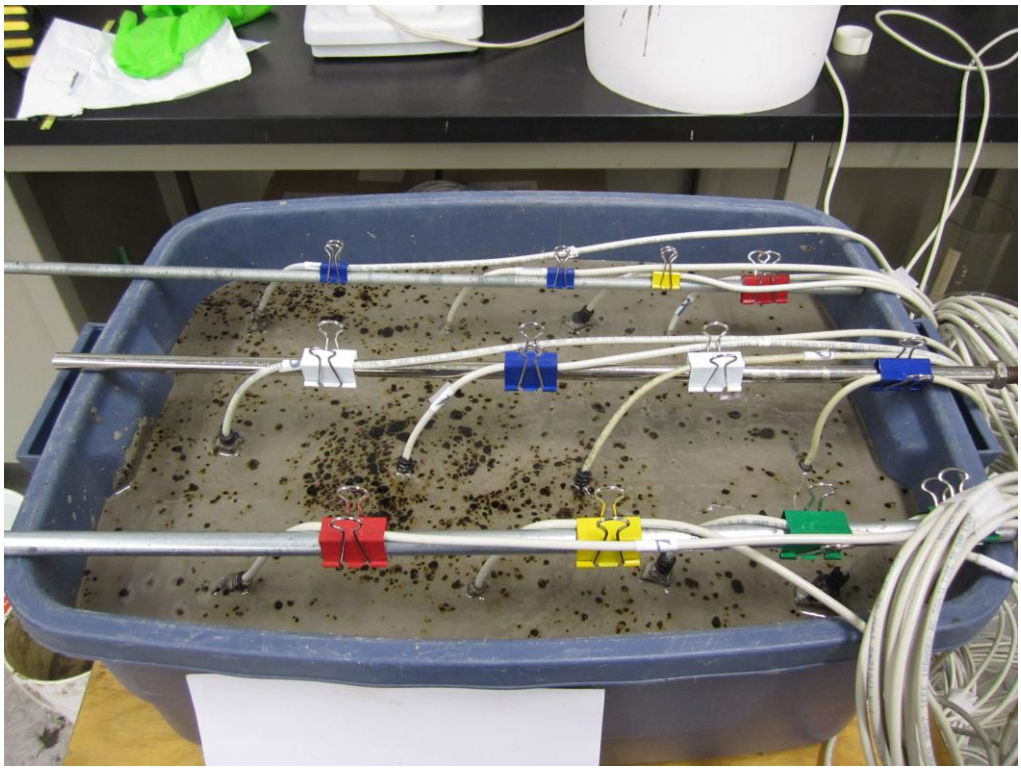

Figure 3.5. Calibration set up for TDR readings in MFT.

3.5 Results and discussions

3.5.1 Raw wave scans of TDR

Various waveforms were collected as the MFT dried (Figure 3.6). The distinction between the post-deflection and pre-deflection points was used by the PCTDR program to determine the dielectric constant. The post-deflection and the pre-deflection points of the waves were significantly different. This distinction was used to determine the apparent length (the distance between the pre and post deflection) and provide an indication of different water content. The results showed that dielectric constant increases with water content. The raw waveforms in Suncor coke and Suncor sand are also presented in Figures 3.7 and 3.8 respectively, which showed a significant distortion of waveforms for coke and sand. The waves reached a plateau within the first two meters. Each plateau represents a different electrical conductivity.

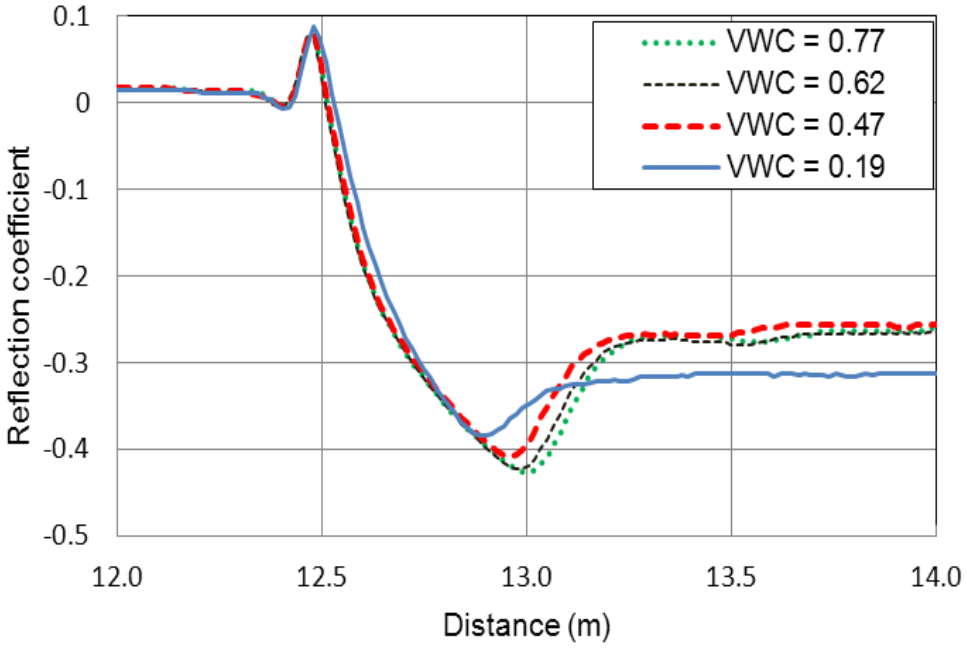

Figure 3.6. The raw scans of waveforms in MFT at various water contents.

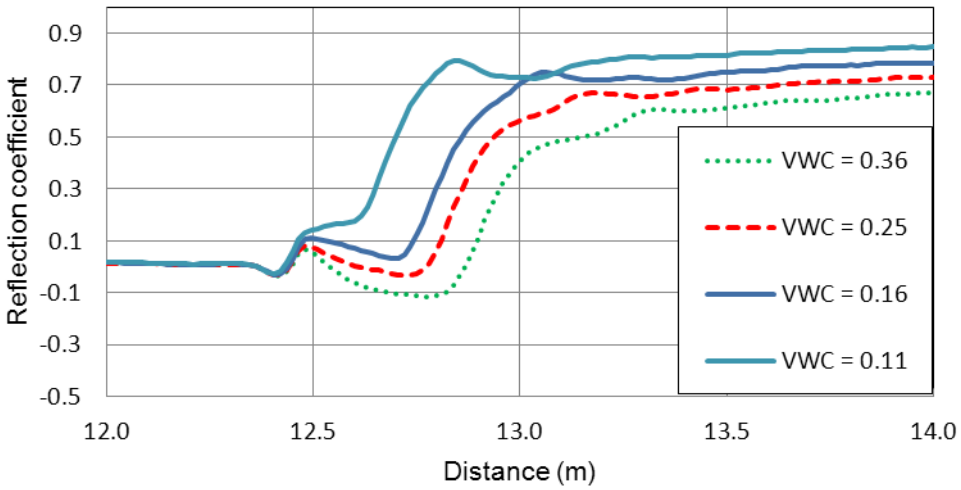

Figure 3.7. The waveforms in Suncor sand at various water contents.

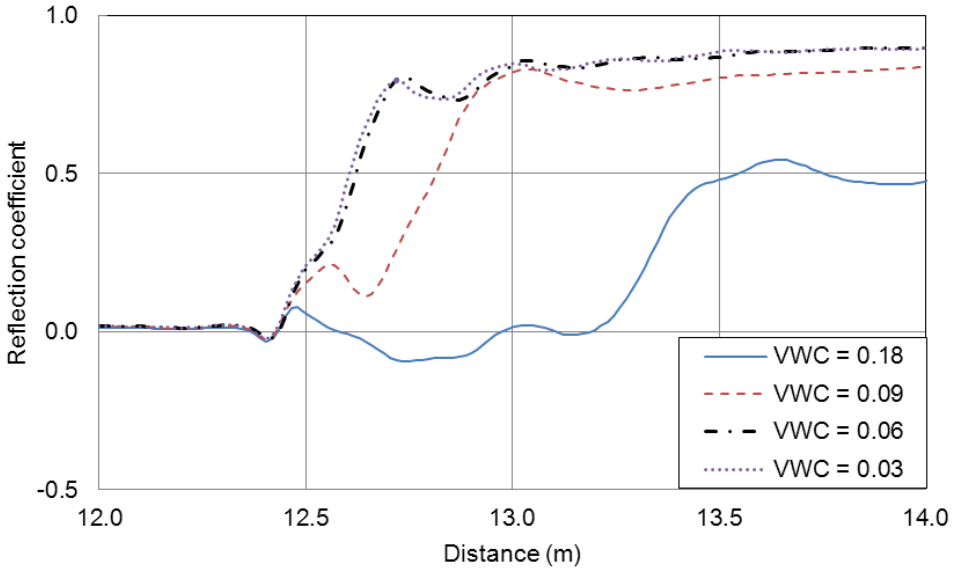

Figure 3.8. The waveforms in Suncor coke at various volumetric water contents.

3.5.2 Volumetric water content versus the apparent length

Topp formulation (Topp et al., 1980) was used in examing the three types of materials. Figure 3.9 presents TDR readings using Topp universal equation (Topp et al., 1980) versus the oven-dry volumetric water content. A slope far from 1 and a non-zero intercept indicates a weak correlation with Topp equation (Topp et al., 1980). It can be seen in this figure 3.9 that the Topp equation (Topp et al., 1980) yields good reuslts for the Suncor sand but does not lead to sufficiently accurate results for MFT and Suncor coke. The results emphasize the need for new calibration of the probes for use in MFT and Suncor coke. Due to hydrophobic property of Suncor coke, only three data points were obtained as the coke particles dry.

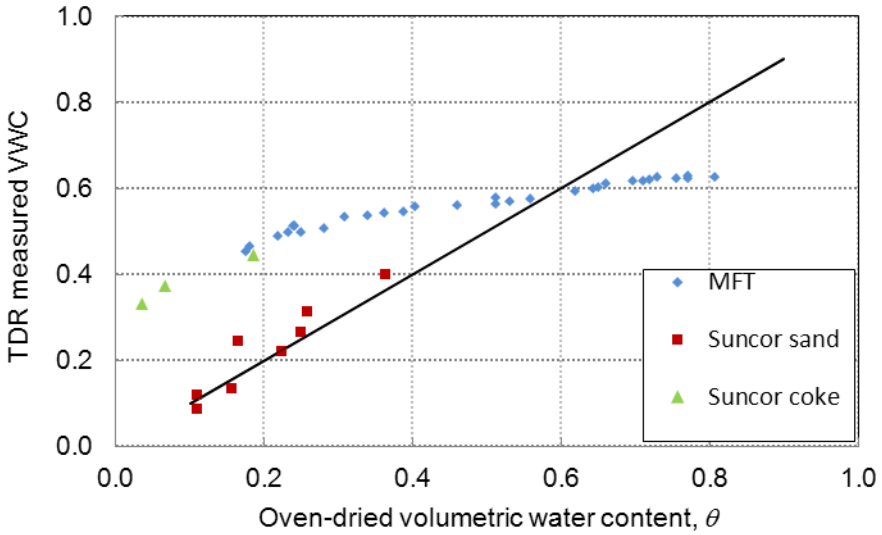

Figure 3.9. The TDR measurement versus oven dry volumetric water content.

3.5.3 Dielectric constant versus volumetric water content

Values of the dielectric constant were plotted against the oven-dried volumetric water content, θ. For comparison, Topp equation (Topp et al., 1980) within a 25% margin range has been presented in Figure 3.10. It can be seen that approximately 50% of the MFT readings fall outside of the 25% margin on either side of the Topp equation. The Suncor sand and Suncor coke readings are also outside the range of Topp equation, indicating the poor functionality of Topp equation to predict the water content of MFT, Suncor coke and Suncor sand.

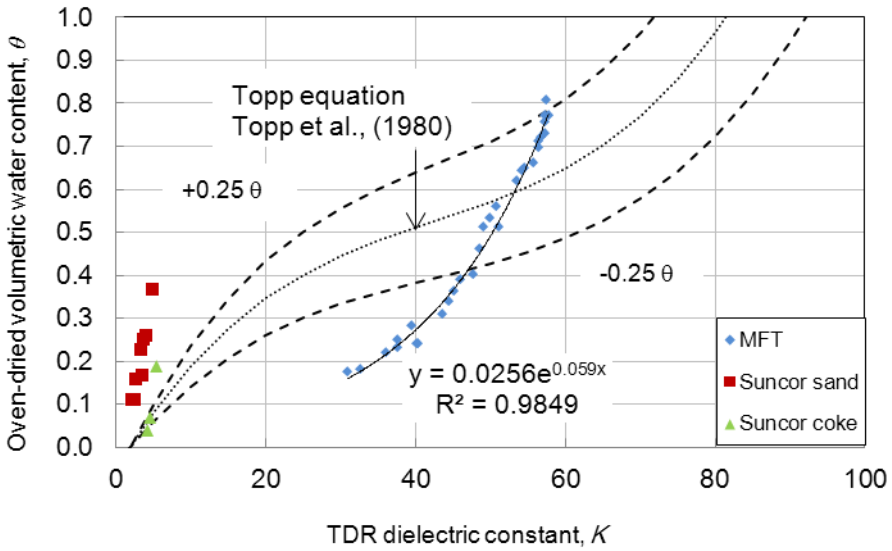

Figure 3.10. The volumetric water content versus the dielectric constant.

Figure 3.11 presents a data set of $\sqrt{K}$ values plotted against volumetric water content, θ. The results are similar to the results presented by other researchers (Siddiqui et al., 2000; Alharthi et al., 1987; Ledieu et al., 1986). An essentially linear relationship was observed for all three materials.

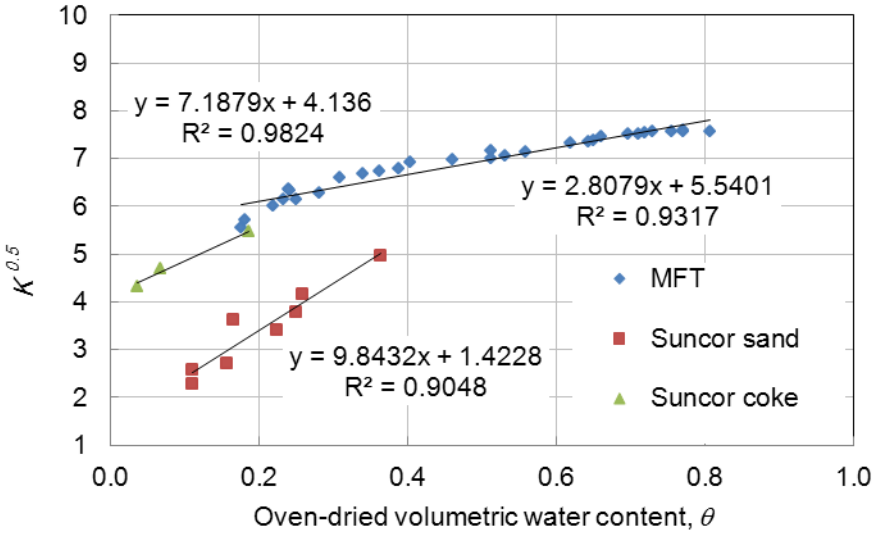

Figure 3.11. The square root of dielectric constant versus volumetric water content.

It has been shown by some authors that the density of soil affects the empirical $K^{0.5}$ versus θ relationship (Siddiqui et al., 2000). To find a relation that is less sensitive to dry density the combined variables $[K^{0.5}\rho_w/\rho_d]$ are plotted versus gravimetric water content. The results presented by Siddiqui et al., (2000) show a similar relationship. Figure 3.12 shows that, $[K^{0.5}\rho_w/\rho_d]$ yields a slightly more linear relationship than the $K^{0.5}$ versus θ.

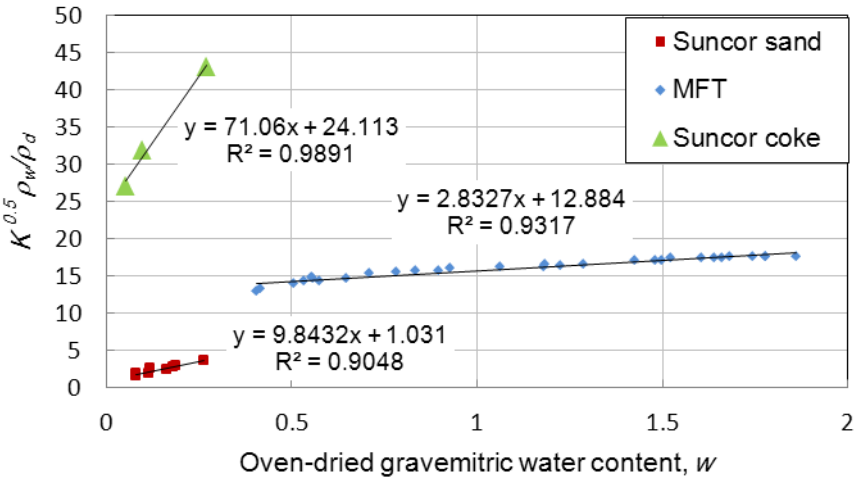

Figure 3.12. The square root of dielectric constant versus the gravimetric water content.

3.5.4 Effect of sample size

The sensitivity of dielectric constant to sample sizes was examined by using three containers of different diameters to ensure the validity of the results. This experiment was only conducted on dry Suncor sand. Three measurements of dielectric constant were taken. Figure 3.13 shows that the dielectric constants were the same, indicating that the container size does not impact the measured dielectric properties.

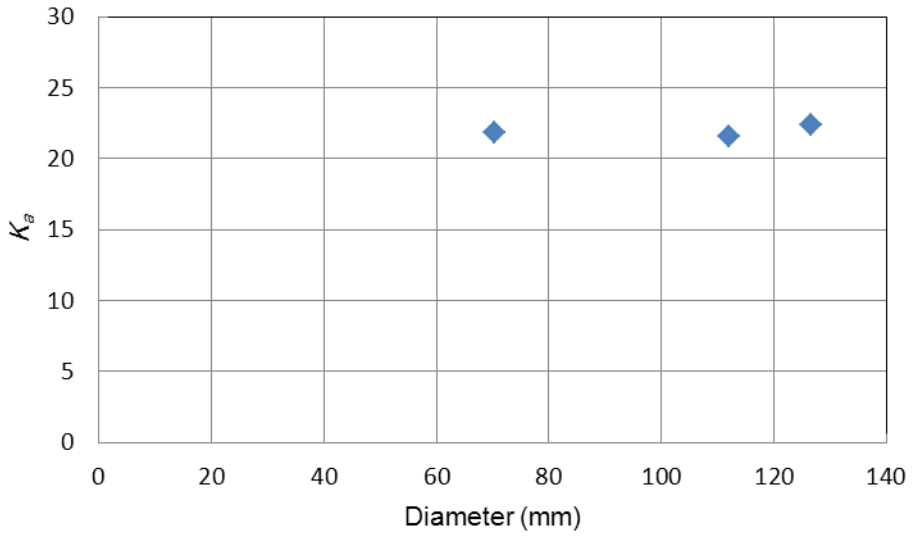

Figure 3.13. The plot of sample size with the dielectric constant of dry Suncor sand.

3.5.5 Effect of density

The effect of the relative density of the material on the dielectric constant was examined by measuring the dielectric constant of four different samples with distinct densities. The results of this experiment was limited to dry Suncor sand. Dry Suncor sand was poured in a container having a diameter of 70 mm and a height of 200 mm. A density of 1.42 g/cm^3 was obtained. Once the first reading is taken the sample is compacted to reach the second density. The process was repeated for the four denisties. Figure 3.14 presents the plot of dielectric constant versus dry density of the Suncor sand samples. Figure 3.14 shows that the variation in density does not have any considerable effect on dielectric constant of the sand.

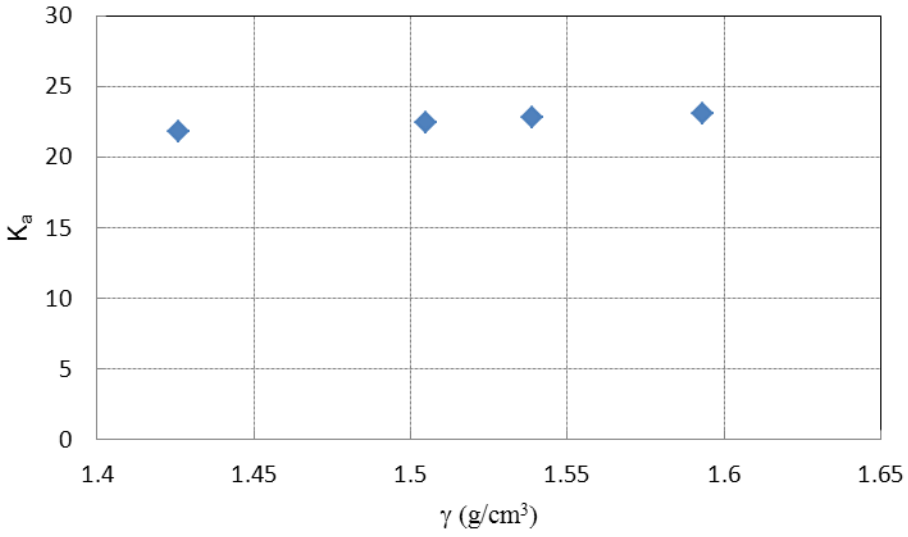

Figure 3.14. The plot of dry density versus the dielectric constant of dry Suncor sand.

3.5.6 Electrical conductivity measurements

Signal loss of electrical waves during TDR measurements are used to determine the electrical conductivity of soils. The experiments are limited to distilled water and MFT. The electrical conductivity of distilled water and MFT are determined to validate the TDR results. The measurements were based on Gies-Tiemann method (Equation 3.5). The raw waveform in distilled water, air and MFT has been presented in Figure 3.15. The picture shows that the reflection coefficient approaches 1.0 as the distance increases, indicative of zero conductivity. The reflection coefficient at infinity, ρ_∞ approaches -0.24 which yields a value of 0.25 *S/m* for the electrical conductivity of MFT.

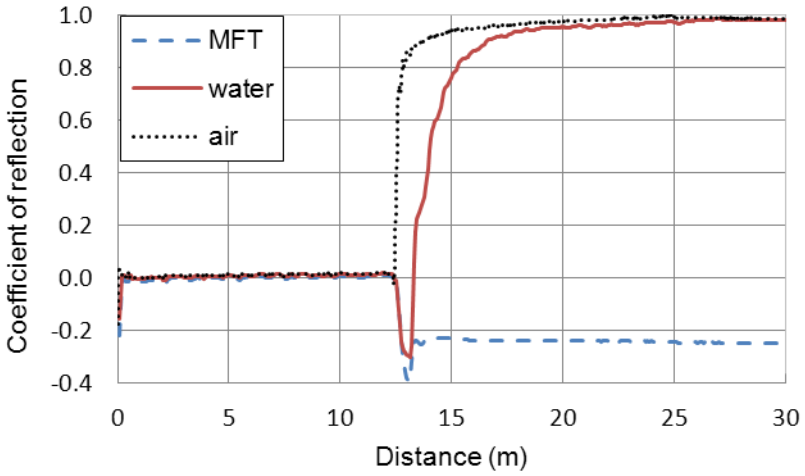

Figure 3.15. The raw scan of the waveform in MFT, distilled water and air.

The electrical conductivity of distilled water and MFT was determined based on Gies-Tiemann method. The geometric constant 6.40 used in Equation [3.5] to determine the electrical conductivity, was provided by the manufacturer (Campbell Scientific Canada Corporation). The actual electrical conductivity of distilled water and MFT was determined using a conductivity meter (Fisher Scientific Accumet Excel XL20) and compared with the TDR results in Figure 3.16. This figure shows a good agreement between the two techniques ensuring the reliability of the TDR method to determine the electrical conductivity of soils.

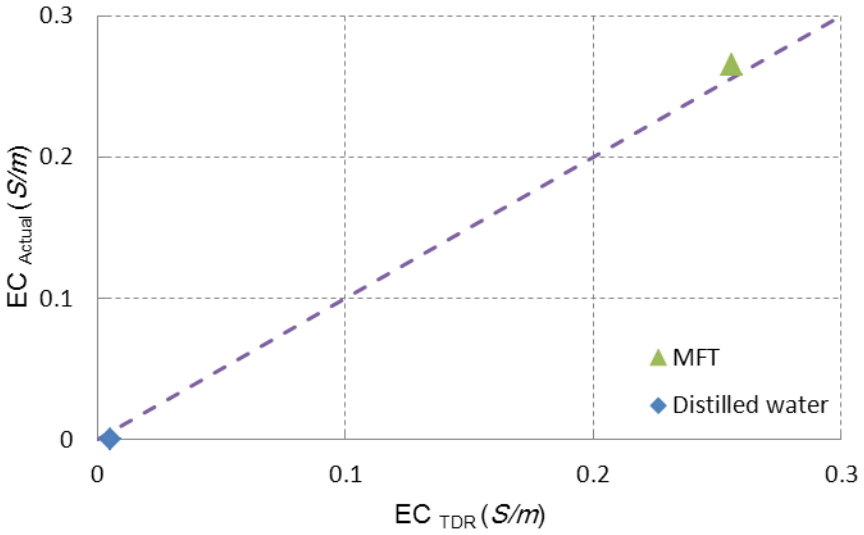

Figure 3.16. The relationship between the TDR-measured electrical conductivity and the actual electrical conductivity.

3.5.7 Distortion of the wave

The water content measurement is based on the evaluation of a pulse reflection from the TDR probe. The pulse and the reflections are prone to distortions during the travel between the TDR100 and the TDR probe. The cable connecting the probe to the reflectometer has characteristic impedance that has both resistive and reactive components. Distortion of the waveform can introduce errors into the system. Figure 3.17 illustrates waveforms gathered from a 3-rod probe for two low water content samples in coke. This study shows the distortion intensifies as the sample becomes completely dry. Thus it is concluded that care must be taken to correctly interpret the results when there is very low water content.

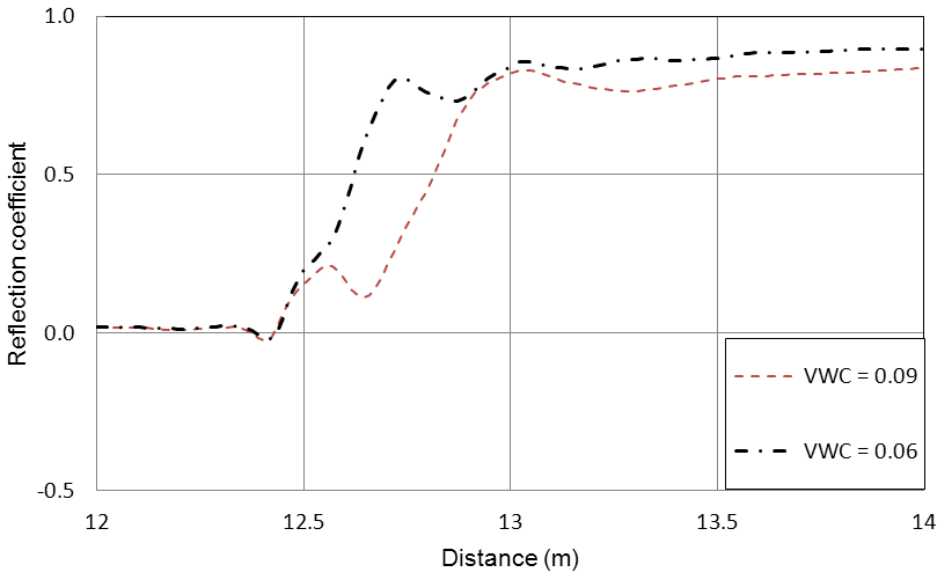

Figure 3.17. The distortion of the waves at low water contents.

3.6 Summary and conclusions

An approach has been developed in this paper to use TDR measurements to estimate water content and electrical conductivity of MFT, Suncor sand and Suncor coke. The different elements of the TDR system are explained for use in measuring soil water content and electrical conductivity. Experimental data were used to compare various types of calibration formulations. It was found that Topp equation (Topp et al., 1980) does not yield reliable results, requiring a new set of equations for each material. It was also found that a linear equation exists between the square root of the dielectric constant, $K^{0.5}$ and θ. It is also shown that small variations in the density and sample size do not have any considerable impact on the determination of dielectric property. The new calibration equation in the form of $[K^{0.5}\rho_w/\rho_d]$ leads to slightly better results by reducing the effect of soil density. The results of the electrical conductivity measurements from TDR also agree well with the actual values.

3.7 Refereneces

Alharthi, A., and Lange, J. (1987). "Soil water saturation: Dielectric determination." *Water Resour.Res.,* 23(4), 591-595.

ASTM. 1997*a*. Standard test method for particle size analysis of soils (D422-63). *In* 1997 Annual Book of ASTM Standards, Vol. 04.08. American Society for Testing and Materials (ASTM), Philadelphia, PA. pp. 10-16

ASTM. 1997*b*. Standard test method for specific gravity of soils (D854-92). *In* 1997 Annual Book of ASTM Standards, Vol. 04.08. American Society for Testing and Materials (ASTM), Philadelphia, PA. pp. 88-91.

ASTM. 1997*c*. Standard test method for amount of material in soils finer than the No. 200 (75 μm) sieve (D1140-92). *In* 1997 Annual Book of ASTM Standards, Vol. 04.08. American Society for Testing and Materials (ASTM), Philadelphia, PA. pp. 92-94.

ASTM. 1997*d*. Standard test method for capillary moisture relationships for coarse and medium textured soils by porous plate apparatus (D2325-68). *In* 1997 Annual Book of ASTM Standards, Vol. 04.08. American Society for Testing and Materials (ASTM), Philadelphia, PA. pp. 195-201.

ASTM. 1997*e*. Standard classification of soils for engineering purposes (unified soil classification system) (D2487-93). *In* 1997 Annual Book of ASTM Standards, Vol. 04.08. American Society for Testing and Materials (ASTM), Philadelphia, PA. pp. 217-227.

ASTM. 1997*f*. Standard test method for liquid limit, plastic limit, and plasticity index of soils (D4318-95). *In* 1997 Annual Book of ASTM Standards, Vol. 04.08. American Society for Testing and Materials (ASTM), Philadelphia, PA. pp. 522-532.

Chen, R., Xu, W., and Chen, Y. (2009). "Measuring dielectric constant in highly conductive soils based on surface reflection coefficients." *J.Geotech.Geoenviron.Eng.,* 135(12), 1883-1891.

Dalton, F. N., and Van Genuchten, M. T. (1986). "The time-domain reflectometry method for measuring soil water content and salinity." *Geoderma,* 38(1-4), 232-250.

Drungil, C. E. C., Abt, K., and Gish, T. J. (1989). "Soil moisture determination in gravelly soils with time domain reflectometry." *Transactions of the American Society of Agricultural Engineers,* 32(1), 177-180.

Ebrahimi-Birang, N., Maule, C. P., and Morley, W. A. (2006). "Calibration of a TDR instrument for simultaneous measurements of soil water and soil electrical conductivity." *Transactions of the ASABE,* 49(1), 75-82.

Heimovaara, T. J., De Winter, E. J. G., Van Loon, W. K. P., and Esveld, D. C. (1996). "Frequency-dependent dielectric permittivity from 0 to 1 GHz: time domain reflectometry measurements compared with frequency domain network analyzer measurements." *Water Resour.Res.,* 32(12), 3603-3610.

Hook, W. R., Livingston, N. J., Sun, Z. J., and Hook, P. B. "Remote Diode Shorting Improves Measurement of Soil Water by Time Domain Reflectometry." *Soil Sci.Soc.Am.J.,* 56(5), 1384-1391.

Hu, Y., Vu, H. Q., and Hubble, D. W. (2010). "Evaluation of dielectric-based probes for expansive soils: Application to Regina clay." *Canadian Geotechnical Journal,* 47(3), 346-358.

Malicki, M. A., Plagge, R., and Roth, C. H. (1996). "Improving the calibration of dielectric TDR soil moisture determination taking into account the solid soil." Eur.J.Soil Sci., 47(3), 357-366.

Nichol, C., Smith, L., and Beckie, R. (2003). "Time domain reflectrometry measurements of water content in coarse waste rock." *Canadian Geotechnical Journal,* 40(1), 137-148.

Noborio, K., (2001). "Measurement of soil water content and electrical conductivity by time domain reflectometry: a review." *Comput.Electron.Agric.,* 31(3), 213-237.

Or, D., and Wraith, J. M. (1999). "Temperature effects on soil bulk dielectric permittivity measured by time domain reflectometry: A physical model." *Water Resour.Res.,* 35(2), 371-383.

Pettinelli, E., Cereti, A., Galli, A., and Bella, F. (2002). "Time domain reflectrometry: calibration techniques for accurate measurement of the dielectric properties of various materials." *Rev.Sci.Instrum.,* 73(10), 3553-62.

Regalado, C. M., Muñoz Carpena, R., Socorro, A. R., and Hernández Moreno, J. M. (2003). "Time domain reflectometry models as a tool to understand the dielectric response of volcanic soils." *Geoderma,* 117(3-4), 313-330.

Siddiqui, S. I., Drnevich, V. P., and Deschamps, R. J. (2000). "Time Domain Reflectometry Development for Use in Geotechnical Engineering." *Geotech Test J,* 23(1), 9-20.

Topp, G. C., Davis, J. L., and Annan, A. P. (1980). "Electromagnetic determination of soil water content: Measurements in coaxial transmission lines." Water Resour.Res., 16(3), 574-582.

Topp, G. C., and Davis, J. L. (1985). "Measurement of soil water content using Time-Domain Reflectometry (TDR): A field evaluation." *Soil Sci.Soc.Am.J.,* 49(1), 19-24.

Topp, G.C., Yanuka, M., Zebchuk, W.D., Zegelin, S., 1988. Determination of electrical conductivity using time domain reflectometry: soil and water experiments in coaxial lines. Water Resour. Res. 24, 945–952.

Zegelin, S. J., White, I., and Jenkins, D. R. (1989). "Improved field proves for soil water content and electrical conductivity measurement using time domain reflectometry." *Water Resour.Res.*, 25(11), 2367-76.

Chapter 4 Vacuum consolidation of Mature Fine Tailings

4.1 Introduction

Stabilization and reclamation of mine tailings -residues or wastes resulting from ore extraction and processing has always been a challenge for engineers. Two concerns in the stabilization for reclamation process are the bearing capacity of the tailings surface and the rate of settlements due to placement of load on the cover (Jakubick et al., 2003).

Dewatering mine and oil sands tailings cover a wide range of methods (Scott and Cymerman 1984): adding binder to the tailings (Qiu et al., 1999); chemical flocculation and coagulation; centrifugation (Theriault et al., 1995); freeze-thaw technique (Dawson et al. 1999); using geotextile to stabilize the surface (Wei et al. 2000); co-disposal of tailings with coarser materials (Wilson 2001); electro-Osmotic dewatering (Vijh 2002); disposal of tailings and sand simultaneously (Tan et al. 1994) and placing alternate layers of tailings and sand (Karunaratne et al. 1991).

Traditional method of disposing tailings involves a settling pond in which tailings are transferred and placed as slurries (Yunxin and Sego 2001). Oil sands tailings in Northern Alberta pose a significant reclamation and environmental challenge for the oil sands industry and mine tailings management in Alberta, Canada. A significant amount of research work has been done on characterization of the oil sands tailings (Scott et al. 1984; Morgenstern and Scott 1995; Chalaturnyk et al. 2002). Due to the nature of fine and ultra fine particles contained in tailings, such as clay, as well as the

ionic chemistry of the process water, the oil sands fine tailings have very low rate of consolidation which leads to slow but large deformation and potential instability of the deposit during preparing for reclamation (Lee et al. 1988; Kasperski 1992).

The permeability and compressibility of the oil sands tailings vary significantly with void ratio as a result of large deformations (Huerta and Rodriguez 1992). Numerous studies have been conducted on the consolidation behavior of fine Oil Sand tailings (Jeeravipoolvarn 2005; Boratynec 2003; Pollock 1988).

Amongst the dewatering methods for tailings, capping is the focus of this research program. Capping oil sands fine tailings involves first covering the surface of a tailings pond with a layer to enhance its bearing capacity. The increase in the effective stress within tailings eventually removes water from the pores and dewaters the tailings. The major impediment to the capping technique is the ability of the tailings to support a layer of another material on top without having it overturn and sink through the deposit (Bromwell and Oxford 1977).

The standard practice for capping oil sands deposits in the tailings ponds at Suncor is to use a layer of geotextile/geogrid to increase the bearing capacity of the underlying tailings. The research undertaken in this study describes a new technique of capping which avoids the need to use a geotextile/geogrid. The schematic diagram for reclaiming tailings is presented in Figure 4.1.

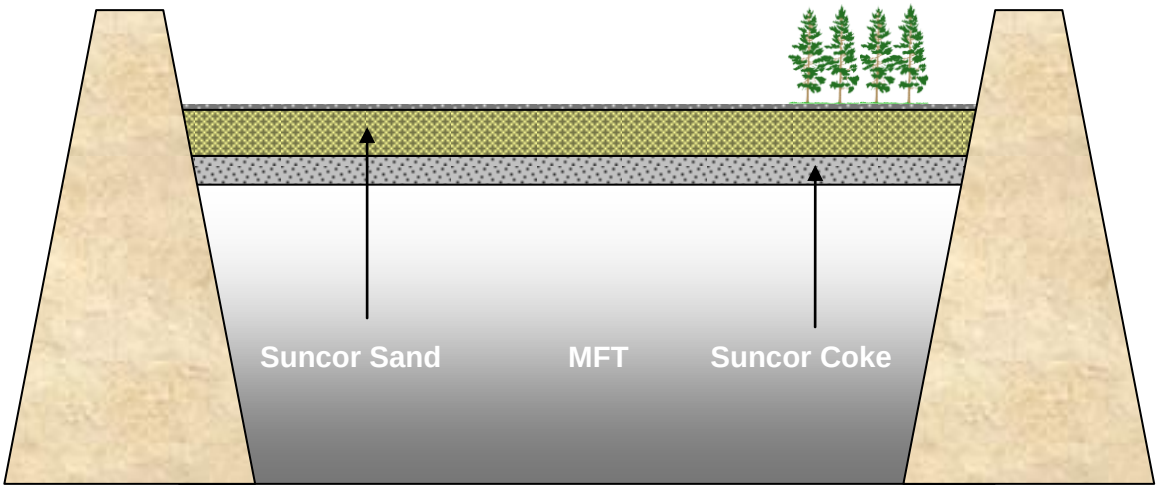

Figure 4.1. Geometry of the stabilized surface of Oil Sand tailings and overlying materials (not to scale)

4.2 Theory

The objective of the current research study is to investigate a novel consolidation technique for oil sand tailings. A three layered system of MFT, Suncor coke and Suncor sand was loaded using the meso-scale column for behavioral observation under vacuum consolidation. The column profile was monitored for settlement, pore-water pressure, matric suction and water content. The profile of the column is composed of 0.5 m of MFT overlain by 0.5 m of coke and then 0.5 m of sand. Initially all three regions were water saturated and the water table was at the top of the sand

layer. Following placement of the overlying sand, a suction (i.e. -5 kPa of pore-water pressure) was applied to the coke layer. Due to air-entry value, AEV, differences between the coke and the sand particles, the coke desaturated while the sand layer remained saturated. At this stage, the saturated sand layer becomes essentially impermeable to air and the suction was transferred to the underlying MFT layer causing the MFT to dewater. The sand and coke layer on top of the MFT also increases the overburden pressure to assist in the consolidation of the underlying MFT (Figure 4.2).

Due to practical limitations, the scope of this research study does not include the investigation of creating a uniform Suncor sand and Suncor coke distribution, operational concerns, cost-benefit analysis and numerical modeling of the layered system. However, they are recognized as being fundamental to the evaluation and implementation of the proposed technique.

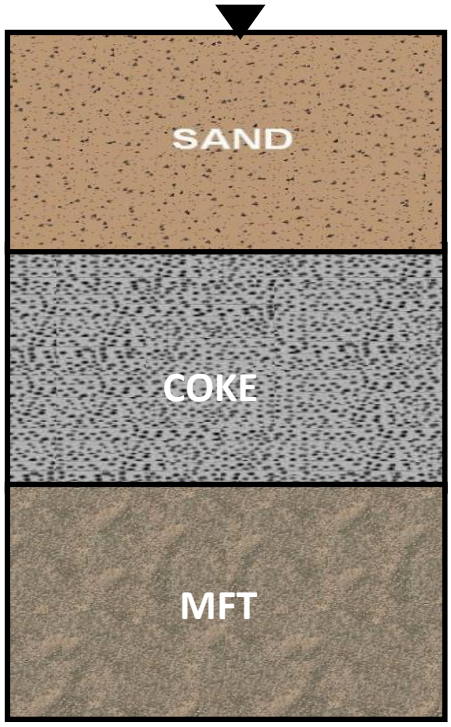

Figure 4.2. Initial configuration of material layers

4.3 Material composition

Approximately 500 litres of Suncor MFT, 500 kg of coke and 500 kg of sand were collected from the Suncor site in Fort McMurray, AB and shipped to the University of Alberta geotechnical laboratory, Edmonton for use as the column fill materials. The basic geotechnical parameters of the materials are summarized in Table 2.1. The Grain size distributions for Suncor sand, Suncor coke and MFT are shown in Figure 2.3. Prior to the placement of materials into the column, the MFT was thoroughly mixed to yield a homogenous slurry. The average initial solids content was 33% by mass. Suncor coke was used as an overburden on top of the MFT because of its low air-entry value and high friction angle. Suncor sand placed on top of the Suncor coke because of its higher air-entry value and lower shear strength. Both materials demonstrate low volume change properties.

4.4 Experimental program

4.4.1 Column apparatus

Figure 4.3 shows a sketch of the column designed for this experiment. The column was made of PVC with an attached base plate. The column was approximately 1 m in diameter and 2.30 m height. The size of the column was selected based on its ability to provide a reasonable data from various elevations. The top of the column was left open to allow irrigation but covered with plastic to minimize the evaporation in the laboratory. The design profile of the column consists of a layer of 0.5 m of MFT, overlain by 0.5 m of Suncor coke and then by 0.5 m of Suncor sand. The materials were placed into the column using a pail. Each pail was mixed before the material was dumped into the column. To simulate the field operation, a water cap was placed on the MFT. Care was taken to place the water cap on the MFT without disturbance of the MFT. The overlying Suncor coke and Suncor sand were pluviated into the water cap. The Suncor coke tended to float on top of MFT due to density similarities and the cohesive characteristic of MFT. Care was taken to create a uniform layer of Suncor coke and Suncor sand to avoid any local failure. The loading time for placing the Suncor coke and Suncor sand occurred over a period of two days to ensure uniform loading conditions. The instrumentations were installed in pre-specified elevations before filling the column (Figure 4.3).

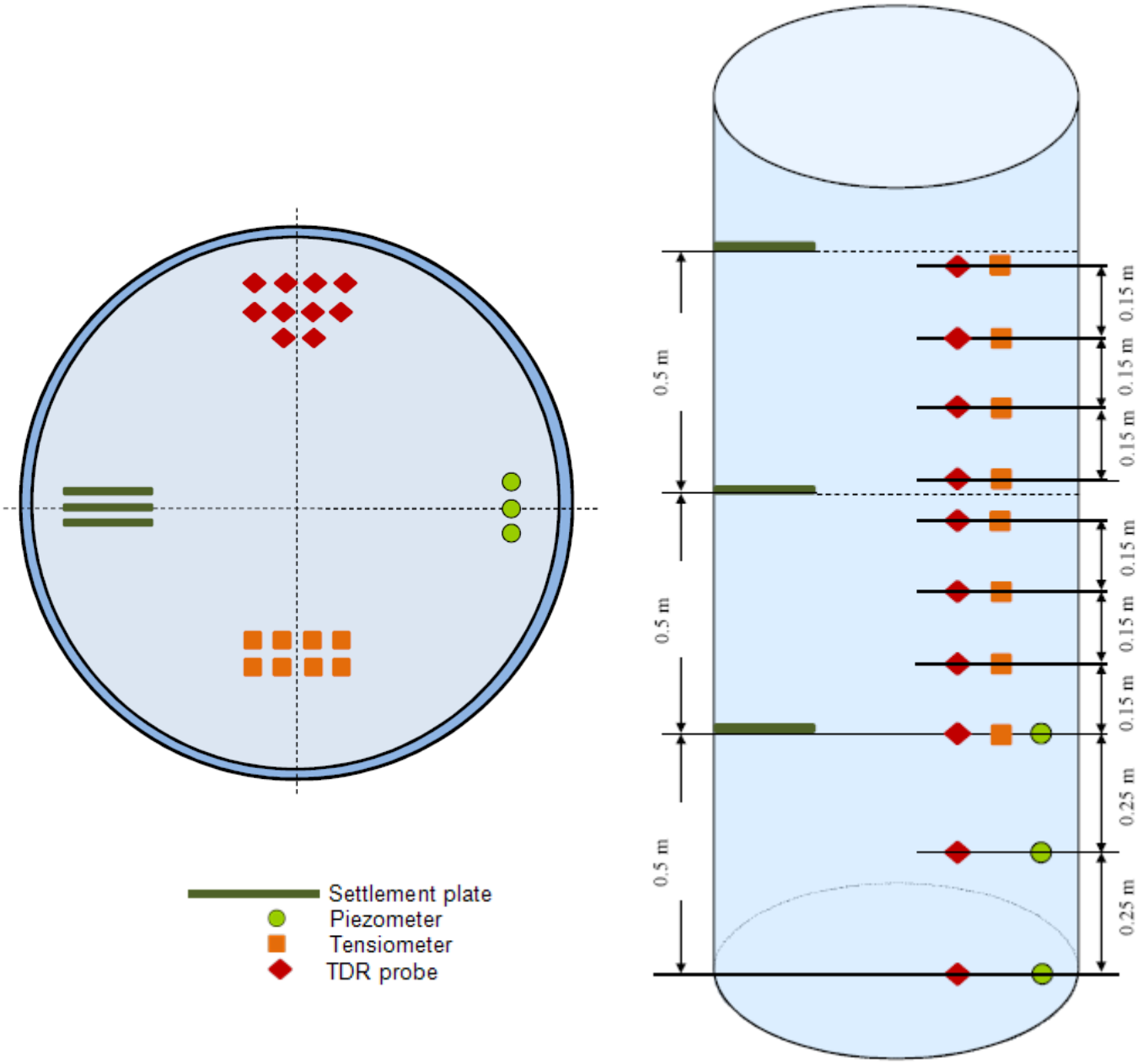

Figure 4.3. Sketch of column showing the location for the instrumentation

4.5 Instrumentation and monitoring

A total of four parameters were selected for monitoring purposes; namely, settlement, pore-water pressure, matric suction and water content. The monitoring continued for a period of six months after the column was filled. The instrumentation was selected based on the requirement to have redundant measurements of various parameters, availability of the devices, long-term durability, stability and the ability to have long cable lengths to allow for continuous monitoring. The instruments floated with the materials inside the column during the test. The instrumentation for the column included strain-gauge piezometers placed at 0 m, 0.25 m and 0.5 m, settlement plates placed at 0.5 m, 1 m and 1.5 m, Tensiometers mounted at 0.5 m, 0.65 m, 0.8 m, 0.95 m, 1 m, 1.15 m, 1.30 m and 1.45 m depths and TDR probes placed at 0 m, 0.25 m, 0.5 m, 0.5 m, 0.65 m, 0.8 m, 0.95 m, 1 m, 1.15 m, 1.30 m and 1.45 m. All the instruments were numbered from bottom to the top; number 1 being closest to the bottom of the column.

4.5.1 Strain gauge piezometers

The first 0.5 m of the column was filled with MFT and the pore-water pressure response and settlement were monitored. The strain gage piezometers (Model ELSGP5000SB-0.05 manufactured by RST Instruments, BC, Canada) were placed near the bottom, middle and top of the MFT layer. Figure 4.4 shows the piezometers used in this study. A filter paper and a piece of geotextile were wrapped around the tip of the piezometer prior to placement inside the column in order to prevent the sensitive surface of the piezoemeter from clogging. The piezometers were placed at least 0.1 m away from the column wall to avoid creation of a preferential vertical flow pathway. Each piezometer was saturated prior to use. All three piezometers used in the test, were calibrated by the manufacturer to a maximum pressure of 55 kPa (Figure 4.5).

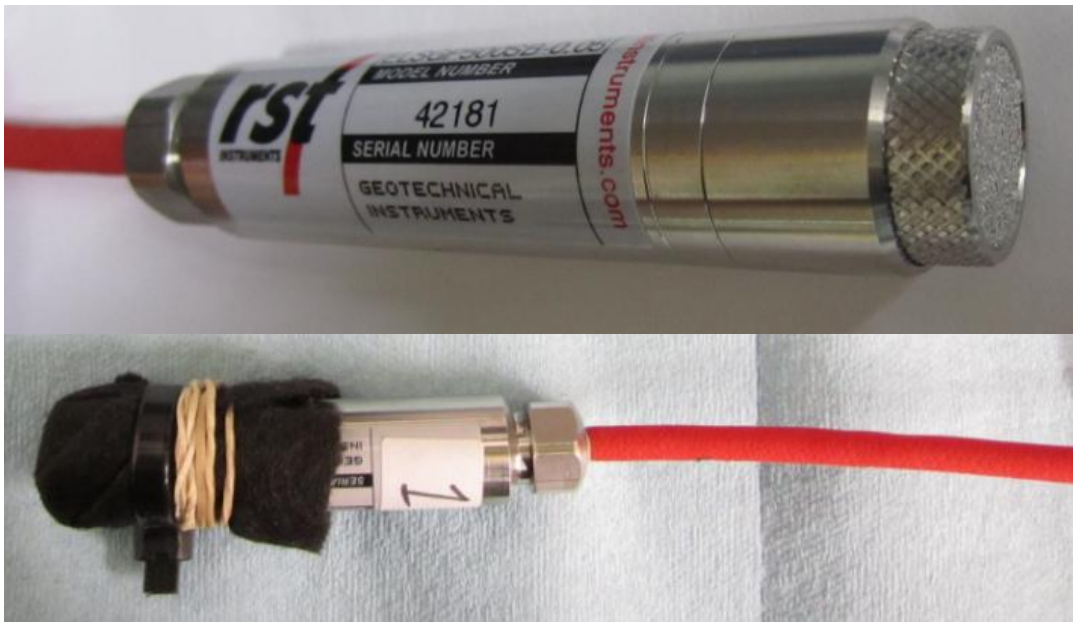

Figure 4.4. Strain gauge piezometer

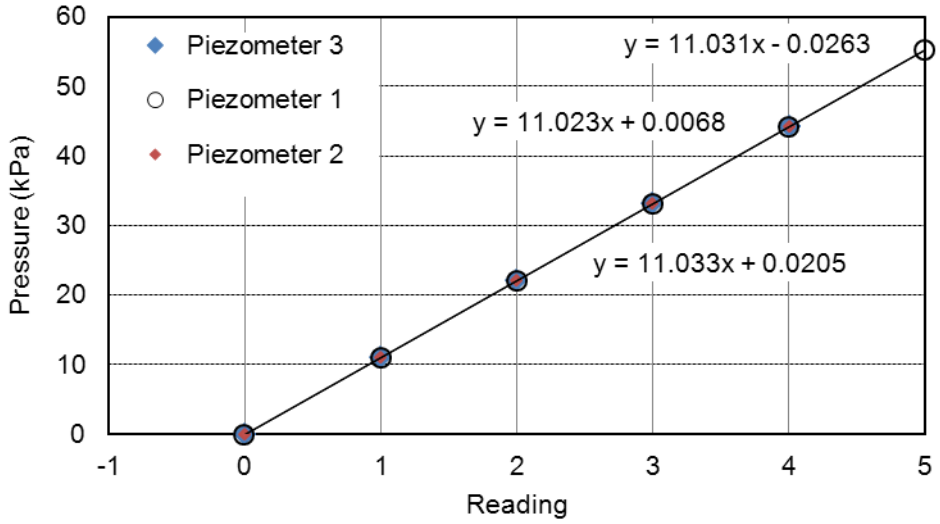

Figure 4.5. Calibration of piezometers

4.5.2 Time Domain Reflectometry probes

Total pore-water pressure coupled with the water content measurement provides valuable insight into the behavior of the MFT. TDR probes were used across the column at 0.25 m intervals in the MFT and at 0.15 m intervals in the other layers to measure the water content change in the column at various elevations during the test. TDR probes (CS640 instruments from Campbell Scientific, Canada) were placed in the interior of the column in accordance with the manufactures guidelines (Figure 4.6). Prior to installation, the probes were calibrated with MFT, Suncor coke and Suncor sand as outlined in Chapter 3. Ten TDR probes were used in this study at the designated elevations.

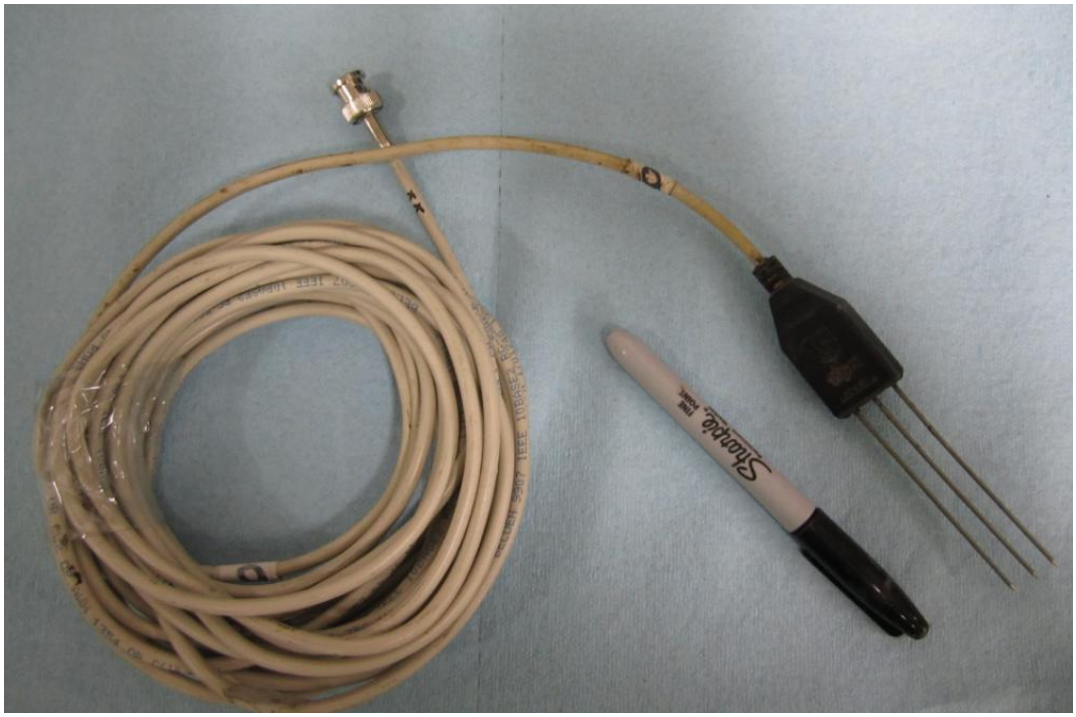

Figure 4.6. A typical CS640 TDR probe used in the column test

4.5.3 Tensiometers

Tensiometers were installed at 0.15 m intervals in the Suncor coke and Suncor sand layers to measure the matric suctions in the two zones that might de-saturate. Eight jet-fill tensiometers (manufactured by SoilMoisture Equipment Corp.) were assembled and checked for saturation and sensitivity for measurement of matric suction. Figure 4.7 shows a jet-fill tensiometer used in the test.

Figure 4.7. Jet-fill Tensiometer

4.5.4 Settlement gauges

Figure 4.8 shows one of the three settlement gauges designed and constructed to measure the amount of deflection taking place as the material loaded. The settlement plates were fabricated from pail lids with a 1 or 2 m long rod attached. The diameter of each plate was 0.3 m. Total settlement was taken as the average settlement of the MFT, Suncor coke and Suncor sand. Differential settlement was determined using two settlement plates at the interface of the upper (coke-sand) and lower (coke-MFT) layers.

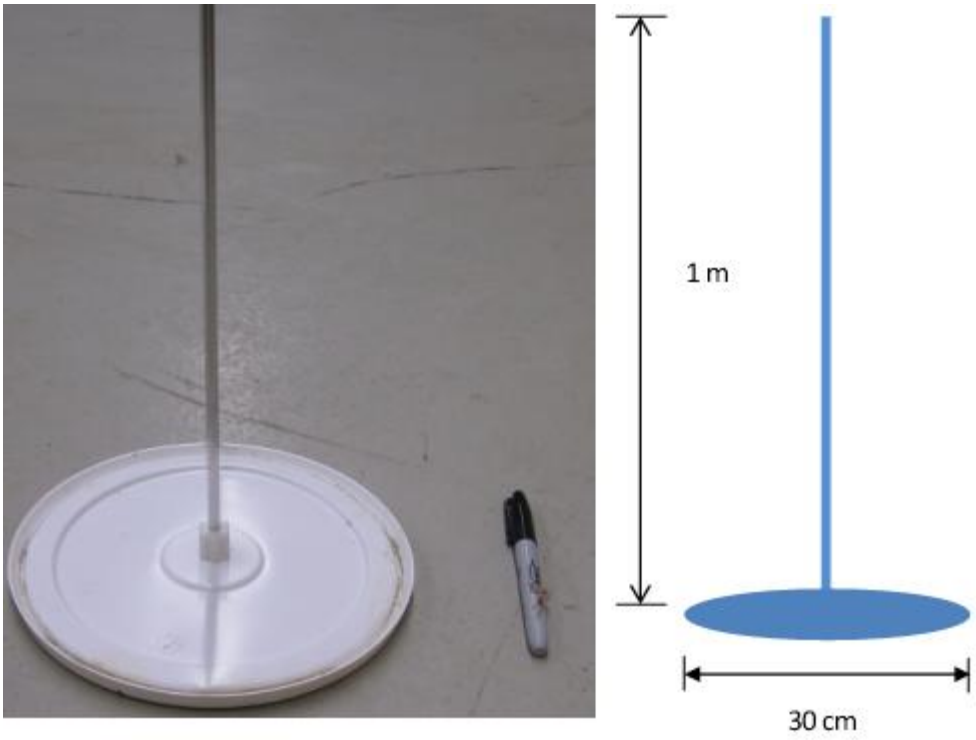

Figure 4.8. Settlement plates

4.5.5 Suction pipes

Negative pore-water pressures were applied to the middle of the Suncor coke layer through suction pipes. The suction pipes were composed of 4 pieces of plastic tubes, approximately 20 cm long with equi-distance slots. To avoid clogging of the slots, a piece of geotextile was wrapped around each pipe (Figure 4.9).

Figure 4.9. Suction pipes

4.5.6 Irrigation and collection of water

The top boundary condition of the soil layer was considered to simulate the precipitation in Fort McMurray in the summer months. To achieve this, the sand layer was irrigated on a daily basis (Silva., 1999). The water removed through the suction pipes was collected in a container and measured daily for mass balance calculations.

4.6 Results and discussions

4.6.1 Pore-water pressure response

Figure 4.10 presents the selected pore-water pressure measurements taken by the strain-gauge piezometers buried in the MFT. The maximum pore-water pressure in the column was approximately 6.5 kPa at the bottom of MFT layer, with pressure measurement decaying with time to below 5.5 kPa after approximately four months. The MFT showed a triangular pressure profile distribution, which dissipated with time. The water pressure measures by the second piezometer remained fairly constant at approximately 5 kPa and did not show consolidation. After the application of the suction to the Suncor coke, the pore-water pressure of the uppermost piezometer dropped below zero and was observed to become negative. The shape of the pore-water pressure distribution shown in Figure 4.11 indicates a minor dissipation of excess pore-water pressure after the application of the suction. Due to the narrow range of the induced pore pressures and the accuracy of the piezometers, no further indications of pore-water dissipations can be inferred from the results. The strain-gauge piezometers produced some anomalies such as the apparent oscillations in the pore-water pressure. Errors in the pore-water pressure response can be attributed to either minor thermal, barometrical air fluctuations during the daytime or clogging. The accuracy for the strain-gauge piezometers used in this test was ± 2 kPa according to the manufacturer. The operating temperature in the laboratory was assumed to remain constant at 22 °C. The water pressures measurements were taken at the same time of the day to minimize the errors induced by minor thermal variations. For future experimentation piezometers with a lower range and higher accuracy are recommended.

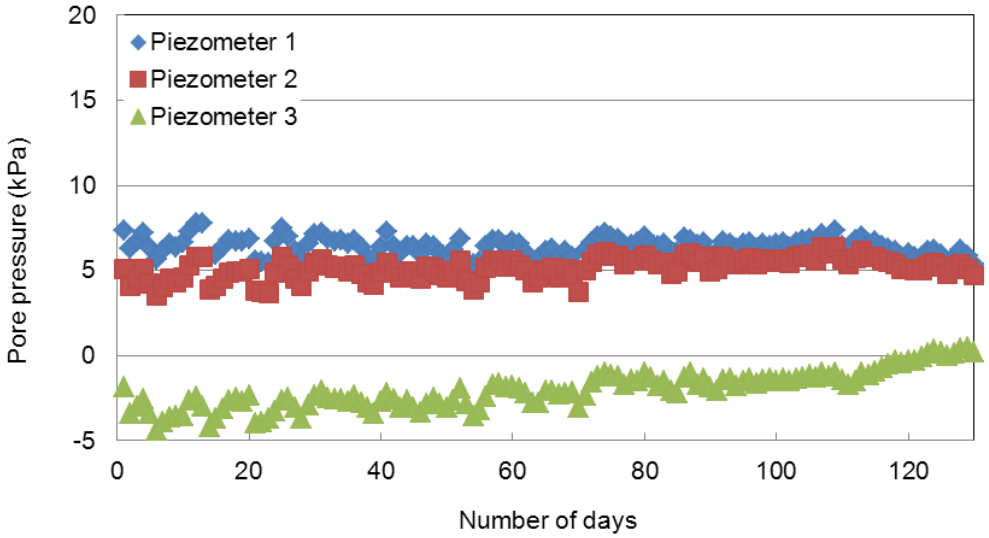

Figure 4.10. Pore-pressure data in MFT

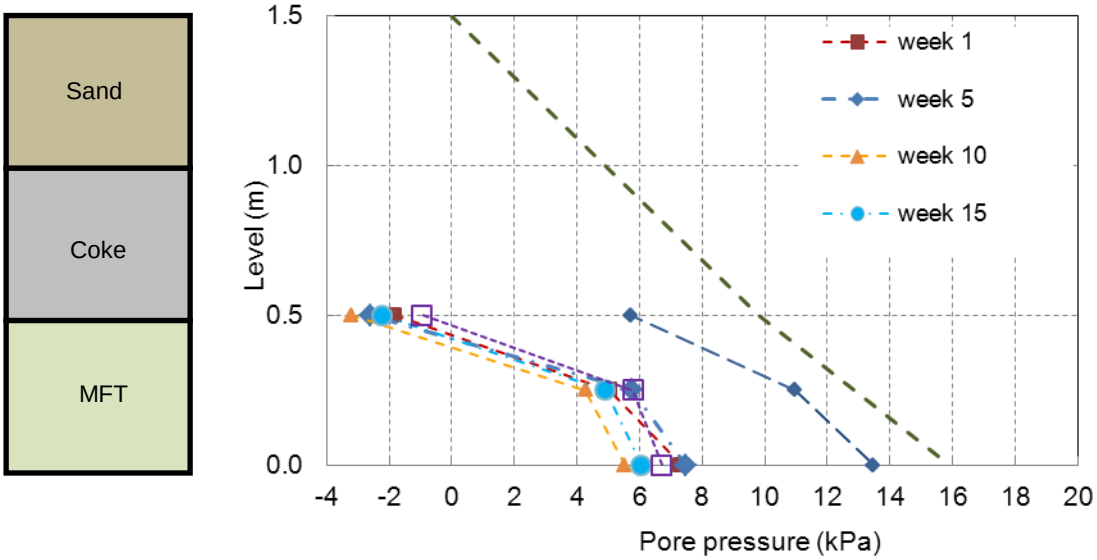

Figure 4.11. The pore-pressure diagram in MFT

4.6.2 Drainage from the Suncor coke layer

The weight of water collected from the suction pipes inside the coke layer and water irrigated on the surface of sand is shown in Figure 4.12. The data collection commenced after 40 days due to operational limitations. The collected water and the irrigated water followed the same pattern. Water was expelled from the coke layer through the suction pipes. The weight of collected water reached a maximum of 114 kg. The error in the water balance was 0.6% at 50 days and 0.1% at 100 days with positive sign indicating that the more irrigated water was added than was collected. It was not feasible to calculate the amount of water that has been removed from MFT through the suction pipes due to the low rate of dewatering and the lack of initial results. Errors in the water balance were attributed to measurement errors and the accuracy of the experiment. No leaks were observed during the loading time and the application of suction in the column. Evaporation in the laboratory was considered minimal due to placement of cover on top of the column.

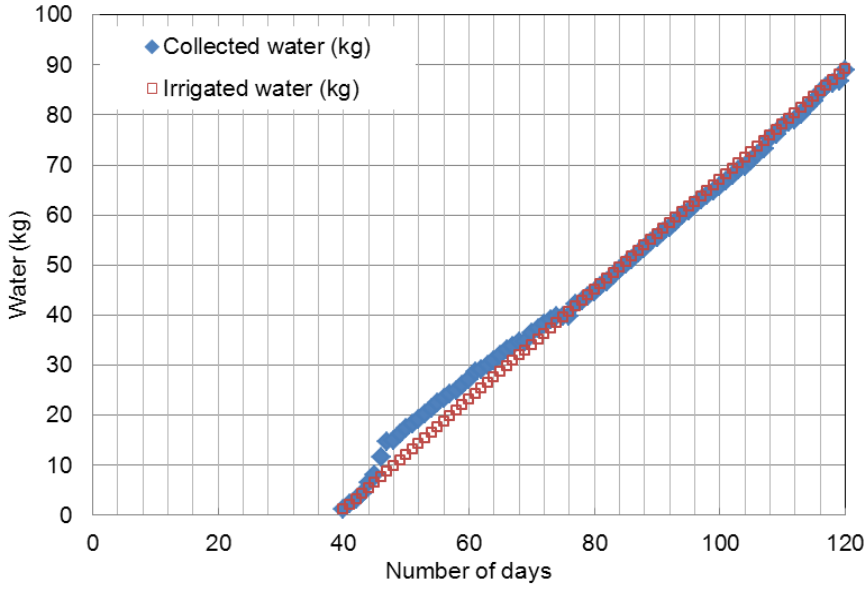

Figure 4.12. The collected and irrigated water during the test

4.6.3 Water content change

Figure 4.13 presents the water content profiles for the Suncor MFT. Figure 4.14 shows that the solids content increased during the 4 months of the test. Some anomalies are seen in this figure due to the algorithm deficiencies. The initial solids content was around 33%. It can be seen from Figure 4.15 that the rate of water content decrease at the interface of MFT with the coke layer was higher than for the other lower layers, indicating that there was a flow of water towards coke layer. The middle and bottom TDR readings also tended to decrease in the water content indicating consolidation of MFT.

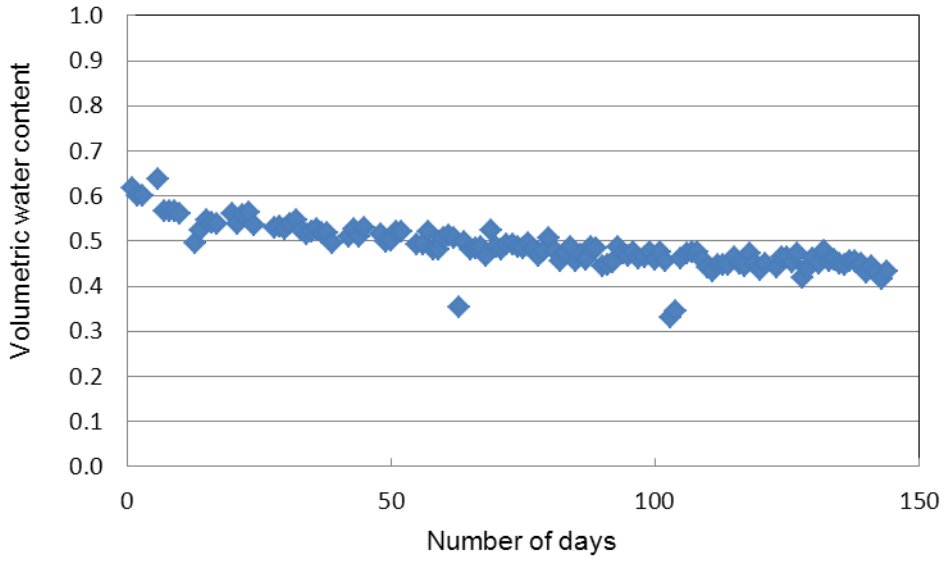

Figure 4.13. Volumetric water content decrease in MFT

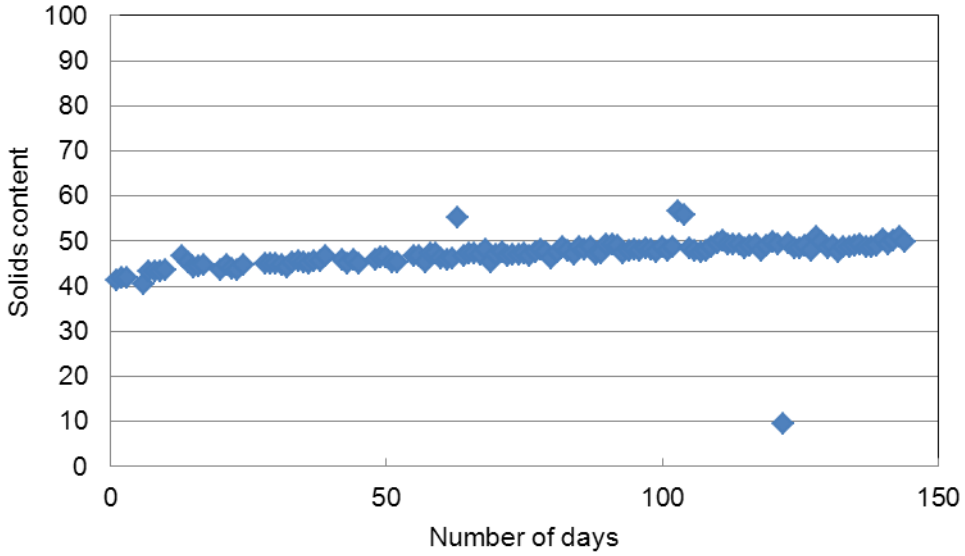

Figure 4.14. Solids content increase in MFT interface

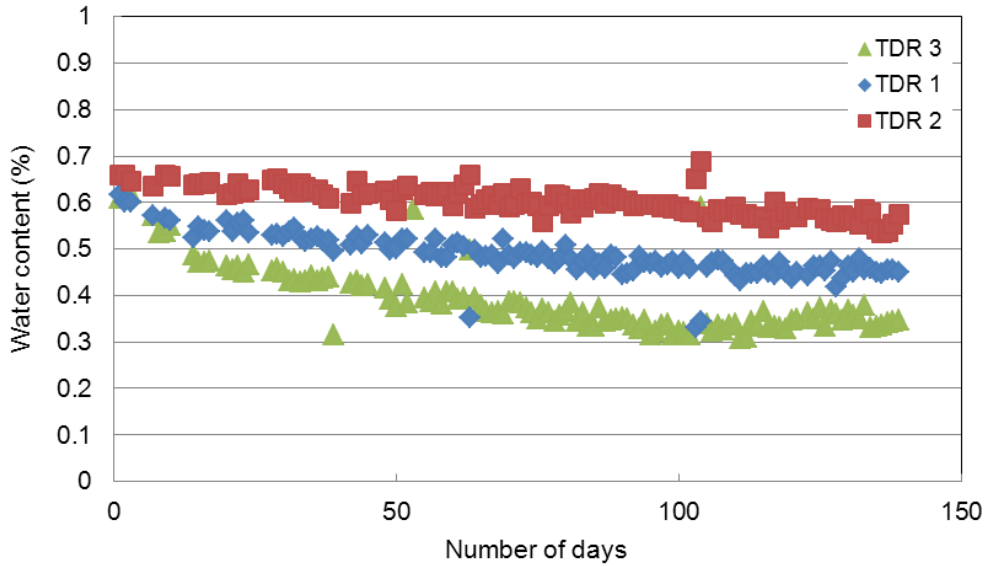

Figure 4.15. Water content decrease in MFT

The water content in the coke layer remained essentially constant and extremely low during the experiment as was anticipated. The coke layer dewatered within the first few hours after the application of the suction (Figure 4.16).

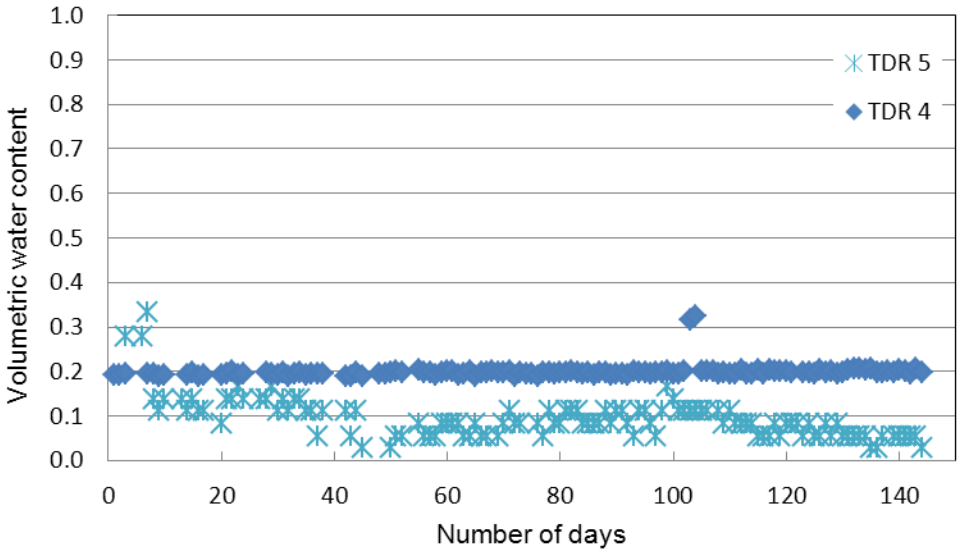

Figure 4.16. Volumetric water content in coke layer

The water content of the Suncor sand layer dropped slowly during the first 50 days of the experiment and then remained constant at a residual value. The results showed that a significant dewatering took place in the sand layer; however, the water content was higher than that in the Suncor coke layer. The reason of the higher water content may be due to the daily irrigation of the surface and the higher air-entry value of the Suncor sand (Figure 4.17).

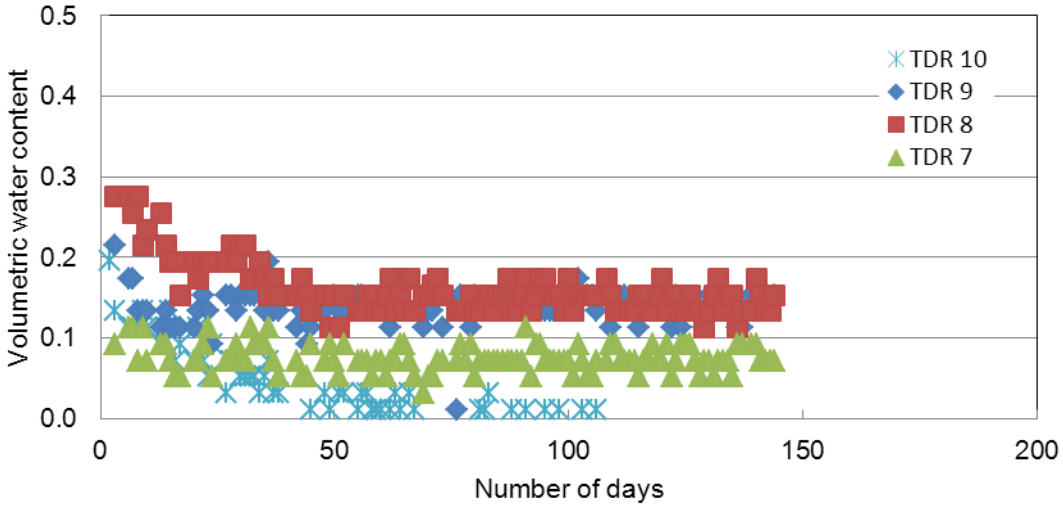

Figure 4.17. Volumetric water content in sand layer

4.6.4 State of water saturation

The MFT, Suncor coke and Suncor sand were water saturated prior to the commencement of the experiment. The measured matric suctions and the in-situ water content measurements were compared to the laboratory-derived SWCC's. The matric suctions (or the negative water pressures) were investigated by direct measurement using Jet-Fill tensiometers. The suction profiles of the MFT, coke and sand layer are shown in Figure 4.18. The MFT was found to remain water saturated during the four months test period due to its high air-entry value (i.e. approximately 2000 kPa).

Comparison of the matric suctions suggests that the coke layer that was initially saturated underwent desaturation shortly after the suction was applied. Desaturation was attributed to the extremely low air-entry value of the Suncor coke (i.e. approximately 0.1 kPa). Observations from the tensiometers on a daily basis indicated that the coke remained desaturated during the four month test. The suction range in the Suncor coke layer was measured 5 to 7 kPa. The suction in the Suncor coke was similar to the negative pressure applied to the coke layer.

The applied matric suction was selected to be -5 kPa which was close to the air-entry value of Suncor sand approximately -2 kPa. Comparison of the tensiometer measurements of matric suction with an SWCC for the Suncor sand layer suggests that the sand layer remained saturated during the four month test. The daily irrigation of Suncor sand surface did not allow for desaturation. Visual inspection also confirmed that the surface of the sand did not dry during the test. Minor desaturation that was observed in the Suncor sand layer was attributed to air flow and evaporation. Low

values of suction (i.e. 2 to 4 kPa) likely occurred at the upper parts of the Suncor coke layer as well as inside the Suncor sand layer. Matric suction values remained fairly constant during the test period and are summarized in Figure 4.19.

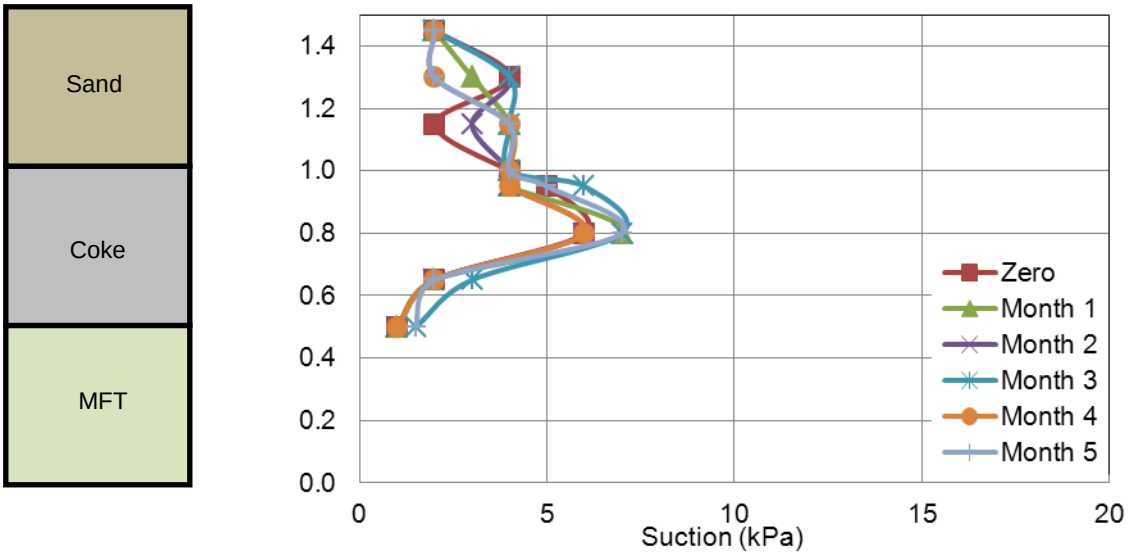

Figure 4.18. Suction profile inside the layers

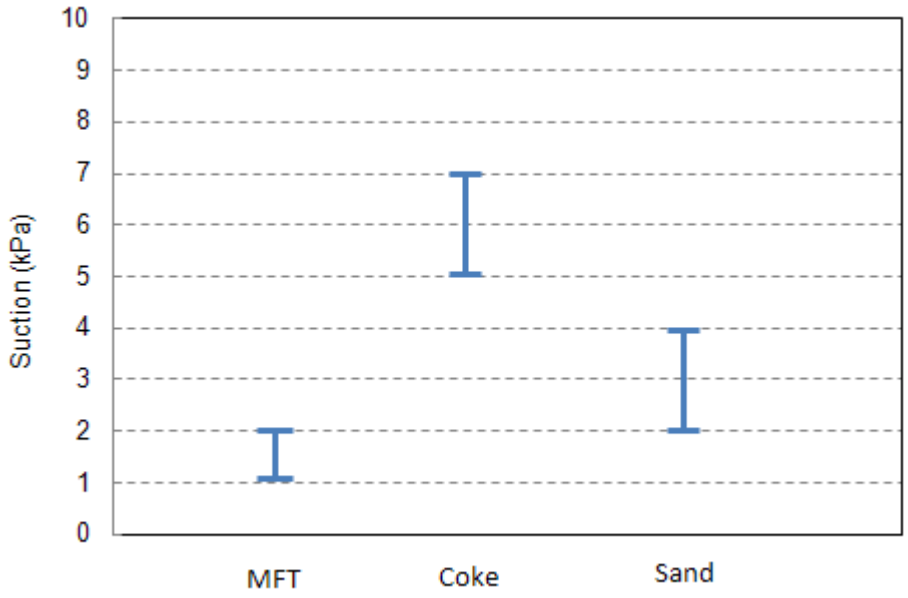

Figure 4.19. Suction range inside the layers during the test

4.6.5 Settlement

The plastic plates used as settlement gauges allowed measurement of settlement. All settlement measurements were referenced to the bottom of the column. Figure 4.20 presents the settlement profiles for each material.

The majority of volume change occurred during dissipation of pore-water pressure in the MFT. The MFT changed volume prior to application of suction and continued to release water afterwards. The total settlement in the MFT after four months was approximately 23% of its initial height. The final settlement of the MFT was 0.115 m. The settlement graph of MFT showed that displacement of MFT had not stopped even after four months. Column wall effects may also have had a confining effect on consolidation.

Differential settlement of the granular Suncor coke and Suncor sand was approximately the same (i.e. 0.012 m for coke and 0.015 for sand). The settlement amounts to about 3% of their original thickness. The settlement in the Suncor sand and Suncor coke layer appears to have occurred evenly with slightly less settlement occurring in the coke layer.

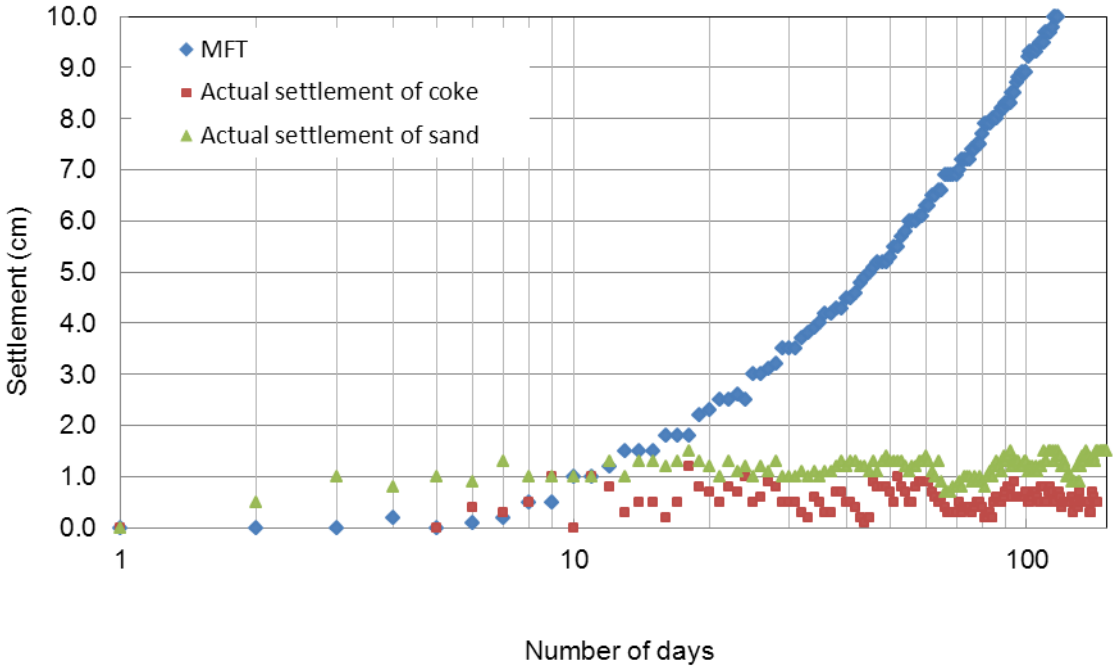

Figure 4.20. The results of the measured settlements

4.7 Summary and conclusions

A meso-scale column apparatus was designed, constructed and installed at the geotechnical laboratory of University of Alberta, Edmonton. The study was part of a long-term research initiative into the investigation of vacuum consolidation on MFT.

Basic geotechnical data and observations of vacuum consolidation of MFT are presented in this paper. The behavior of MFT dewatering under vacuum consolidation was investigated in an instrumented column. The data presented in this research are specific to Suncor MFT and the conditions in this experiment; however several general conclusions can be drawn from the study.

1- The visual inspection indicated no failure of the MFT as the coke particles were pluviated. This suggests the feasibility of placing a uniform layer of coke directly on top of the MFT provided it is pluviated through a water column.
2- The solids content measurement of MFT using the TDR probes indicated that the solids content of the MFT increased throughout the experiment and consolidation.
3- The sand layer maintained water saturated after 100 days indicating the feasibility of maintaining the saturation of the sand layer above the coke layer.
4- The amount of settlement in the MFT was 12 cm over 100 days indicating that consolidation was occurring.

The results are promising, however it should be noted that this study is preliminary and further investigation of the vacuum consolidation is recommended.

4.8 References

Boratynec, D. J. (2003). "Fundamentals of rapid dewatering of composite tailings". M.Sc. University of Alberta (Canada), Canada.

Bromwell, L. G., and Oxford, T. P. 1977. *Waste Clay Dewatering and Disposal.* 1801 Alexander Bell Drive, Reston, VA, 20191-4400, USA, American Society of Civil Engineers.

Chalaturnyk, Richard J., J. D. Scott, and Baki Ozum. 2002. Management of oil sands tailings. *Petroleum Science and Technology* 20, no. 9-10:1025-1046.

Dawson, R. F., D. C. Sego, and G. W. Pollock. 1999. Freeze-thaw dewatering of oil sands fine tails. *Canadian Geotechnical Journal* 36, no. 4:587-598.

Jakubick, Alex T., Gord McKenna, and Andy M. Robertson. 2003. Stabilisation of Tailings Deposits: International Experience. *international Experience. Mining and the Environment III* Sudbury, Ontario, Canada, 25-28 May, pp. 1-9.

Jeeravipoolvarn, Silawat. 2005. Compression behaviour of thixotropic oil sands tailings. Ph.D. diss., University of Alberta (Canada).

Karunaratne, G. P., et al. 1991. *Instrumentation and monitoring of a layered clay-sand reclamation.* Rotterdam, Neth: Publ by A.A. Balkema.

Kasperski, Kim L. 1992. *A review of properties and treatment of oil sands tailings.* Devon, Alberta: AOSTRA J. Res. 8.

Lee, S. L., et al. 1988. CONSOLIDATION OF DREDGED CLAY IN RECLAMATIONS. *Soils and Foundations* 28, no. 2:1-13.

Morgenstern, N. R., and Scott, J. D. 1995. *Geotechnics of fine tailings management.* New York, NY, USA: ASCE.

Pollock, Gordon W. 1988. Large strain consolidation of oil sand tailings sludge. Ph.D. diss., University of Alberta (Canada).

Qiu, Y., D. C. Sego, and Jozef Szymanski. 1999. Innovative tailings backfill using HSM. *Tailings and mine waste*169-176.

Scott, J. D., and Cymerman, G. J. 1984. *PREDICTION OF VIABLE TAILINGS DISPOSAL METHODS.* New York, NY, USA: ASCE.

Scott, J. D., Maurice B. Dusseault, and W. D. I. Carrier. 1984. Behaviour of the clay/bitumen/water sludge system from oil sands extraction plants. *Applied Clay Science* 1, no. 1-2:207-218.

Tan, T., T. Goh, G. P. Karunaratne, and S. Lee. 1994. Shear strength of very soft clay-sand mixtures. *Geotechnical Testing Journal* 17, no. 1:27-34.

Theriault, Yvon, et al. 1995. The effect of chemical, physical and enzymatic treatments on the dewatering of tar sands tailings. *Fuel* 74, no. 9:1404-1412.

Vijh, Ashok. 2002. *Electro-Osmotic Dewatering of Clays, Soils, and Suspensions.*

Wilson, G. Ward, 2001. Co-disposal of tailings and waste rock. *Geotechnical News* 19, no. 2:44-49.

Wei, J., et al. 2000. *CAPPING OF A SILT POND FILLED WITH SILTY-CLAY SLURRY.*Geoeng 2000, Melbourne, Australia ed.

Yunxin, Q., and D. C. Sego. 2001. Laboratory properties of mine tailings. *Canadian Geotechnical Journal* 38, no. 1:183-190.

Chapter 5 Numerical analysis of vacuum consolidation

5.1 Introduction

The prediction of consolidation in oil sands tailings is central to the long term behavior of tailings. The typical hydraulic deposition of oil sand tailings causes large potential consolidation. Such large deformations can no longer be over-looked and necessitate the modeling using large-strain methodology.

This paper presents the use of the finite element method to address the complex combination of large-strain consolidation and the unsaturated behavior of the three and four layered system. In this system, MFT is overlain by a layer of coke which is in turn overlain by another layer of sand (Figure 5.1). Negative water pressure is applied to the coke layer to expedite the consolidation process. The top boundary consists of a constant flux of 0.0014 m^3/day corresponding to the field data. In the four layered system another layer of MFT is placed on the sand layer to avoid intrusion of air into the suction system.

The theoretical context for the analysis of vacuum consolidation involves the numerical modeling of large strain consolidation associated with unsaturated behavior of coke and sand upon the application of suction. Numerical advances in computing technology have made feasible long-term analysis of various practical geotechnical problems in which both saturated and unsaturated soil parameters are included in the analysis. Until recently the coupling seepage analysis with stress-strain analysis has been unfeasible due to software and computational limitations.

Two scenarios, one with the use of suction and one without, are presented. This approach allows the determination of the vertical displacement and pore-pressure response developed in the model. Information is also provided about the interpretation of the modeling. A comparison of the results of the proposed new technique is provided to demonstrate the advantages of the new technique.

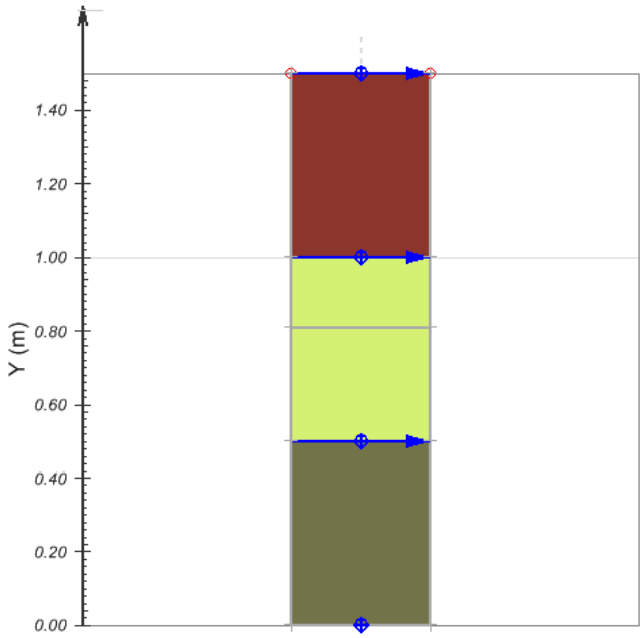

Figure 5.1. The three layered model generated in SVOffice

5.2 Theory

The finite element software package developed by SoilVision Systems Ltd. has the capability of solving the water phase continuity (seepage) equation and the equilibrium (stress-strain) equations simultaneously. The two computer programs made available for the purpose of this study were SVFlux and SVSolid, were capable of bridging the gap between unsaturated seepage analysis and large-strain consolidation. The coupled analysis is the option best suited for consolidation modeling. The model is initially constructed in the SVFlux environment with flow properties and then coupled with SVSolid to analyze consolidation (SVOffice Manual, 2009). The pore-water pressure values determined by SVFlux were used in SVSolid to modify the effective stress to determine deformation. The deformation which is represented by the void ratio change modifies the hydraulic conductivity which is used again in the next step by SVFlux. This process continues until the predetermined end time is achieved (SVOffice manual, 2009). In the following sections, the seepage and stress-strain relationships are described.

5.2.1 Seepage equations

The decrease in water content of saturated soil without replacement of water by air is called consolidation (Terzaghi 1943; Haase et al.). The rate at which the water dissipates is related to the hydraulic conductivity (*k*) and the pore pressure gradient (*i*). During consolidation the soil matrix continues to readjust itself by continuous compression. The classical consolidation theory assumes that the deformations in the soil matrix are infinitesimal which results in a constant hydraulic conductivity and compressibility. In consolidation of tailings the compressibility and hydraulic conductivity are not constant due to excessive deformation. The governing equation for highly nonlinear finite strain consolidation can be written as follows (Gibson et al., 1967):

$$(\frac{\gamma_s}{\gamma_f}-1)\frac{d}{de}[\frac{k(e)}{(1+e)}]\frac{\partial e}{\partial z}+\frac{\partial}{\partial z}[\frac{k(e)}{\gamma_f(1+e)}\frac{d\sigma'}{de}\frac{\partial e}{\partial z}]+\frac{\partial e}{\partial t}=0 \qquad [5.2]$$

where:

γ_s = the unit weight of solids,

γ_f = the unit weight of fluids,

e = the void ratio,

k(e) = hydraulic conductivity,

z = material coordinate,

σ' = the effective stress

and *t* = time.

Numerous studies have been conducted on determining large strain consolidation parameters and prediction of fine tailings (Lee et al. 1988; Fox et al. 2003; Bartholomeeusen et al. 2002; Huerta and Rodriguez 1992; Carrier and Bromwell 1983; Gustavsson and Oppelstrup 2001; Cargill 1984; Townsend and McVay 1990; Consoli and Sills 2000; Bartholomeeusen et al. 2002; Azam, Jeeravipoolvarn, and Scott 2009). Effective stress and hydraulic conductivity versus void ratio are the large-strain consolidation parameters required for the finite element analysis of fine tailings and may be determined using large-strain consolidation cells. The relations used as input parameters in the finite element analysis provide an increased accuracy in the analysis of the pore-pressure and settlement of the tailings.

As water is drawn from a saturated medium the soil experiences an unsaturated behavior. The unsaturated behavior of a soil can be very well explained by its Soil Water Characteristic Curve (SWCC). The SWCC relates the matric suction to the gravimetric water content. The SWCC is a function of soil type and can be used as the basis to determine the unsaturated hydraulic conductivity. Unsaturated hydraulic conductivity is used as an input parameter in the finite element simulation. (Yang et al. 2004; Fredlund and Rahardjo 1993).

The governing, partial differential equation for the water phase in the consolidation equation is (Fredlund and Rahardjo, 1993):

$$\frac{\partial}{\partial y}(k_y(\psi,e)\frac{\partial h}{\partial y}) = m_w{}^2\gamma_w\frac{\partial h}{\partial t} \quad [5.2]$$

where:

h = total head

$k_y(\psi,e)$ = hydraulic conductivity of the soil in y direction

γ_w= the unit weight of water (9.81 kN/m^3) and

$m^2{}_w$= the slope of the soil water characteristic curve

As seen in the above equation, the hydraulic conductivity in the general case is a function of soil suction and void ratio. The m_w is the slope of the SWCC of the soil.

5.2.2 Stress-strain relationship

The 1D equation governing the static equilibrium for a general case of unsaturated soil is given below (Fredlund and Vu, 2003):

$$c_{33}\frac{\partial}{\partial x}(\frac{\partial u}{\partial y})+\frac{\partial}{\partial y}(c_{22}\frac{\partial v}{\partial y})-d_s\frac{\partial(u_a-u_w)}{\partial y}+b_y=0 \qquad [5.3]$$

where:

$$c_{22}=\frac{(1-\mu)E}{(1+\mu)(1-2\mu)}; \qquad c_{33}=\frac{E}{2(1+\mu)}; \qquad d_s=\frac{E}{(1-2\mu)H}$$

E= is the elasticity parameter for the soil structure with respect to a change in the net normal stress,

H = is the elasticity parameter for the soil structure with respect to a change in matric suction

μ = Poisson's ratio

b_y = the body weight downward

u and v are the displacements in vertical and horizontal direction and

(u_a- u_w) = the matric suction.

To solve equation [5.3], the boundary conditions, initial conditions, such as initial effective stress conditions and initial matric suction should be known.

5.3 Material description

Suncor MFT, Suncor sand and Suncor coke are the three types of materials used in modeling. The model is composed of 1D soil column with three materials of equal thickness of 0.5 m.

Vu (Vu, 2003) proposed a six parameter equation (equation 5.3) capable of fitting both the SWCC and the large strain consolidation formulation. Vu equation for void ratio is presented below:

$$e = A + B\log\left[\frac{1 + C(\sigma - u_a) + D(u_a - u_w)}{1 + M(\sigma - u_a) + N(u_a - u_w)}\right] \qquad [5.4]$$

where:

A and *B* are constant soil parameters. *C* and *M* are soil parameters related to the effective stress and *D* and *N* are soil parameters related to the soil suction to satisfy the logarithmic equation.

Similarly the same equation is used to relate soil suction and the effective stress to the soil saturation:

$$Sr = a + b\log\left[\frac{1 + c(\sigma - u_a) + d(u_a - u_w)}{1 + m(\sigma - u_a) + n(u_a - u_w)}\right] \qquad [5.5]$$

where:

a and *b* are constant soil parameters. *c* and *m* are soil parameters related to the effective stress and *d* and *n* are soil parameters related to the soil suction to satisfy the logarithmic equation.

The Vu equation was found to be capable of modeling a smooth and continuous model for representation of the constitutive surfaces. The Vu six parameter equations were utilized for the fitting of the constitutive surfaces in both SVSolid and SVFlux. Optimal fits of the six-parameter equation were found with the help of a least squares algorithm in MATLAB.

The initial stages of this study involved determining the parameters for the constitutive surfaces. For the seepage analysis a minimum of 20 data-points were entered directly into the SVFlux program for the hydraulic conductivity of each material. The permeability functions of Suncor coke, Suncor sand and MFT are presented in Figures 5.2 and 5.3.

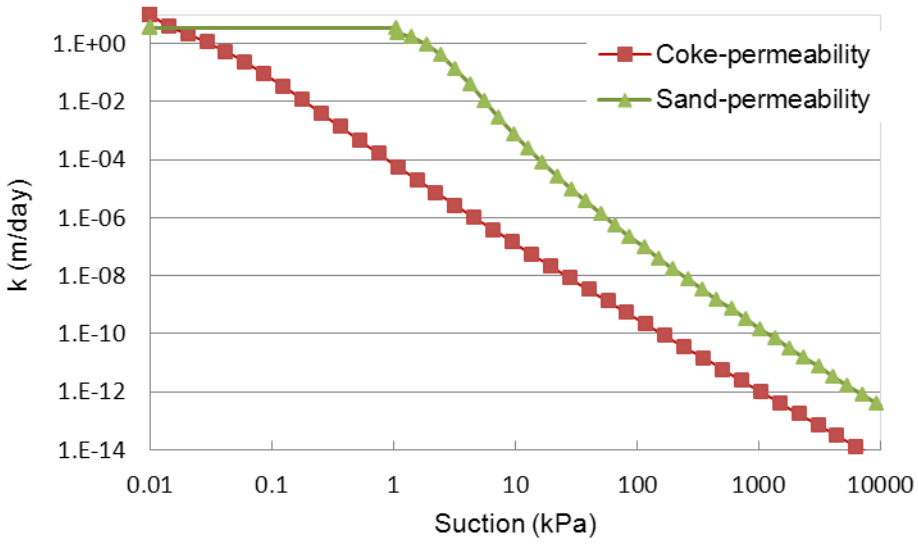

Figure 5.2. Permeability data for the coke and sand

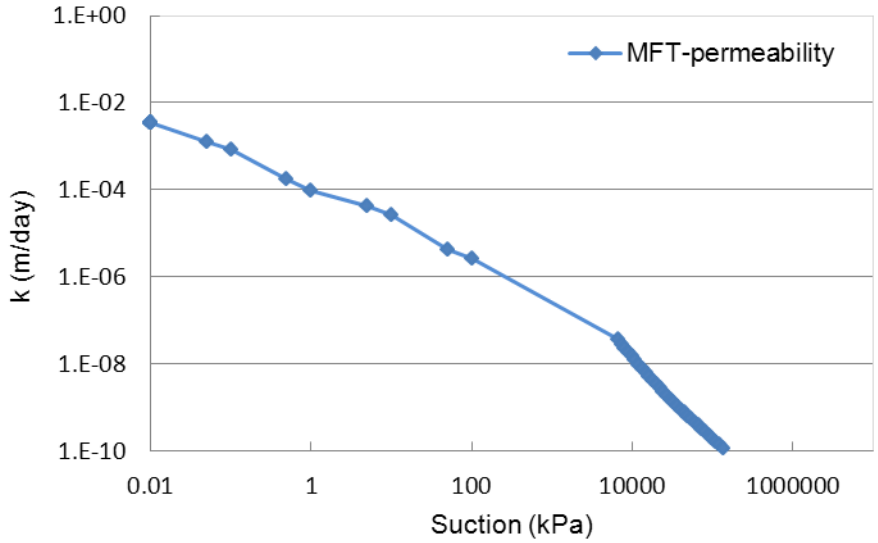

Figure 5.3. Permeability data for the MFT

For the saturation constitutive surface, the data-points were fitted with Vu constitutive surface (Vu 2003). Table 5.1 presents the soil properties used in the seepage analysis.

Table 5.1. Soil properties used in the seepage analysis

	Suncor Coke	Suncor sand	MFT
Unified Soil Classification System	GW	SP	ML
Void ratio, *e*	0.94	0.77	4.63
Poisson ratio, ν	0.48	0.43	0.82
Vu parameters			
a	1.2679	12.7	1.4305
b	-2.0871	-37	0.4988
c	1.1033	2321.1	23.8202
d	5.2407	77.3	2E-8
m	0.7895	1119.1	232.1565
n	1.3139	35	0.0053

Finite element programs typically require the compressibility equation to represent volume change of the soil. The relation between the effective stress and void ratio determined by the large-strain consolidation cells was used and fitted with Vu constitutive surface (Vu 2003). Difficulties were encountered when fitting the model to the granular coke and sand samples having low compressibility. To avoid such instability problems, the zero compressibility curves of both coke and sand was considered to have a smooth and physically realistic slope. The continuous and smooth model minimizes numerical instability and convergence problems when used in any finite-element package. Table 5.2 presents the parameters utilized in the Vu constitutive model.

Table 5.2. Soil properties used in the stress-strain analysis

	Suncor Coke	Suncor sand	MFT
Unified Soil Classification System	GW	SP	ML
Void ratio, *e*	0.94	0.77	4.63
Poisson ratio, ν	0.48	0.43	0.82
A	0.9514	0.78	5.389
B	-0.0098	-0.0098	-7.181
C	19.68	19.68	2.554
D	42.39	42.39	0.0791
M	0.0005	0.0005	0.6854
N	0.0225	0.0225	0.0169

5.4 Modeling approach

The 1D model composed of three soil regions is depicted in Figure 5.4. The seepage boundary conditions used includes a normal constant flux of 0.0014 (m^3/day) at the uncovered top of the sand layer (ground surface). This allowed the soil profile to mimic the real conditions in the field. The complexity of the model increased by the incorporation of suction along the exposed boundaries. The suction pressure profile applied to the middle of the coke layer is given in Figure 5.4.

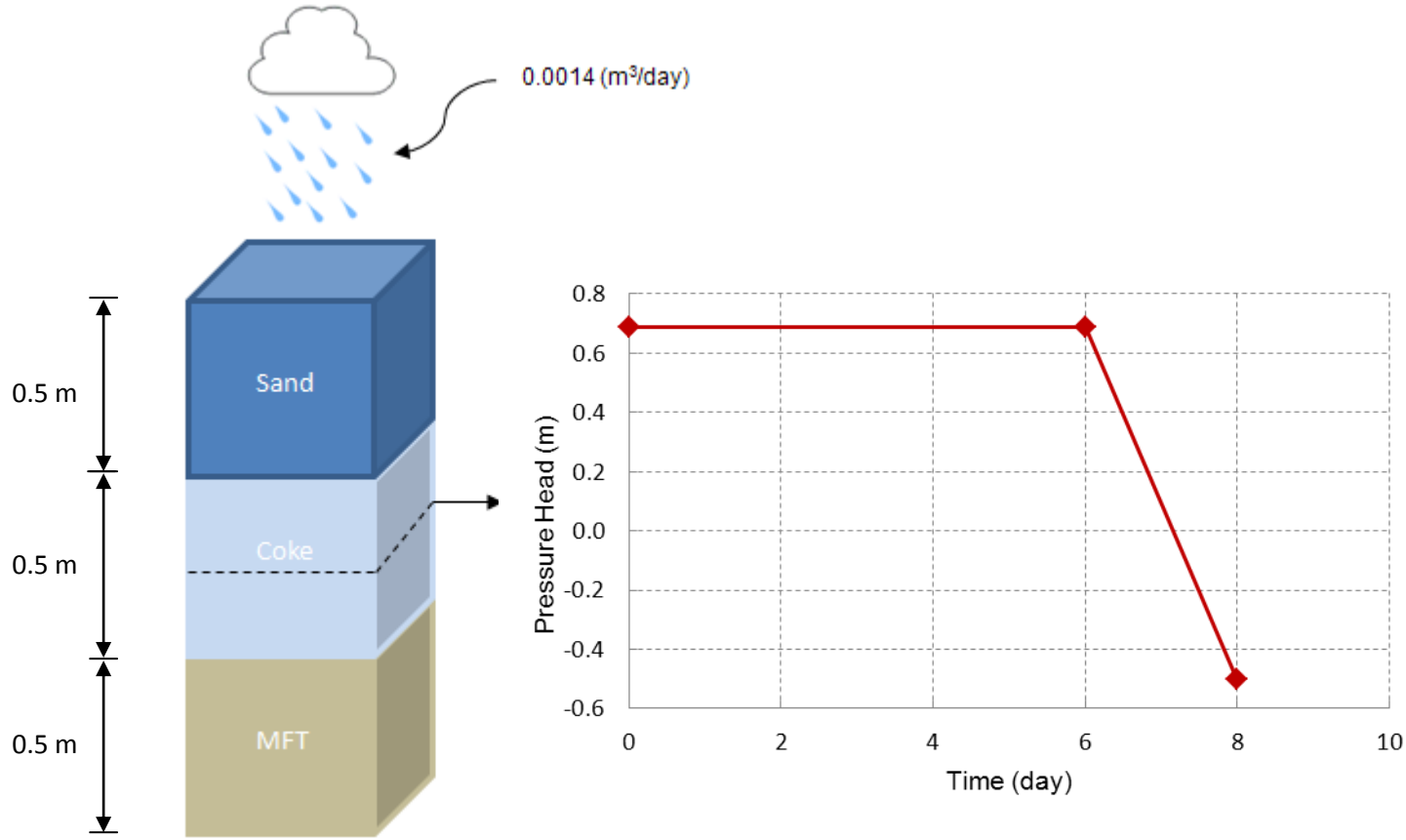

Figure 5.4. Geometry and boundary conditions in the model

In order to remove convergence problems, a smooth function was generated to simulate the application of suction over time. As seen in Figure 5.4, the function generates (-0.5 m) of pressure head corresponding to (-5 kPa) of negative water pressure at the end of eight days.

Stability caused difficulties when running the model with the suction being applied to the middle of the coke layer (0.25 m above the MFT layer). In order to alleviate the stability problem the suction point was adjusted slightly higher than the middle of the coke layer (0.31 m above the MFT layer).

The initial condition in seepage analysis involved a constant head of 1.5 m in the entire model, equivalent to a water table at the surface of the model. The boundary condition in seepage analysis consists of no flux at the bottom of the model. No boundaries are included on MFT-coke and coke-sand interfaces.

The stress-strain boundary condition at the bottom is fixed in the y-direction. The top boundary is free to move vertically. The initial total stress state in the model is determined from the total unit weight multiplied by the height of each layer. The horizontal stress is determined from the vertical stress by applying the coefficient of earth pressure at rest, *Ko.* The coefficient of earth pressure of each material is estimated from its friction angle using equation [5.6]: Jaky (1948) for normally consolidated soils:

$$K_o = 1 - \sin(\phi) \qquad [5.6]$$

where ϕ is the friction angle of each material.

Body load of each material was applied in two days. Large strain theory involves the solution of stress/deformation equations using a Lagrangian reference frame, meaning that the nodes in the mesh move as the body deforms to capture large deformations of MFT. The model was run for 365 days with a time step resolution of 0.1 day.

The simulation consisted of a few separate models with various boundary conditions. The same modeling procedure was followed for all cases. To investigate the effect of suction and fluxes on the model, a set of models with various suctions and fluxes were created and analyzed.

5.5 Results of simulation

The investigation into the effect of various parameters on the consolidation uncovered a number of facts relevant to the behavior of the MFT. The effect of such parameters involved in the vacuum consolidation has been documented to various degrees in the following sections.

5.5.1 Displacement

The estimation of displacement has been computed for various models including a single MFT layer, MFT overlain by a coke layer and MFT overlain by coke and sand with/without the suction (Figure 5.5). Figure 5.6 shows that the deformation increases drastically as MFT is overlain by coke and sand. This implies that the overburden has the dominant effect on the MFT. The graph also shows that application of (-5 kPa) has negligible influence on the amount of settlement that occurred in MFT.

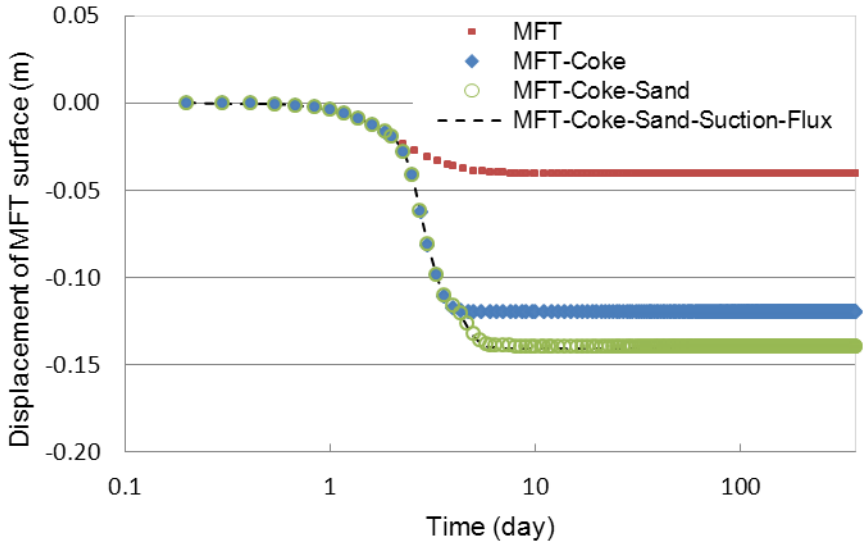

Figure 5.5. Vertical displacement of MFT in various models

The experimental results are plotted alongside the predicted results in Figure 5.6. Figure 5.6 confirms our lab observation that the majority of the settlement takes place in MFT. The predicted displacement is in the same order of the experimental result but the rate of the settlement is different. The difference in rate of consolidation may be due to the difference in large-scale and small scale permeabilities, simplifications made in loading time of MFT in the model and the intrusion of coke layer into the MFT. The magnitude of the predicted settlement of coke and sand match up well with the lab data indicating a negligible compressibility of granular coke and sand (0.02 m).

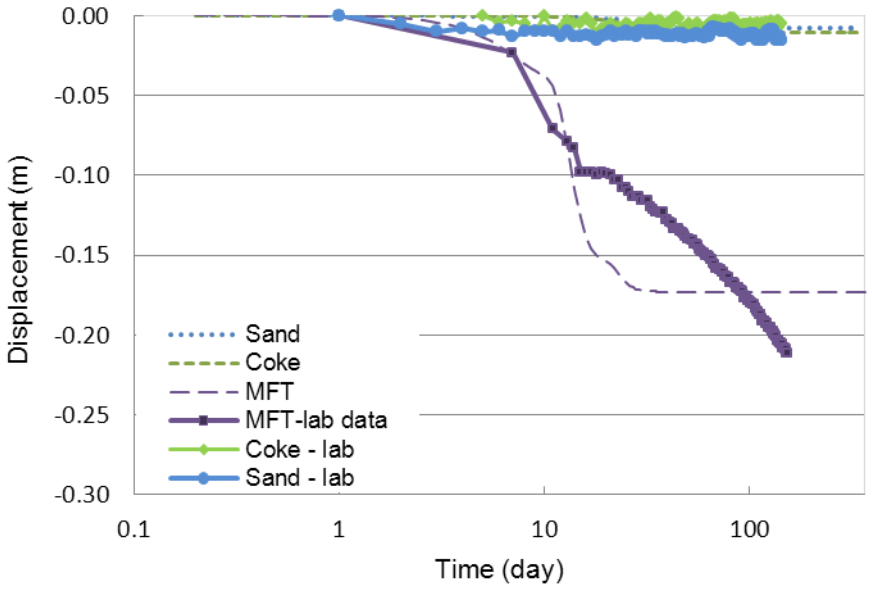

Figure 5.6. Comparison of experimental and predicted data

Figure 5.7 illustrates the effect of suction on the final displacement profile in the three models with various suction values. Figure 5.7 confirms the previous results that the amount of suction does not have primary influence on the total displacement taken place on MFT. The displacements in coke and sand with and without suction are

slightly different. However, this difference becomes negligible as the suction increases.

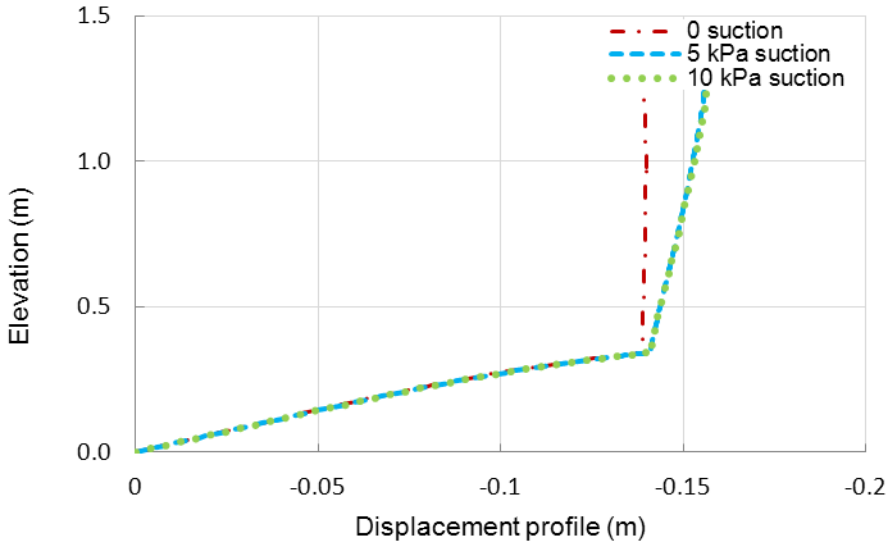

Figure 5.7. Effect of suction value on total displacement

Figure 5.8 illustrates the effect of various fluxes on the displacement profile. As in the previous case, the results indicate that the amount of flux has almost no influence on the displacement patterns of the three models.

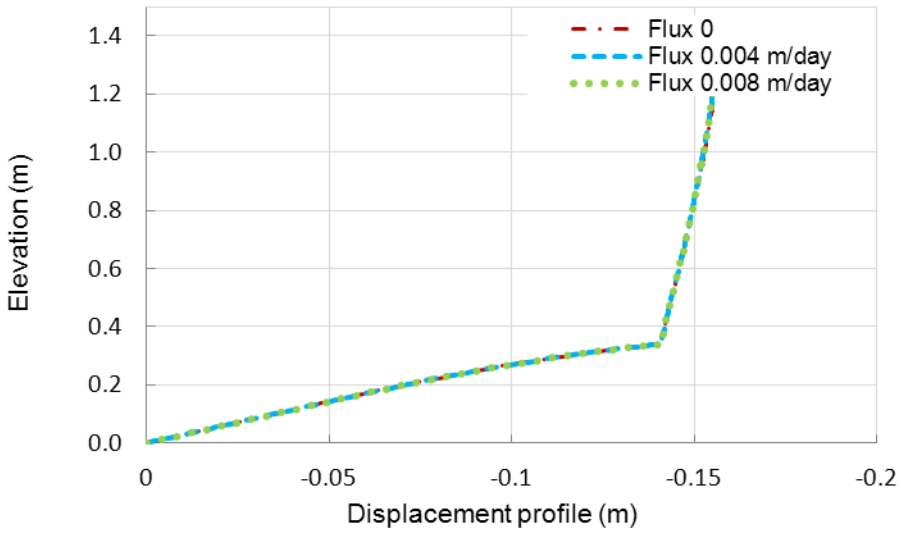

Figure 5.8. Effect of flux value on displacement

5.5.2 Pore-water dissipation response

The pore pressure dissipation in MFT has been investigated by comparing various scenarios (Figure 5.9). The initial water table is at the top of each model creating an initial pore-water pressure head of 0.5 m for MFT; 1 m for MFT overlain by the coke layer and 1.5 m for the three layered system of MFT, coke and sand. The sharp rises in each pore-pressure graph is the result of the increase in the pore-pressure due to the loading of MFT, coke and sand. The pore pressure in MFT converges to the hydrostatic pore pressure in all cases, in 10 days. The application of suction to the coke layer dramatically decreases the pore pressure in MFT.

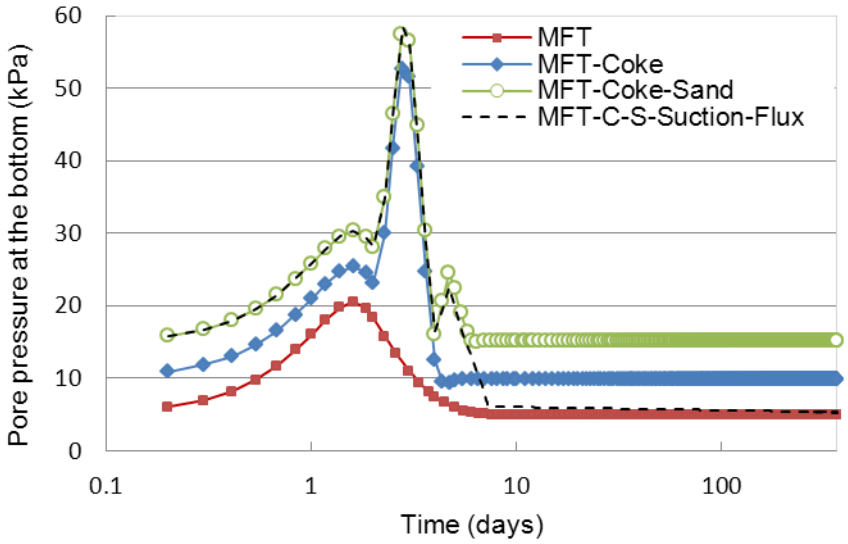

Figure 5.9. Pore pressure of MFT in various models

Figure 5.10 compares the predicted pore pressure and the results obtained from the lab. The first rise in the predicted pore pressure pertains to placement of MFT within the first two days. As MFT is placed, consolidation starts simultaneously and pore-

pressure drops slightly at the end of the second day. Loading the column with coke raises the MFT pore-pressure again to a maximum of 58 kPa while consolidation continues and the generated pore-pressure decreases at the end of the fourth day. Placement of the sand layer generates excess pore-pressure again but the rate of consolidation is faster and the pore-pressure almost reaches the hydrostatic pressure at the end of eight days. The difference between the predicted and the modeled pore-pressure may be due to clogging of the piezometers, barometric or temperature variation reasons. The results obtained from the models and experiments seem to converge as the excess pore-water dissipates.

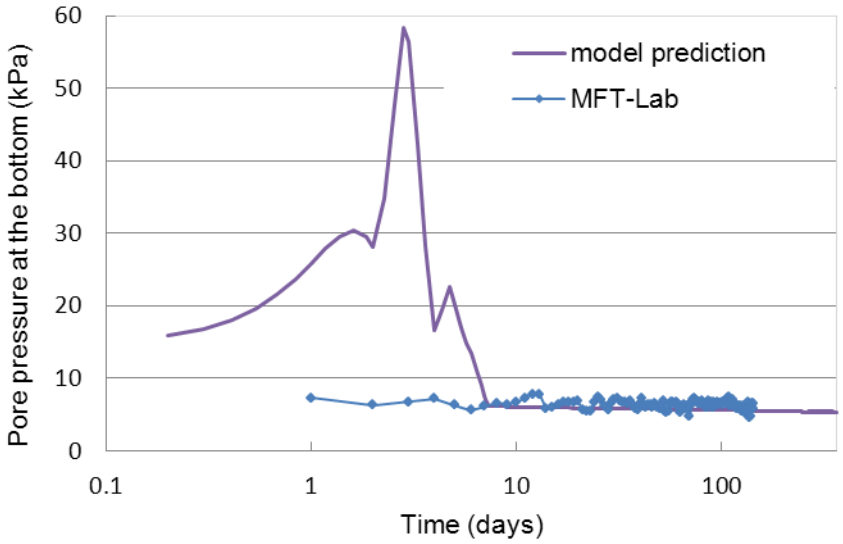

Figure 5.10. Representation of experimental and predicted pore pressure in MFT

The pore pressure diagram at the end of the test is also presented in Figure 5.11. It is seen in Figure 5.11 that all regions experience negative water pressure induced by the suction in the coke layer except for the MFT layer in which hydrostatic pressure prevails. The model without any suction experiences an increase in the water pressure due to the constant flux of water irrigated on top of the sand layer without any drainage.

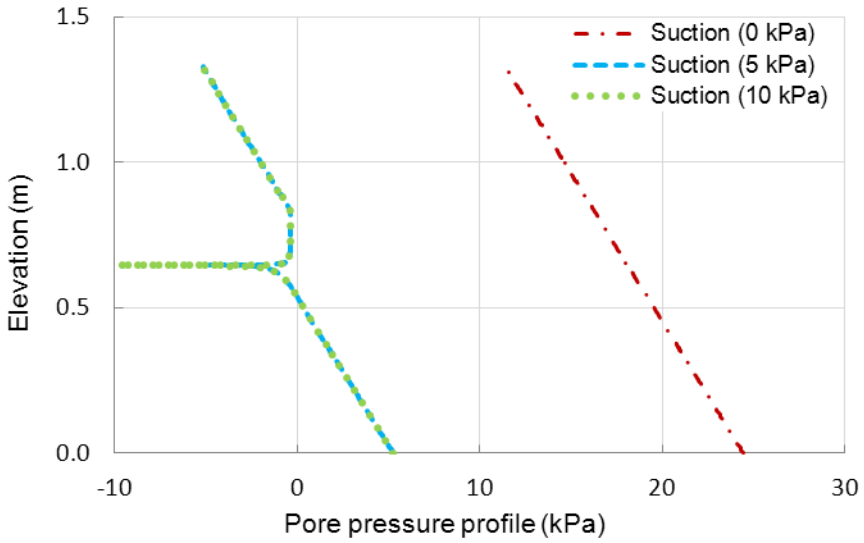

Figure 5.11. Pore pressure diagram in the model at the end of the test

Figure 5.12 demonstrates the effect of flux on the pore pressure. The model with no precipitation experiences more negative water pressure in the coke and sand layer due to suction. The predicted model shows that with a constant suction of (-5 kPa), increasing the flux of water has no effect on the final pore pressure profile.

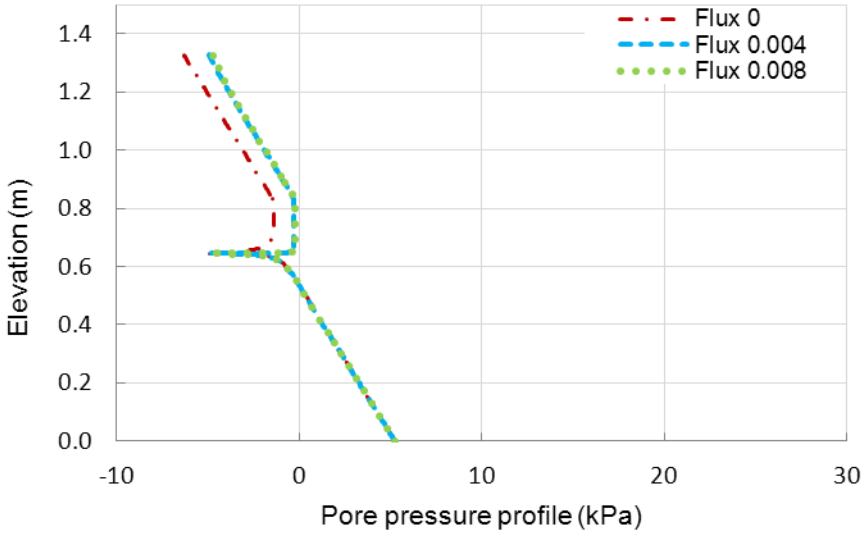

Figure 5.12. Effect of flux value on pore-pressure

5.5.3 Effective stress

The effective stress plot has been presented in Figure 5.13. Significant deterioration of the reliability of the prediction found in this graph was due to considerable variation of both the compressibility parameters of the materials and the application of suction. The instability occurs at the coke-MFT interface and at the point in the coke layer where the suction is applied. The effective stress in MFT decreases slightly with depth due to the increase in hydrostatic water pressure.

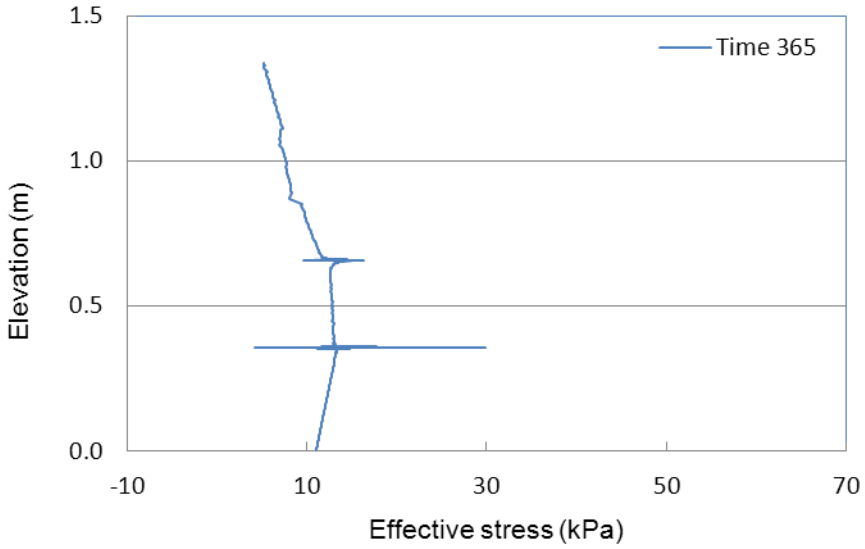

Figure 5.13. Effective stress profile

Further analysis of the effect of suctions on the effective stress reveals that increasing the suction from 5 kPa to 10 kPa has no effect on the final effective stress pattern (Figure 5.14).

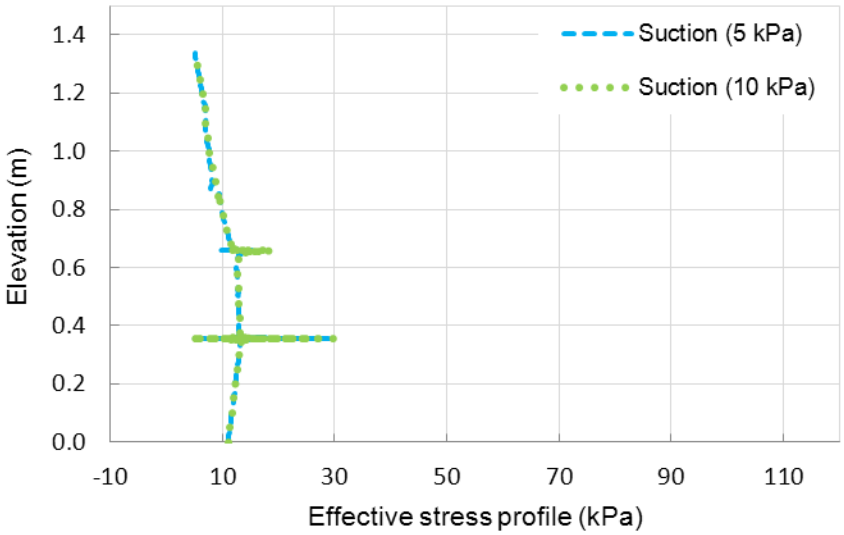

Figure 5.14. Effect of suction value on effective stress

Figure 5.15 reveals that precipitation has no influence on the effective stress pattern of models.

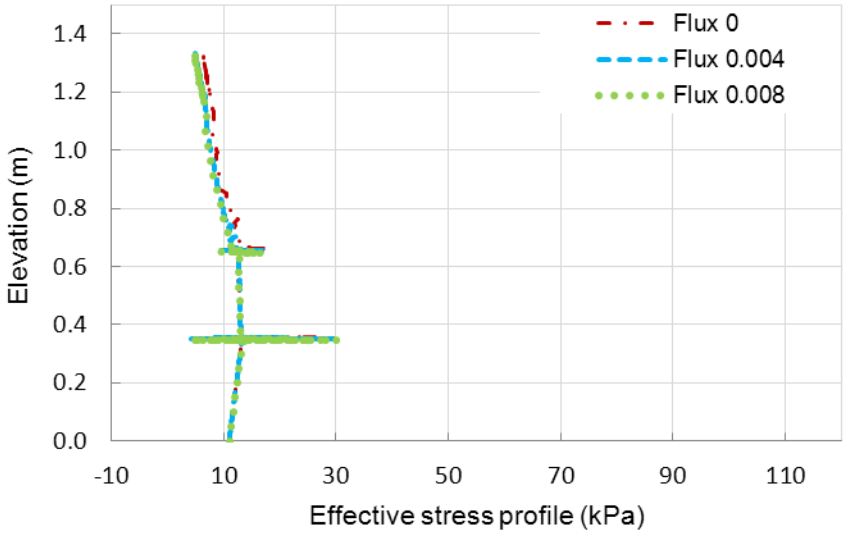

Figure 5.15. Effect of flux value on effective stress

5.5.4 Volume of water

The movement of water from MFT has been investigated by comparing the accumulative fluxes in different situations; with and without suction. The flux profiles suggest that negligible amount of water was drained from the MFT layer in both all three cases (Figure 5.16). Negative sign indicates an outward flow.

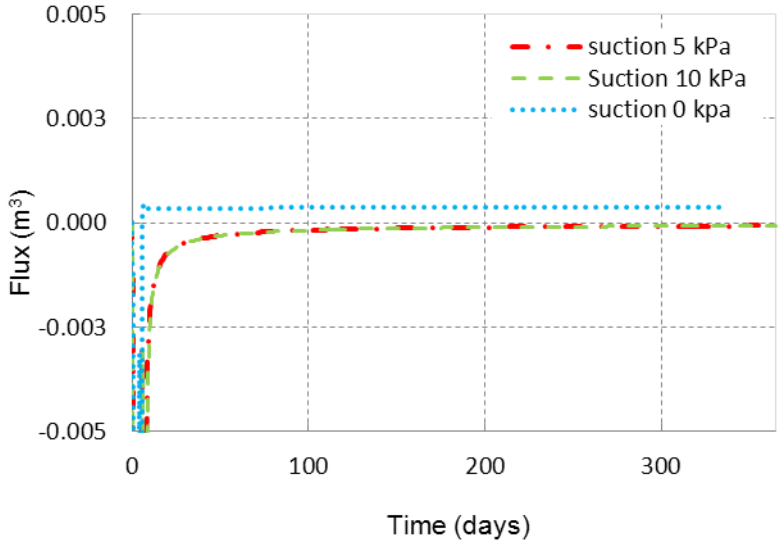

Figure 5.16. Instantaneous flux of water removed from the MFT

The effect of the flux of water on the amount of water removed from the MFT surface is depicted in Figure 5.17. The results presented in Figure 5.17 indicate that the flux on the sand layer has no influence on dewatering MFT. This is consistent with our understanding of the problem, since the flux of water on the sand layer will keep the sand saturated and the excess water is removed through the suction pipes having on influence on dewatering MFT.

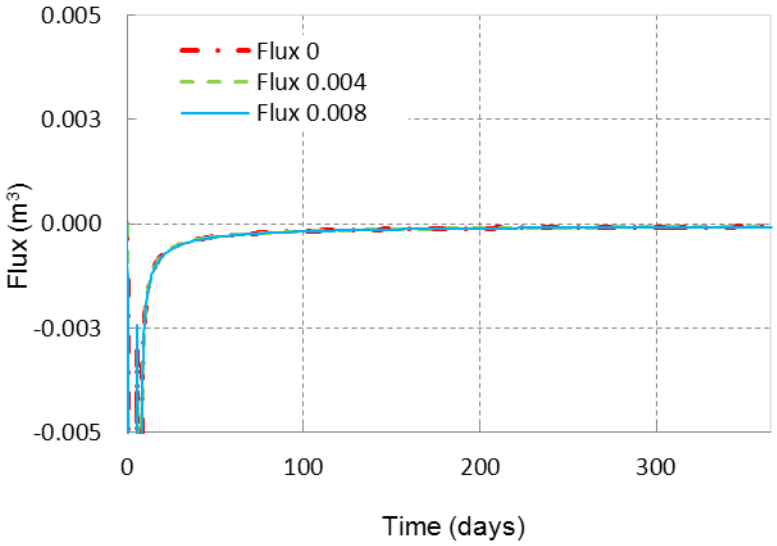

Figure 5.17. Effect of flux value on volume of water

Figure 5.18 compares the instantaneous outward flux from the suctions pipes in the experiment and in the model. This figure shows that apart from the fluctuations at the loading time of the materials, the experimental results and the predicted values match well during the test.

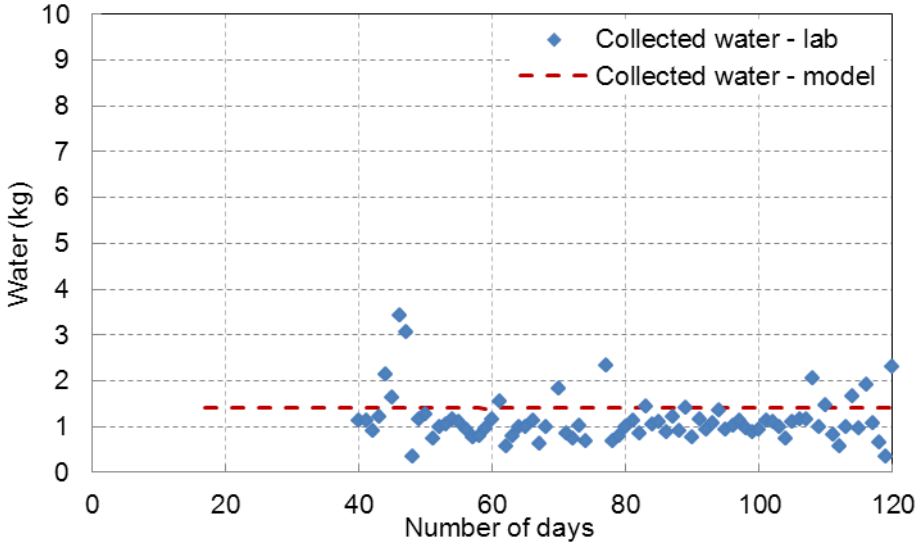

Figure 5.18. Comparison between the experimental and the predicted amount of water removed from the suction pipes

5.5.5 Saturation

The constant flux of water on the sand profile was found to be able to maintain the saturation of the sand layer for the whole test period (Figure 5.19). Coke 1 in Figure 5.19 refers to the lower half of the coke layer on top of MFT while Coke 2 refers to the upper half of the coke layer underlying the sand layer. All materials have the initial saturation of approximately 100%. After the application of the suction, the coke layer desaturates and remains unsaturated for the rest of the test. The upper coke layer experiences a higher desaturation since the water flows downward towards the suction point. Degree of saturation in MFT remains constant before and after the application of suction due to its high air-entry value.

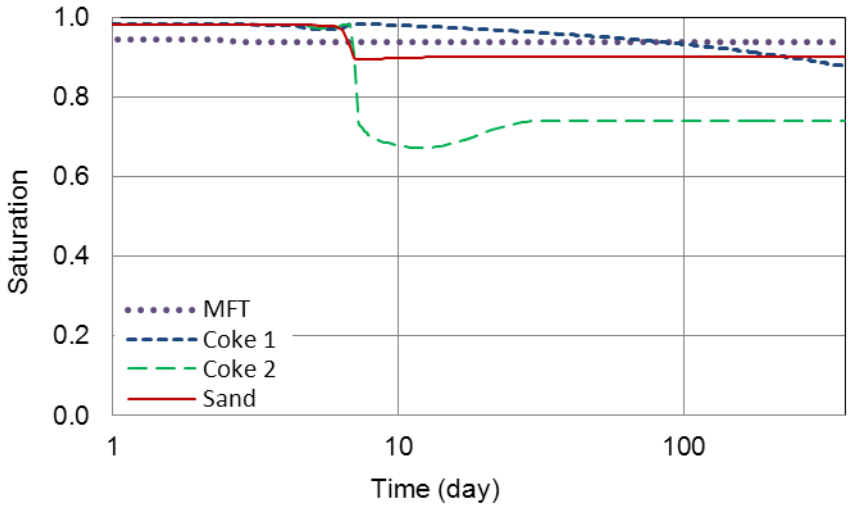

Figure 5.19. The graph of saturation during the test

The effect of suction in the saturation of the sand layer is depicted in Figure 5.20. In all three cases, a constant flux of water was placed on top of the sand layer. In the zero suction case, the sand layer remains completely saturated for the whole test period while in the other cases the sand desaturates slightly to 90% due to suction. Flux of

water on the sand layer (0.0014 m^3/day) maintains the saturation of the sand layer to 90%.

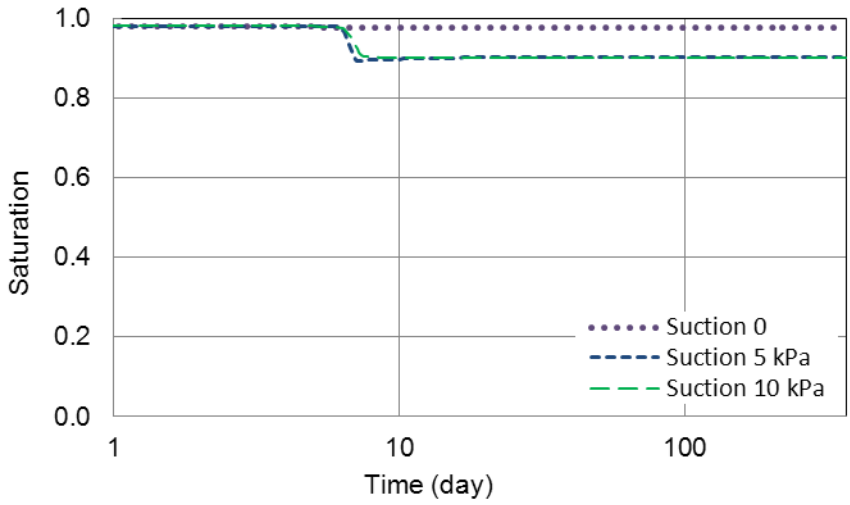

Figure 5.20. Effect of suction value on saturation of sand

The effect of various fluxes on the saturation of the sand layer is depicted in Figure 5.21. In all three cases, suction of (-5 kPa) was maintained in the middle of the coke layer. Application of the (-5 kPa) suction caused a drop in the saturation. Due to the flux of water, the degree of saturation in the sand layer did not change. The model with zero flux experienced a decreasing trend in saturation due to suction.

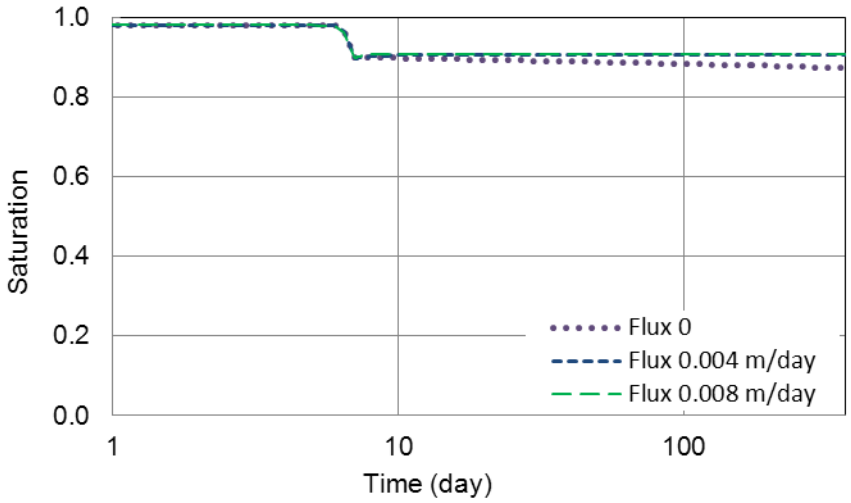

Figure 5.21. Effect of flux value on saturation

Figure 5.22 compares the experimental and the predicted results of the suction in the coke and the sand layer. The experimental results show a higher suction taking place in the test. The amounts of suction in the sand layer in both cases are less than its air-entry value, indicating the ability to keep the top of the sand layer saturated.

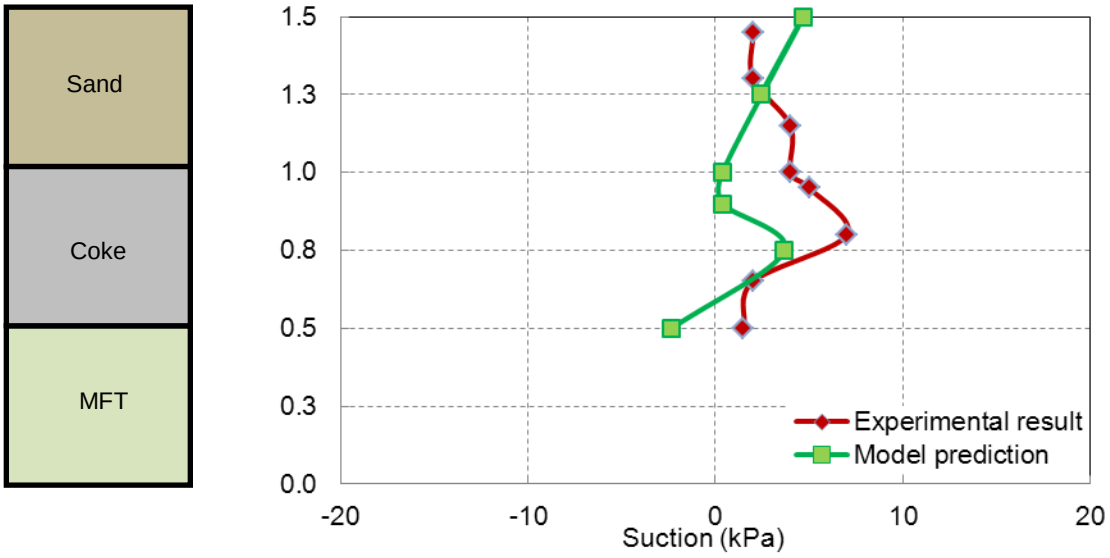

Figure 5.22. Suction profile in the coke and sand layer

5.5.6 Permeability

As the coke and the sand layer desaturate, the permeability of the each material decreases according to their unsaturated permeability functions. Figure 5.23 shows the final permeability profile for each of the three layers in the model. The permeability of MFT remains constant. Part of the coke layer adjacent to the sand layer desaturates fairly rapidly due to gravity while the other part on top of MFT remains fairly saturated unaffected from the suction.

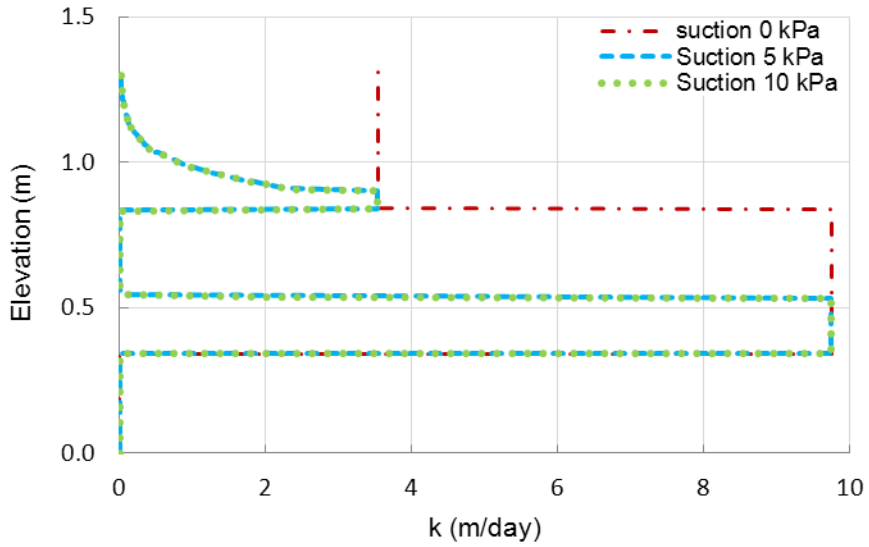

Figure 5.23. Effect of suction value on permeability

The effect of various fluxes on the permeability function is presented in Figure 5.24. As it can be seen in the figure, an increase in the amount of irrigation does not have any effect on the permeability of the model except for the sand in which zero flux decreases the permeability of the sand layer due to the application of suction.

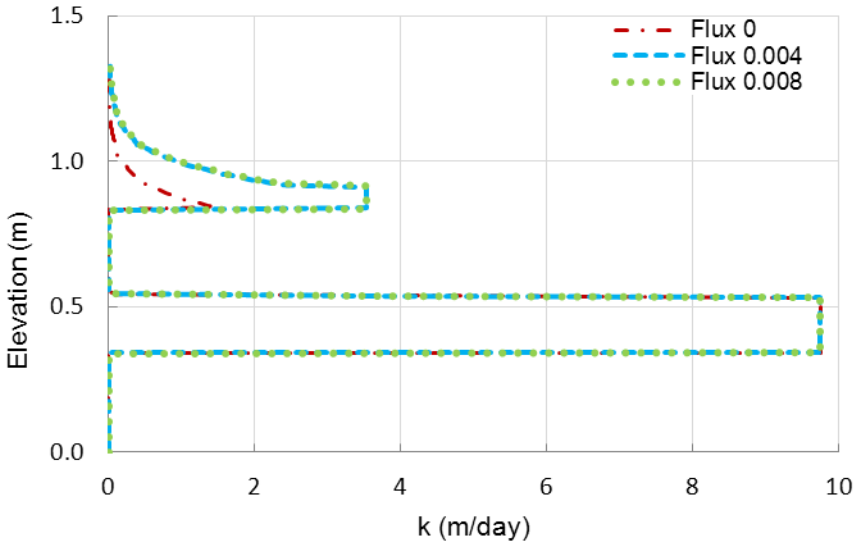

Figure 5.24. Effect of flux value on permeability

5.6 Four layered system

As explained in the previous results, application of the suction has a negligible effect on the consolidation of capped MFT. In this section a four layered system is examined in which a 0.5 m of MFT is placed on the sand layer (Figure 5.25). The configuration of the model is similar to the three-layered system. The results of suction on the pore-pressure dissipation and displacement are presented below.

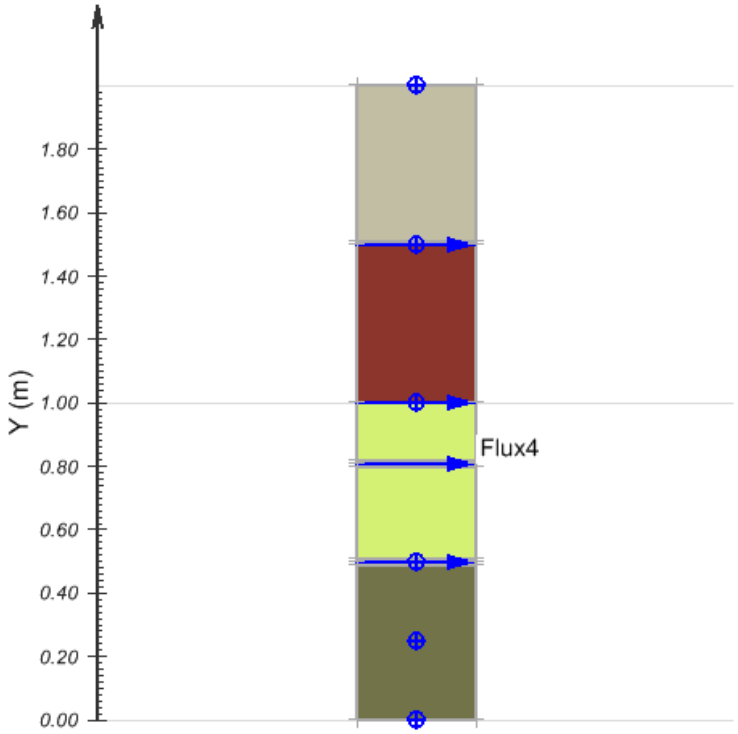

Figure 5.25. Four layered system

5.6.1 Displacement

Figure 5.26 compares the displacement of MFT which is placed on the sand layer. The logarithmic graph shows a settlement of MFT (-0.06 m) within the 100 days of the application of suction. The increase in the settlement is due to the double drainage system as well as the suction.

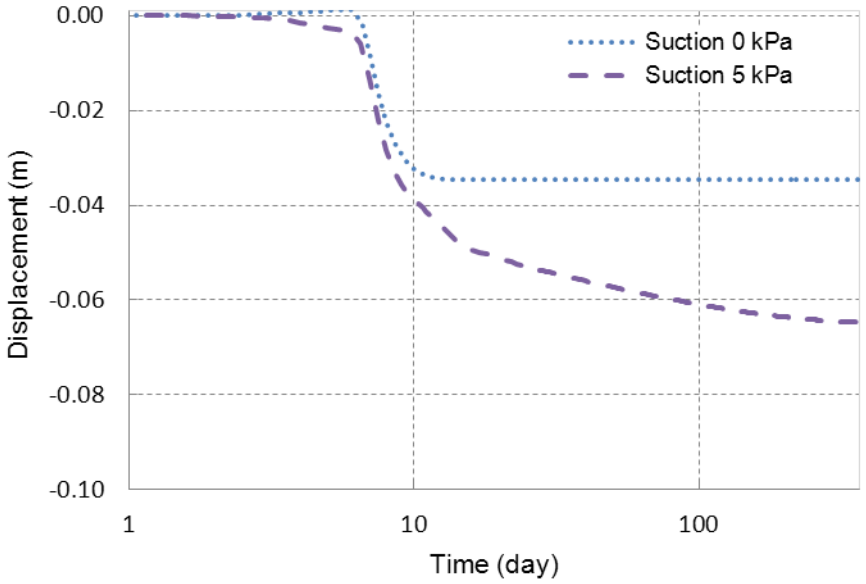

Figure 5.26. Displacement of the overlying MFT in the four-layered system

The settlement of the lower MFT layer has been depicted in Figure 5.27. As it can be seen in the logarithmic plot, the suction has only a small effect on the settlement of the MFT.

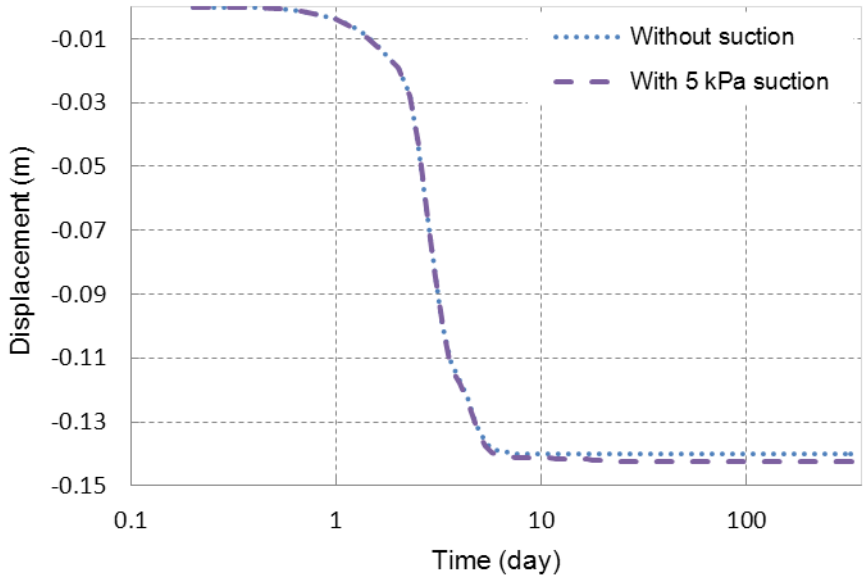

Figure 5.27. Displacement of the lower MFT layer in the four-layered system

5.6.2 Pore pressure dissipation

Figure 5.28 illustrates the effect of the suction on the dissipation of the overlying MFT. The sharp rises in the pore pressure is due to the loading period when the MFT is placed and the pore-pressure build-up takes place. As the suction applies to the coke layer, pore-pressure drops considerably to less than (-7.8 kPa) within 100 days of experiment.

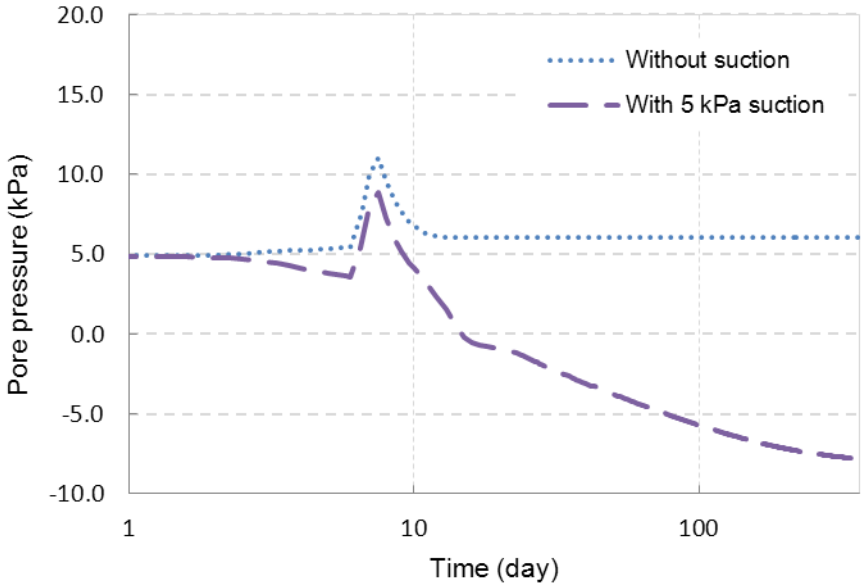

Figure 5.28. Pore-pressure dissipation in MFT in the four-layered models

Figure 5.29 shows the effect of suction on the pore-pressure dissipation of the lower MFT layer. The model without suction shows a hydrostatic pressure after the first 10 days. As the suction applies to the coke layer within 20 days, pore-pressure drops considerably to less than (5.2 kPa) within 100 days of experiment.

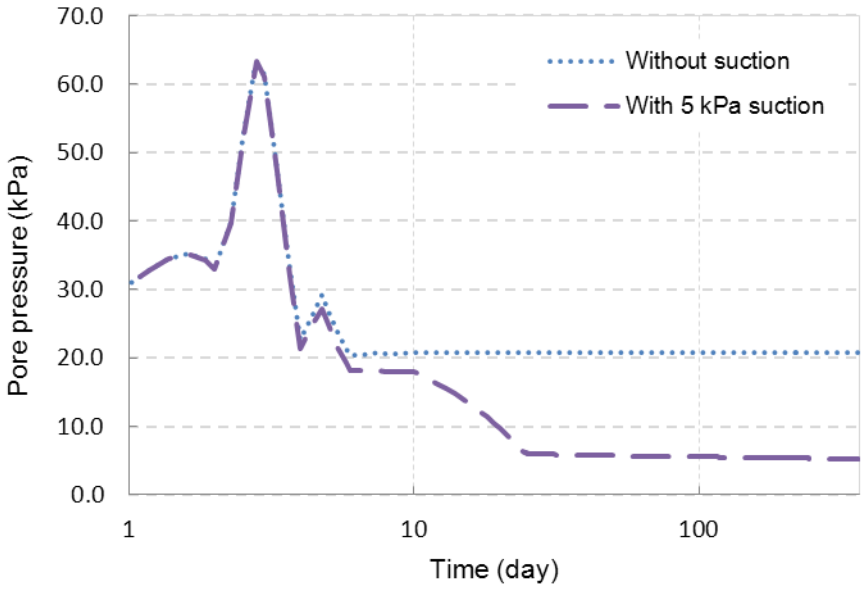

Figure 5.29. Pore-pressure dissipation in the lower MFT layer

5.7 Full scale model

Figure 5.30 depicts the hypothetical image of a reclaimed tailings pond. The sand layer is overlain by a layer of MFT. MFT works as seal to avoid intrusion of air into the saturated sand layer. The suction pipes are placed inside of the coke layer. Applying suction to the coke layer using suction pumps at the ground surface develops a gradient and draws the water from the upper and lower MFT layers out of the system. Due to the head difference between the top and bottom of the suction pipes, the water starts to flow out of the system once the initial required suction is provided by the suction pump.

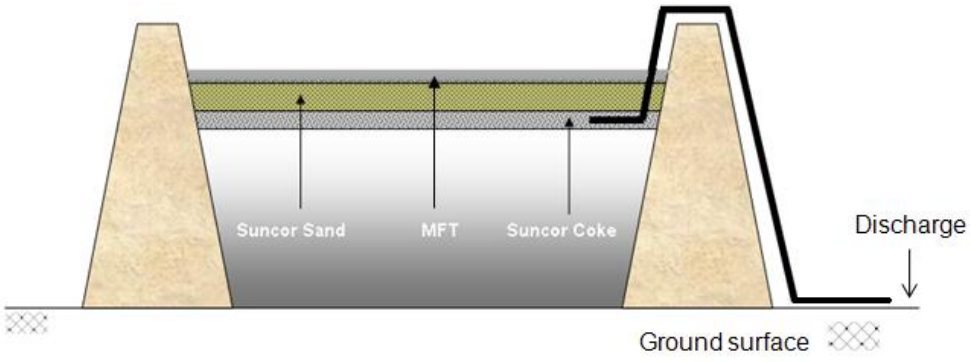

Figure 5.30. Hypothetical image of the reclaimed tailings pond and vacuum consolidation (not to scale)

5.7.1 Boundary/initial conditions

The modeling approach is very similar to the four layered system. A 20 m MFT represents the MFT in the tailings pond. MFT is overlain by a 2 m layer of coke. A 2 m layer of sand overlies the coke layer. The sand is covered by a 0.5 m of MFT (Figure 5.31).

The initial condition in seepage analysis involved a constant head of 24.5 m in the entire model, equivalent to a water table at the surface of the model. The boundary condition in seepage analysis consists of no flux at the bottom of the model. No boundaries are included on MFT-coke and coke-sand interfaces.

In order to remove convergence problems, suction in the coke layer was applied using a smooth function over several days.

The stress-strain boundary condition was similar to previous models; i.e. the bottom of model is fixed in the y-direction. The top boundary is free to move vertically.

Body load of each material was applied in 30 days to simulate placement of a large amount of MFT, coke and sand into the tailings pond. The model was run for 365 days with a time step resolution of 0.1 day.

The simulation consisted of a few separate models with various suctions. The same modeling procedure was followed for all cases.

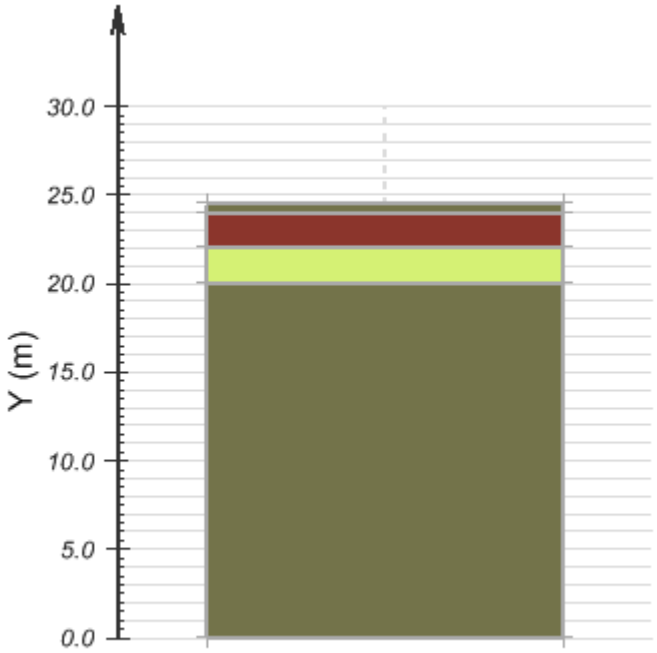

Figure 5.31. Hypothetical image of the reclaimed tailings pond and vacuum consolidation (not to scale)

5.7.2 Displacement

Figure 5.32 illustrates the displacement of MFT at the top of the sand layer. Various models with different suction values have been evaluated. The amount of displacement of MFT without suction indicates a settlement of 0.03 m under its self-weight after nearly 150 days. Applying suction improves the settlement to 0.09 m after one year. Figure 5.32 shows a significant improvement of settlement of MFT after the application of suction. It is also seen in the figure that increasing the amount of suction does not have any significant effect on the settlement in the MFT overlying the sand.

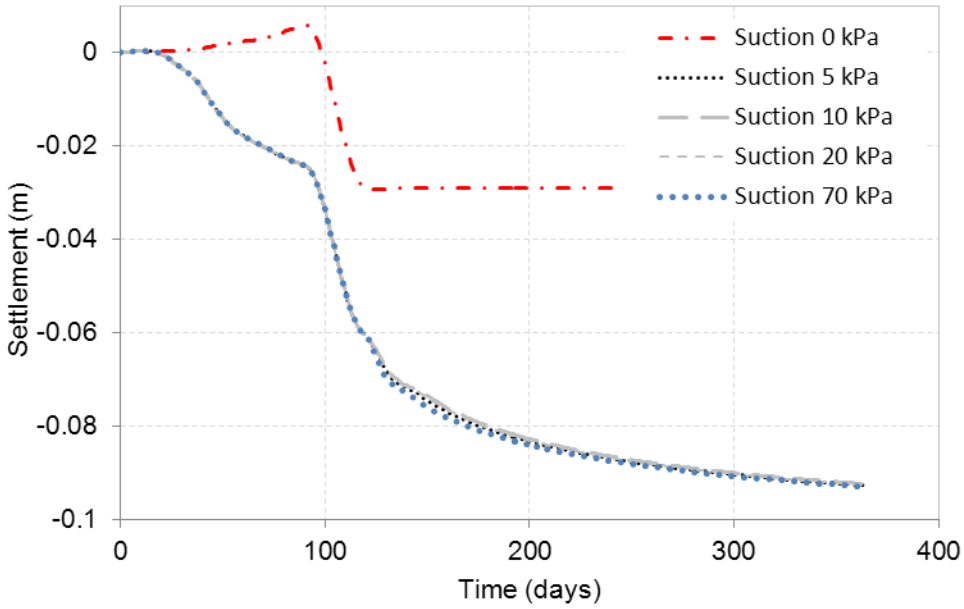

Figure 5.32. Settlement of MFT on top of the sand layer

The displacement of the 20 m MFT layer is depicted in Figure 5.33. The model without any suction shows a settlement of 1 m due its self-weight under the overburden. Application of suction increases the settlement slightly to 1.05 m. It can be seen in the figure that increasing the suction does not increase the settlement of the MFT.

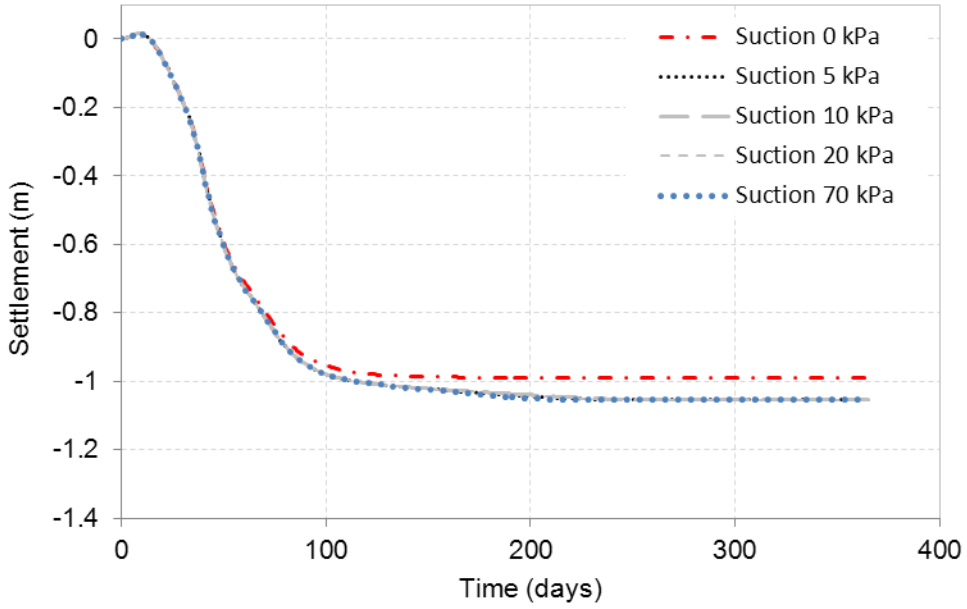

Figure 5.33. Settlement of 20 m MFT

5.7.3 Pore-pressure response

Figure 5.34 illustrates the pore-pressure response of the 0.5 m MFT on top of the sand layer. The initial water table is at the top of MFT creating an initial pore-water pressure head of 0.5 m for MFT. The rise in pore-pressure graph is the result of the increase in the pore-pressure due to the loading of MFT in 30 days. The pore pressure in MFT decreases to reach the hydrostatic pressure of 5 kPa, but due to the release of water from underlying 20 m MFT it increases to a value of 18 kPa. The application of suction to the coke layer dramatically decreases the pore pressure in MFT to a value of -13 kPa.

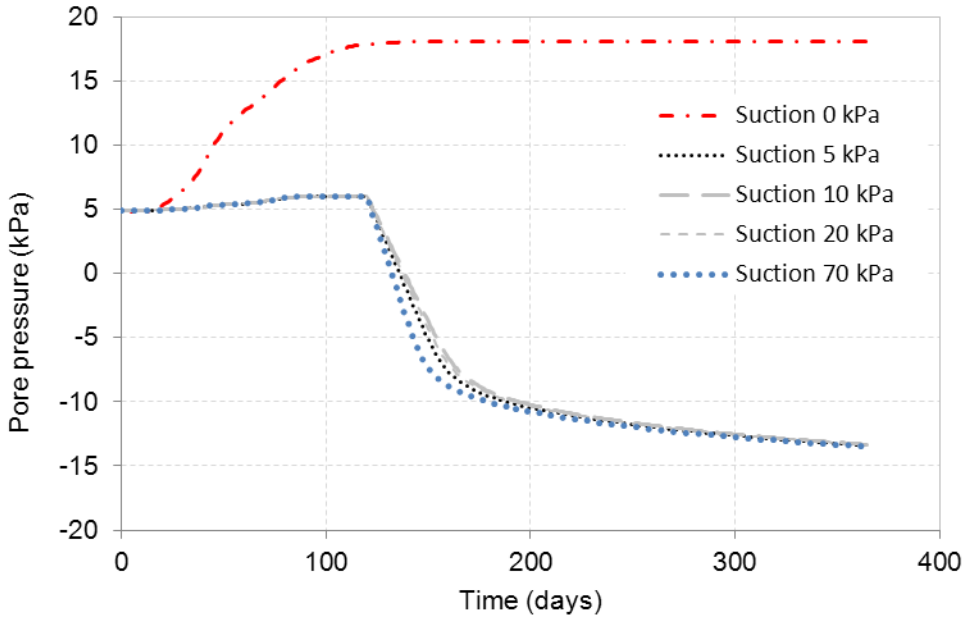

Figure 5.34. Pore-pressure response of 0.5 m MFT on top of the sand layer

Figure 5.35 compares the predicted pore pressure in the 20 m MFT layer with various suction values. The initial water table is at the top of MFT creating an initial pore-water pressure head of 24.5 m for MFT (245 kPa). The first rise in the predicted pore pressure pertains to placement of MFT within the first 30 days. As MFT is placed, consolidation starts simultaneously. Placement of coke and sand decreases the rate of consolidation in MFT and creates local flat zones in the pore-pressure graph of MFT. Figure 5.35 shows an improved consolidation of the 20 m MFT using various suctions. Applying suction decreases the final pore-pressure from 243 kPa to 193 kPa.

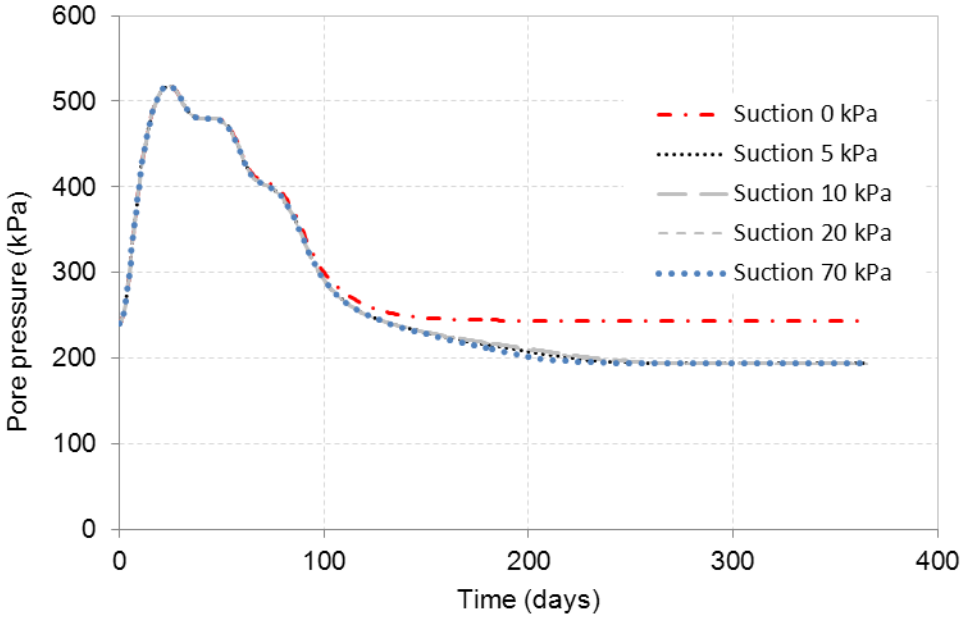

Figure 5.35. Pore-pressure response of 20 m MFT

5.8 Parametric analysis of Poisson's ratio

The effects of various Poisson ratios on the displacement and pore pressure dissipation in MFT are examined to ensure the validity of the results with the assumed values. Figure 5.36 and Figure 5.37 show the effect of Poisson's ratio on displacement and pore-pressure. In these models, the Poisson ratio varied from 0.25 to 0.4 while other parameters remained constant. As illustrated in this graph, the effect of varying Poisson ratio in the pore-pressure distribution and displacement can be ignored.

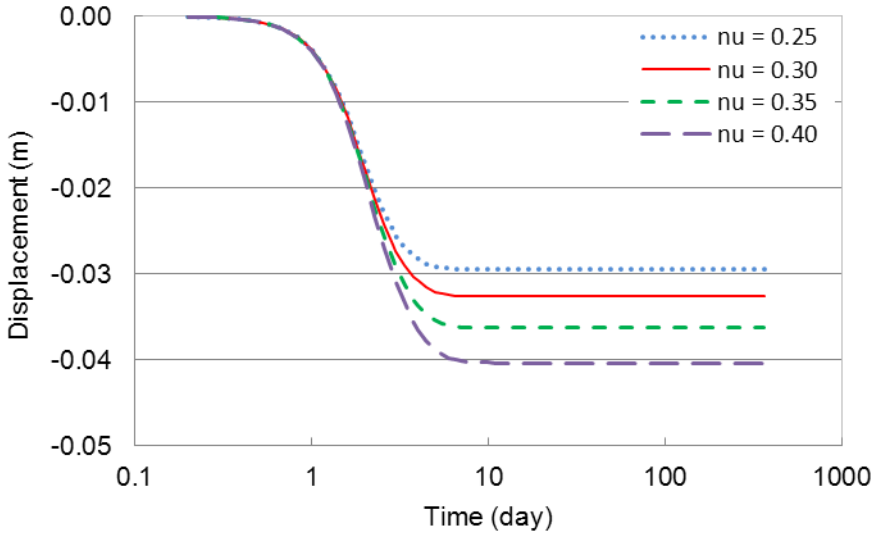

Figure 5.36. Effect of Poisson ratio on displacement in MFT

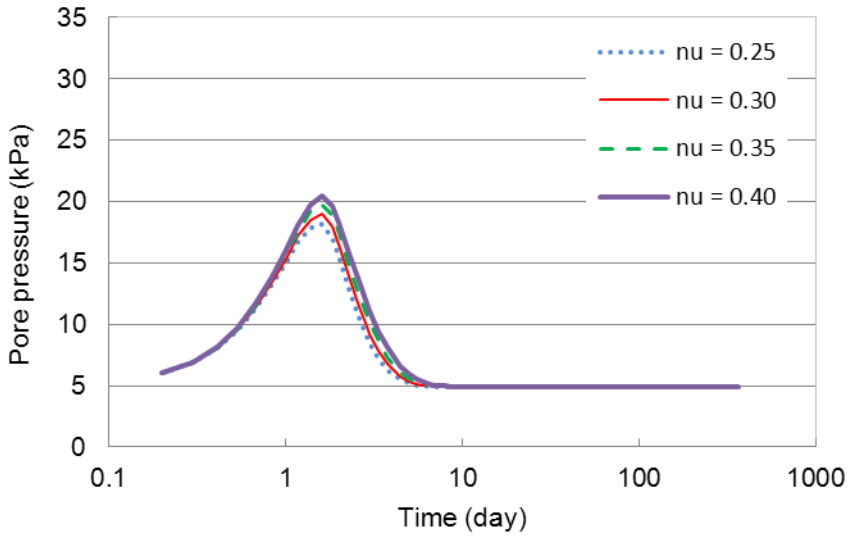

Figure 5.37. Effect of Poisson ratio on pore pressure in MFT

5.9 CONCLUSION

This research study investigated the effect of suction on the long term consolidation behavior of a three-layered and a four-layered system. Factors, including the amount of suction, precipitation and overburden on MFT were assessed. The outcome from this study can be applicable to improving consolidation behavior of soft deposits in tailings management. The research findings are summarized below:

1- The incorporation of suction has little effect on the settlement of the MFT in the three layered system but significantly expedites the consolidation of the overlying MFT in the four-layered system.

2- Applying a flux rate to the surface of the sand layer avoids desaturation of the sand layer.

3- Application of suction changes the pore pressure profile of the model. The decrease in pore-pressure is much more considerable in the upper MFT layer in the four-layered system where the pore-pressure in MFT becomes negative in fifteen days.

4- Application of suction changes decreases the pore pressure in the 0.5 m MFT layer in the full-scale model. It also increases the settlement in the overlying and underlying MFT layers.

5- Increasing the suction does not have any significant effect on the settlement of the 20 m MFT layer but reduces its pore-pressure drastically.

6- Using a parametric study, it is demonstrated that consolidation is not affected by the Poisson's ratio.

5.10 REFERENCES

Azam, S., S. Jeeravipoolvarn, and J. D. Scott. 2009. Numerical modeling of tailings thickening for improved mine waste management. *Journal of Environmental Informatics* 13, no. 2:111-118.

Bartholomeeusen, G., et al. 2002. Sidere: numerical prediction of large-strain consolidation. *Geotechnique* 52, no. 9:639-648.

Bromwell, L. G., and Oxford, T. P. 1977. *Waste Clay Dewatering and Disposal.* 1801 Alexander Bell Drive, Reston, VA, 20191-4400, USA, [journal-services@asce.org], [:http://www.asce.org]: American Society of Civil Engineers.

Cargill, Kenneth W. 1984. PREDICTION OF CONSOLIDATION OF VERY SOFT SOIL. *Journal of Geotechnical Engineering* 110, no. 6:775-795.

Carrier, W. D. I., and Bromwell, L. G. 1983. *DISPOSAL AND RECLAMATION OF MINING AND DREDGING WASTES.* Montreal, Quebec, Canada: Canadian Geotechnical Society.

Consoli, N. C., and G. C. Sills. 2000. Soil formation from tailings: Comparison of predictions and field measurements. *Geotechnique* 50, no. 1:25-33.

Fox, Patrick J., Mario Di Nicola, and Donald W. Quigley. 2003. Piecewise-linear model for large strain radial consolidation. *Journal of Geotechnical and Geoenvironmental Engineering* 129, no. 10:940-950.

Fredlund, Delwyn G., and Hung Q. Vu. "Numerical modeling of swelling and shrinking soils around slabs-on-ground." In Post-Tensioning Institute Conf, pp. 125-132. 2003.

Fredlund, D. G., and Rahardjo, H. 1993. *Soil mechanics for unsaturated soils.* New York: Wiley.

Gibson, R. E., G. L. England, and M. J. L. Hussey. 1967. Theory of one-dimensional consolidation of saturated clays -- 1. *Geotechnique* 17, no. 3:261-273.

Gustavsson, K., and J. Oppelstrup. 2001. Numerical 2D models of consolidation of dense flocculated suspensions. *Journal of Engineering Mathematics* 41, no. 2-3:189-201.

Haase, Matthias, Mario Exner, and Uwe Reichel. 2D modeling of the consolidation of soft soils.

Huerta, A., and A. Rodriguez. 1992. Numerical analysis of non-linear large-strain consolidation and filling. *Computers and Structures* 44, no. 1-2:357-365.

Jakubick, Alex T., Gord McKenna, and Andy M. Robertson. 2003. Stabilization of Tailings Deposits: International Experience. I*nternational Experience. Mining and the Environment III* Sudbury, Ontario, Canada, 25-28 May, pp. 1-9.

Lee, S. L., et al. 1988. CONSOLIDATION OF DREDGED CLAY IN RECLAMATIONS. *Soils and Foundations* 28, no. 2:1-13.

Martinez, R. E., et al. 1987. Reclamation of Phosphatic Clay Waste Ponds by Capping. Volume 6. Consolidation Properties of Phosphatic Clays from Automated Slurry Consolidometer and Centrifugal Model Tests. Ph.D. diss., .

Qiu, Y., D. C. Sego, and Jozef Szymanski. 1999. Innovative tailings backfill using HSM. *Tailings and mine waste*169-176.

SVOffice Manual, 2009, SoilVision Systems Ltd.

TAN, THIAM-SOON, and SENG-LIP LEE. 1990. AN INVESTIGATION OF SHEAR STRENGTH OF SLURRY CLAY. *Soils and Foundations* 30, no. 4:.

Townsend, F. C., et al. 1988. *Reclamation of Phosphatic Clay Waste Ponds by Capping. Volume 1: Centrifugal Model Evaluation of Reclamation Schemes for Phosphatic Waste Clay Ponds.* United States: .

Townsend, F. C., and M. C. McVay. 1990. SOA. Large strain consolidation predictions. *Journal of Geotechnical Engineering* 116, no. 2:222-243.

Townsend, Frank C., M. C. McVay, D. G. Bloomquist, and S. A. McClimans. 1989. Clay waste pond reclamation by sand/clay mix or capping. *Journal of Geotechnical Engineering* 115, no. 11:1647-1666.

Vu, H. Q. (2003). "Uncoupled and coupled solutions of volume change problems in expansive soils". Ph.D. The University of Saskatchewan (Canada), Canada.

Wei, J., et al. 2000. *CAPPING OF A SILT POND FILLED WITH SILTY-CLAY SLURRY.*Geoeng 2000, Melbourne, Australia ed.

Yang, Hong, Harianto Rahardjo, Eng-Choon Leong, and D. G. Fredlund. 2004. Factors affecting drying and wetting soil-water characteristic curves of sandy soils. *Canadian Geotechnical Journal* 41, no. 5:908-920.

Chapter 6

Summary and Future work

6.1 Introduction

This PhD dissertation consists of a series of sections that come together to investigate a novel idea in dewatering oil sand tailings. Summaries of each chapter with recommendations are presented in the following sections.

6.2 Conclusions

Chapter 1 provides an overview of oil sand tailings and objectives of this study. It also establishes the approach followed in this research to address the dewatering problem in oil sand tailings while limiting the scope of work to materials and testing conditions specified in the thesis. The organization of the thesis is outlined in the last part of chapter 1.

- Traditional approach of disposing oil sands tailings into the settling ponds has become too costly primarily because of the costs associated with slow consolidation of the tailings and the area required to accommodate the tailings. Novel approaches are thus required to be assessed to expedite the consolidation time of the oil sand tailings.
- Application of vacuum consolidation is introduced as the major focus of this research program. The intent is to stabilize MFT by creating a sand cap capable of supporting light traffic which is an essential step in further reclaiming the land. In the proposed technique, a layer of saturated coke is placed on top of the tailings surface, overlain by a layer of saturated sand.

Applying a vacuum to the coke layer will consolidate the MFT by removing the water. Creating a trafficable surface on top of MFT can set the stage for the application of numerous dewatering techniques to expedite the consolidation process.

- Characterizing the unsaturated properties of MFT, Suncor coke and Suncor sand is an essential step in this meso-scale study.
- Prior to commencing the test, the meso-scale column must be designed and instrumented with the desired devices to measure the required parameters.
- Numerical modeling of the experiment is carried out after the test to show that the results are consistent.

Chapter 2 details how the unsaturated parameters of the Suncor coke, Suncor sand and MFT were determined.

- Drying and wetting SWCC's of Suncor coke, Suncor sand and MFT were determined in the lab using Tempe cells and Open-rise tubes respectively.
- The laboratory results were fitted with two well-known models, namely the van Genuchten model (1980) and the Fredlund-Xing model (1994).
- The results confirm our understanding of the basic concepts of unsaturated soil mechanics, demonstrating that coarser materials have a lower air-entry value, a lower residual suction and a lower water-entry value than fine-grained soil.
- The unsaturated permeability functions necessary for the numerical modeling were also estimated based on their SWCC's and their saturated permeabilities.

Chapter 3 presents the results of calibrating the Time Domain Reflectometry probes as part of the instrumentation of the meso-scale column.

- Various components in a TDR system for use in measuring soil water content and electrical conductivity were described.
- It was generally found that the universal Topp equation (Topp et al., 1980) did not yield reliable results, requiring a new series of equations to be developed for each material.
- The linear equation between the square root of the dielectric constant, $K^{0.5}$ and θ confirmed the results obtained by other researchers.
- The materials were tested with small variations in the density and sample size and it was observed that neither has any significant impact on the determination of dielectric constant.
- A new calibration equation was developed in the form of $[K^{0.5}\rho_w/\rho_d]$ leading to slightly better results by reducing the effect of soil density.
- The electrical conductivity measurements from TDR also agreed well with the actual values from the electrical conductivity indicator.

Chapter 4 describes the main body of this research study, a meso-scale column test, for which a meso-scale column apparatus was constructed and installed at the geotechnical laboratory of University of Alberta.

- Clear indication of consolidation was observed, with a total of 12 cm of settlement in MFT in 100 days.
- No failure of MFT was recorded, as the coke particles were pluviated, indicating the feasibility of placing a uniform layer of coke on top of MFT.

- Visual inspection of the surface sand cap, along with the data obtained from tensiometers, indicated that water saturation is maintained in some parts of the sand layer after 100 days, illustrating that the sand layer remained saturated.

Chapter 5 introduces finite element modeling of the highly-nonlinear boundary value problem encountered in the three-layered system.

- Investigating various scenarios demonstrated that the overburden has the highest impact on the amount of settlement in MFT.
- It was observed from the results that minor variations in suction and precipitation do not have considerable effect on consolidation.
- It was shown that application of suction changes the pore pressure profile of the model.
- Comparisons between various scenarios indicate that the flux rate applied to the surface of the sand layer was enough to avoid desaturating the sand layer.
- A parametric study was conducted to justify the presumed Poisson ratios for the materials, indicating a negligible influence of the Poisson ratio on the results.
- The four- layer system with another layer of MFT on top of the sand layer was also investigated. The suction and the double drainage path in the MFT led to expedited consolidation of MFT.

6.3 Recommendations for future research studies

This thesis opens a window to various topics associated with vacuum consolidation which can be addressed for future studies.

In chapter 2, there is need for further testing on the effect of relative density on unsaturated parameters of Suncor coke and sand. Relative density deviations in the column test can vary the unsaturated permeability functions of the materials, in turn affecting the physics of the three-layered soil system.

In chapter 3, there is a need to utilize other algorithms to determine the dielectric constant of water. The traditional algorithm used in TDR100 program did not seem to yield reliable results in low water content situations.

In chapter 4, there is need for more experimentation on the effect of suction applied to the coke layer. Application of various amounts of suction would determine the flexibility of the method and provide a solution to an optimum suction value that can be applied to the coke layer while maintaining the saturation of the sand layer.

In chapter 5, various constitutive models can be used to facilitate the convergence problems associated with the high-nonlinearity of the boundary value problem. The effect of the thickness of the sand and coke layers on top of the MFT is another area of study that needs further investigation.